

1-1-2008

## Nitrate ion effects on uranium chemistry in the tributylphosphate-dodecane system

Amber Dawn Wright  
*University of Nevada, Las Vegas*

Follow this and additional works at: <https://digitalscholarship.unlv.edu/rtds>

---

### Repository Citation

Wright, Amber Dawn, "Nitrate ion effects on uranium chemistry in the tributylphosphate-dodecane system" (2008). *UNLV Retrospective Theses & Dissertations*. 2439.  
<http://dx.doi.org/10.25669/gc07-43ur>

This Thesis is protected by copyright and/or related rights. It has been brought to you by Digital Scholarship@UNLV with permission from the rights-holder(s). You are free to use this Thesis in any way that is permitted by the copyright and related rights legislation that applies to your use. For other uses you need to obtain permission from the rights-holder(s) directly, unless additional rights are indicated by a Creative Commons license in the record and/or on the work itself.

This Thesis has been accepted for inclusion in UNLV Retrospective Theses & Dissertations by an authorized administrator of Digital Scholarship@UNLV. For more information, please contact [digitalscholarship@unlv.edu](mailto:digitalscholarship@unlv.edu).

**NITRATE ION EFFECTS ON URANIUM CHEMISTRY IN THE  
TRIBUTYLPHOSPHATE-DODECANE SYSTEM**

**By**

**Amber Dawn Wright**

**Bachelor of Science in Chemistry  
University of Nevada, Las Vegas  
2005**

**Bachelor of Science in Mathematics  
University of Nevada, Las Vegas  
2005**

**A thesis submitted in partial fulfillment  
of the requirements for the**

**Master of Science Degree in Chemistry  
Department of Chemistry  
College of Sciences**

**Graduate College  
University of Nevada, Las Vegas  
December 2008**

UMI Number: 1468387

### INFORMATION TO USERS

The quality of this reproduction is dependent upon the quality of the copy submitted. Broken or indistinct print, colored or poor quality illustrations and photographs, print bleed-through, substandard margins, and improper alignment can adversely affect reproduction.

In the unlikely event that the author did not send a complete manuscript and there are missing pages, these will be noted. Also, if unauthorized copyright material had to be removed, a note will indicate the deletion.

**UMI<sup>®</sup>**

---

UMI Microform 1468387  
Copyright 2009 by ProQuest LLC  
All rights reserved. This microform edition is protected against  
unauthorized copying under Title 17, United States Code.

---

ProQuest LLC  
789 East Eisenhower Parkway  
P.O. Box 1346  
Ann Arbor, MI 48106-1346



**Thesis Approval**  
The Graduate College  
University of Nevada, Las Vegas

December 2, 20 08

The Thesis prepared by

Amber Dawn Wright

Entitled

Nitrate Ion Effects on Uranium Chemistry in the  
Tributyl Phosphate-Dodecane System

is approved in partial fulfillment of the requirements for the degree of

Master of Science Degree in Chemistry

Examination Committee Chair

Dean of the Graduate College

Examination Committee Member

Examination Committee Member

Graduate College Faculty Representative

## ABSTRACT

### **Nitrate Ion Effects on Uranium Chemistry in the Tributylphosphate-Dodecane System**

By

Amber Dawn Wright

Dr. Kenneth Czerwinski, Examination Committee Chair  
Associate Professor of Chemistry  
University of Nevada, Las Vegas

Understanding the role of nitrate in the speciation of actinides is important in order to determine the necessary data for extraction modeling of the UREX process. The focus of this project is on the fundamental chemistry of uranium (U) in the tributyl phosphate (TBP) extraction system, with emphasis on the effect of nitrate on actinyl speciation. Speciation calculations can be performed if stability and solubility constants for the chemical species formed under the examined conditions are known. The stability constant of the uranyl-TBP complex was evaluated under a variety of conditions. The variables were nitric acid, uranyl, total nitrate concentration, and ionic strength. The thermodynamic data collected can be incorporated into extraction modeling codes used to predict distribution in reprocessing. The methods used in this research will be modified for corresponding experiments with plutonium and provide necessary data for optimizing the modeling codes.

## TABLE OF CONTENTS

ABSTRACT.....	iii
LIST OF FIGURES .....	vi
LIST OF TABLES.....	viii
ACKNOWLEDGEMENTS.....	x
CHAPTER 1 INTRODUCTION .....	1
1.1 Thesis Overview .....	1
1.2 Separation Chemistry of Spent Nuclear Fuel.....	2
1.2.1 Solvent Extraction.....	3
1.2.2 Extraction studies of actinides in TBP.....	8
1.3 PUREX .....	21
1.4 UREX.....	24
1.5 Process Modeling.....	27
1.6 Project Rationale.....	28
CHAPTER 2 EXPERIMENTAL METHODS .....	30
2.1 Reagents.....	30
2.2 Extractions .....	31
2.2.1 General Extraction Procedure.....	32
2.2.2 Aqueous Phase Variation.....	32
2.3 Determination of Analysis Methods.....	37
2.3.1 Acid Concentration Determination.....	37
2.3.2 Nitrate Concentration Determination.....	40
2.3.3 Uranium Concentration Determination.....	51
CHAPTER 3 RESULTS AND DISCUSSION.....	74
3.1 Uranium Extraction.....	74
3.2 Nitric Acid Extraction.....	79
3.3 Lithium Nitrate Extraction.....	84
3.4 Perchlorate Species Extraction .....	86
3.5 Stability Constant Calculation .....	88
CHAPTER 4 CONCLUSIONS .....	93
4.1 Analytical Methods.....	93
4.2 Extractions .....	94

4.3	Future Work.....	96
	REFERENCES .....	98
	VITA.....	103

## LIST OF FIGURES

Figure 1.1	HDEHP molecule.....	5
Figure 1.2	TBP molecule.....	5
Figure 1.3	CMPO molecule.....	6
Figure 1.4	TIOA molecule .....	7
Figure 1.5	Distribution of actinides in 50% TBP /kerosene.....	10
Figure 1.6	Plot of Pu(IV) distribution ratio against vol % TBP in kerosene to establish stoichiometry of extraction .....	12
Figure 1.7	U(VI) distribution ratio as a function of nitric acid concentration .....	13
Figure 1.8	Distribution of U(VI) from solutions of varying nitric acid and total nitrate concentration.....	14
Figure 1.9	Comparison of distribution ratios determined from the reported stability constant values of 1.65 and 2.67 with experimental data .....	18
Figure 1.10	PUREX process .....	23
Figure 1.11	AHA molecule .....	25
Figure 1.12	Diagram of UREX +3 reprocessing scheme.....	26
Figure 1.13	Schematic of AMUSE code .....	28
Figure 2.1	Comparison of titrations performed in H <sub>2</sub> O and in (NH <sub>4</sub> ) <sub>2</sub> C <sub>2</sub> O <sub>4</sub> .....	39
Figure 2.2	Calibrations of the nitrate specific ion selective electrode with and without the presence of an ionic strength adjuster.....	42
Figure 2.3	Response of the ion selective electrode as a function of nitrate .....	43
Figure 2.4	Response of ion selective electrode over linear range .....	44
Figure 2.5	Measurement of LiNO <sub>3</sub> and HNO <sub>3</sub> standards as calculated based on opposing calibration curve.....	45
Figure 2.6	Response slope as a function of pH .....	46
Figure 2.7	Nitrate calibration curves as determined by ion chromatography .....	48
Figure 2.8	Test for accuracy and acid effects of ion chromatography based measurements.....	49
Figure 2.9	ICP-AES diagram .....	52
Figure 2.10	Diagram of UV-vis system .....	54
Figure 2.11	Molecular orbital diagram of uranyl ion.....	56
Figure 2.12	Absorption spectrum of uranyl ion .....	57
Figure 2.13(a)	UV Spectra of UO <sub>2</sub> (NO <sub>3</sub> ) <sub>2</sub> aqueous solutions in 1 mm cuvettes .....	58
Figure 2.13(b)	Expansion of spectra of UO <sub>2</sub> (NO <sub>3</sub> ) <sub>2</sub> aqueous solutions in 1 mm cuvettes .....	59
Figure 2.14	Calibration using maximum UV absorbance at 415 nm.....	60
Figure 2.15	Effect of counting time on the minimum detection limit of liquid scintillation counting.....	62
Figure 2.16	Effects of sample and scintillation fluid volume on the minimum detection limit of liquid scintillation counting.....	63
Figure 2.17	Partial decay chain of <sup>238</sup> U .....	64
Figure 2.18	LSC spectra of aqueous and organic standards.....	65

Figure 2.19	Calibration curves generated by liquid scintillation counting .....	67
Figure 2.20	Comparison of [U] of aqueous samples determined by liquid scintillation counting and ICP-AES.....	68
Figure 2.21	Comparison of [U] of organic samples determined by liquid scintillation counting and ICP-AES.....	69
Figure 2.22	Difference between concentration values measured by LSC and ICP-AES .....	70
Figure 2.23	LSC spectra of 0.02 M U standard with and without addition of <sup>233</sup> U.....	71
Figure 2.24	Comparison of three methods used to determine uranium concentration.	72
Figure 3.1	K <sub>d</sub> as initial [NO <sub>3</sub> <sup>-</sup> ] increases in the presence of 0.05 M U.....	75
Figure 3.2	K <sub>d</sub> as initial [HNO <sub>3</sub> ] increases in the presence of 0.05 M U.....	75
Figure 3.3	K <sub>d</sub> comparison to literature values at initial [U] of 0.1 M .....	76
Figure 3.4	Extraction of U from 1 M HNO <sub>3</sub> .....	77
Figure 3.5	NO <sub>3</sub> <sup>-</sup> stoichiometry determined via extraction from 1 M HNO <sub>3</sub> and 0.01 M U solutions .....	78
Figure 3.6	TBP stoichiometry determined via extraction from 1 M HNO <sub>3</sub> and 0.01 M U solutions .....	79
Figure 3.7	Acid extraction from 1 M HNO <sub>3</sub> and varied [NO <sub>3</sub> <sup>-</sup> ] .....	80
Figure 3.8	NO <sub>3</sub> <sup>-</sup> stoichiometry determined via acid extraction from 1 M HNO <sub>3</sub> and 0.02 M U solutions.....	81
Figure 3.9	TBP stoichiometry determined via acid extraction data from 1 M HNO <sub>3</sub> and 0.02 M U solutions.....	82
Figure 3.10	Extraction of [NO <sub>3</sub> <sup>-</sup> ] into TBP phase .....	85
Figure 3.11	Mass balance of nitrate ions.....	86
Figure 3.12	Mass balance of acid in the organic phase.....	88
Figure 3.13	Comparison of calculated K <sub>d</sub> values with those previously reported .....	91

## LIST OF TABLES

Table 1.1	Distribution ratios for spent fuel components in 50% TBP from 1 M HNO <sub>3</sub>	9
Table 1.2	K <sub>d</sub> values of actinides in 19% TBP from 5 M HNO <sub>3</sub>	11
Table 1.3	Table of previously reported log β values	19
Table 2.1	List of stock solutions	30
Table 2.2	List of reagents	31
Table 2.3	Range of concentrations	32
Table 2.4	Initial aqueous phase conditions with 0.1 M UO <sub>2</sub> (NO <sub>3</sub> ) <sub>2</sub>	33
Table 2.5	Initial aqueous phase conditions with 0.05 M UO <sub>2</sub> (NO <sub>3</sub> ) <sub>2</sub>	34
Table 2.6	Initial aqueous phase conditions with 0.01 M UO <sub>2</sub> (NO <sub>3</sub> ) <sub>2</sub> and 1 M HNO <sub>3</sub>	35
Table 2.7	Initial aqueous phase conditions with 0.02 M UO <sub>2</sub> (NO <sub>3</sub> ) <sub>2</sub> and 1 M HNO <sub>3</sub>	35
Table 2.8	Initial aqueous phase conditions with I = 6 M	36
Table 2.9	Initial aqueous phase conditions with I = 4 M	36
Table 2.10	Effects of bubbling argon gas on [H <sup>+</sup> ] (M) measured during titration	39
Table 2.11	Effects of ammonium oxalate on [H <sup>+</sup> ] (M) measured during titration	40
Table 2.12	Relative standard deviation in titration measurements	40
Table 2.13	Effects of ionic strength adjuster on calibration slope	43
Table 2.14	Method detection limit of [NO <sub>3</sub> <sup>-</sup> ] determination by ion chromatography	48
Table 2.15	Relative standard deviation in nitrate concentration of 1.2 M LiNO <sub>3</sub> determined by ion chromatography	50
Table 2.16	Method detection limit of [U] determined by ICP-AES	53
Table 2.17	Comparison of [U] (mM) in organic phase as determined by direct ICP-AES measurement vs. by mass balance	53
Table 2.18	Molar absorptivity measured at 415 nm	59
Table 2.19	Difference between [U] (mM) in organic phase of samples extracted from 20 mM UO <sub>2</sub> (NO <sub>3</sub> ) <sub>2</sub> as determined by UV-Visible spectroscopy and ICP-AES	60
Table 2.20	Method detection limits of liquid scintillation counting	64
Table 2.21	Deviation in LSC calibration slopes	66
Table 2.22	Concentration of uranium measured in aqueous and organic phases as determined by LSC and compared to initial [U]	66
Table 2.23	Ratio of [U] values as obtained by LSC and ICP-AES	68
Table 2.24	Comparison of % difference in [U] results from LSC and ICP-AES with and without the addition of <sup>233</sup> U	73
Table 2.25	Relative standard deviation in uranium concentration determined by ICP-AES of 1.1 M uranyl nitrate stock solution	72
Table 3.1	Calculation of log β <sub>H</sub> for samples with [TBP] <sub>free</sub> less than 0.6 M	83
Table 3.2	Calculation of log β <sub>H2</sub> for samples with [TBP] <sub>free</sub> greater than 0.7 M	83

Table 3.3	Reported $\log \beta_H$ and $\log \beta_{H2}$ values for nitric acid-TBP.....	84
Table 3.4	Comparison of error in speciation calculation based on reported stability constants from Table 3.3.....	84
Table 3.5	Comparison of the $UO_2(NO_3)_2 \cdot 2TBP$ stability constant evaluated with and without $[NaClO_4]$ extraction.....	87
Table 3.6	Calculated $\log \beta$ values at $I = 6$ as initial conditions vary.....	89
Table 3.7	Calculated $\log \beta$ values at $I = 4$ as initial conditions vary.....	90

## ACKNOWLEDGEMENTS

First and foremost I would like to thank my thesis committee members for their patience and dedication to this work. I especially would like to thank my advisor Dr. Ken Czerwinski for his many hours of effort toward this project. I also want to give special recognition to Dr. Cynthia-May Gong for repeatedly going out of her way to help me any time I needed guidance.

I need to mention a few students who assisted me with my experiments in the lab, namely Jamie Warburton, Ira Racoma, and Jade Morgan. I appreciate the radiochemistry group as a whole, and especially Tom O'Dou and Trevor Low for making the lab run smoothly. Most importantly I need to thank my friends and family for their encouragement and emotional support because I could have never done it without them.

## CHAPTER 1

### INTRODUCTION

#### 1.1 Thesis Overview

This thesis will discuss a project designed to determine the stability constant of the uranyl nitrate tributylphosphate (TBP) complex through a series of solvent extraction experiments as part of a larger task to understand the fundamental chemistry involved in the reprocessing of spent nuclear fuel. The goals of the larger task include understanding nitrate ion effects on the extracted species of Pu(IV) and determining the stability constant for the formation of plutonium nitrate – TBP complexes. The goals of the project presented in this document are to study the speciation in the U(VI) – HNO<sub>3</sub> – TBP system and to determine the stability constant of the UO<sub>2</sub>(NO<sub>3</sub>)<sub>2</sub>•2TBP complex. The uranium system will be studied first as a prelude for future work with plutonium.

Chapter 1 will provide necessary background information on solvent extraction of uranyl nitrate into TBP. This chapter discusses reasons for and application of separations technology. The background includes previous work on TBP extraction of uranium(VI), nitric acid, lithium nitrate, and sodium perchlorate at 25°C. Chapter 2 will present the details involved in the experimental methods employed in this work. An explanation of the development of the methods used to determine acid, nitrate and uranium concentration of the samples at equilibrium is given. The results of the extraction experiments will be discussed in Chapter 3, including speciation and the calculated value

for the stability constant. The extraction of  $\text{UO}_2(\text{NO}_3)_2$ ,  $\text{HNO}_3$ ,  $\text{LiNO}_3$ ,  $\text{NaClO}_4$ , and  $\text{HClO}_4$  into TBP at room temperature is investigated. This study is distinctive from the previous work because equilibrium concentrations of the various extraction components are measured, whereas previous studies only determined equilibrium concentrations of the metal. Another unique aspect of this work is that ionic strength is held constant in the aqueous phase of the extractions. Chapter 4 will provide a summary of conclusions and ideas for future work.

## 1.2 Separation Chemistry of Spent Nuclear Fuel

A major concern with nuclear power is the ultimate fate of the spent fuel. Reprocessing the spent fuel not only reduces the volume and radiotoxicity of the high level waste, but can be used to produce new fuel, for example, mixed oxide fuel (1, 2). These advantages make a case for reprocessing which is not employed commercially in the U.S., but is currently used in the U.K., France, Japan and Russia (2, 3). In order to reprocess, techniques must be established to selectively separate certain radionuclides from the dissolved spent fuel. The mass of spent nuclear fuel from reactors used in the United States is typically comprised of about 95% uranium (the starting material), 4% fission products, and 1% neutron capture products (transuranium actinides) (4). Separating the uranium helps reduce the volume, while removing the transuranic elements substantially decreases the radiotoxicity. The extent of the benefits of reprocessing is determined by the efficiency of the separation process.

Many actinide separation methods have been investigated for radioanalytical purposes in laboratories. Not all of these radioanalytical methods can be applied to

reprocessing of spent nuclear fuel. This is due to conditions relevant to reprocessing, including tolerance to radiolysis, chemical hydrolysis, engineering considerations, and formation of degradation products that could impede the process conditions. In order to achieve the large-scale separations necessary for reprocessing, the method chosen must meet some basic criteria: reversibility, adaptability to remote operations, rapid kinetics, and an ability to operate continuously (4). The separations techniques for reprocessing include pyroprocessing, precipitation, ion exchange, and solvent extraction. Solvent extraction has several advantages for use in the large scale reprocessing of spent nuclear fuel, including the ability for continuous operation, high throughput, solvent recycling, and remote handling, all of which are important to reprocessing (4, 5). Solvent extraction is the only method of concern to this work, and will be discussed in detail.

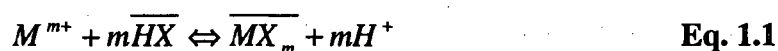
#### 1.2.1 Solvent Extraction

Solvent extraction is a common method which has been widely researched and used for actinide separations (4, 6, 7, 8, 9). For nuclear fuel considerations, this method employs the transport of select actinide ions between two phases and offers adjustable parameters, including concentrations, contact times, temperature, addition of chemicals to change component oxidation state or pH, and the solvent itself. These parameters can be altered in order to optimize and fine tune the process performance based on the chemistry of the particular system. For example, changing the concentration of nitric acid can control the separation of actinides by extraction with TBP (4) (see Section 1.2.2.).

Solvent extraction consists of the transfer of a solute from one phase to another, usually an aqueous phase to an organic phase. The phases must be immiscible. Typically, the organic phase contains the extractant ligand which coordinates to the metal

ion. The transportation of a neutral complex from the polar to the nonpolar solvent results in extraction from an aqueous phase to an organic phase. As the solvent extraction method allows for numerous permutations in system parameters, a myriad of such systems have been investigated for the separation of actinides (1, 4, 8, 9). Three major classifications for the type of extractants are acidic extractants, solvating extractants, and ion pairing extractants (4, 9).

Acidic extractants operate by the cation exchange of hydrogen ions for the selected cations (9). A general equation for the reaction of an acidic extractant with a metal follows:



where  $M^{m+}$  is the metal ion of interest,  $HX$  is the acidic extractant molecule, and the bar over the top denotes organic phase species. Here  $m$  provides the number of protons exchanged between phases and the stoichiometry of the extracted molecule, and is based on the charge of the metal cation. For these systems, pH is an important consideration since it can drive the reaction equilibrium. One example of an acidic organophosphorus-based extractant molecules that have been studied for the purpose of actinide and lanthanide separations (4). Currently, HDEHP (bis(2-ethylhexyl)phosphoric acid) (Figure 1.1), and is one of many acidic organophosphorus-based extractant molecules that have been studied for the purpose of actinide and lanthanide separations (4). Currently, HDEHP is the extractant in the TALSPEAK (Trivalent Actinide Lanthanide Separation by Phosphorous reagent Extraction from Aqueous Komplexes) process. With the addition of an aqueous complexant, DTPA (diethylene triamine pentaacetic acid), and the use of a lactate buffer (pH =3), this process can achieve actinide lanthanide separation factors of over 100 (Eq. 1.5) (10, 11).

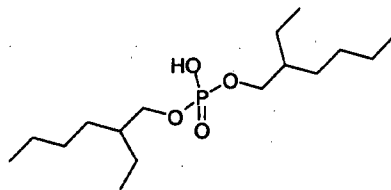


**Figure 1.1** HDEHP molecule

Solvating extractant systems are the most prevalent technology for actinide purification. Of these systems, PUREX, which exploits tributylphosphate (TBP), is the most dominant (4) (see section 1.3). Extraction with TBP is discussed in detail throughout the rest of this work, starting in section 1.2.2.

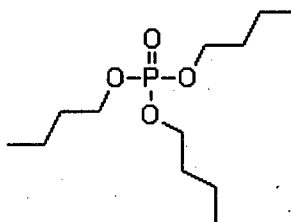
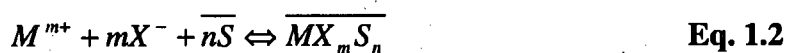


**Figure 1.2** TBP molecule

In general, a solvating extractant operates by carrying a neutral salt into the organic phase. An equation for this type of reaction follows:



where  $M^{m+}$  is the metal ion of interest,  $X^{-}$  is the complexing anion,  $S$  is the solvating extractant molecule, and the bar denotes organic phase species. First the stoichiometric amount of anions must be present to form the neutral complex which is then coordinated with the solvate at the interface and brought into the organic phase. Another example of a solvating extractant used in nuclear reprocessing is CMPO (octyl(phenyl)-N,N-

diisobutylcarbamoylmethylphosphine oxide) (Figure 1.3). Both of these solvating extractants, as well as many others, coordinate with the metal through the phosphoryl oxygen. The CMPO extractant is used for the separation of trivalent actinides and lanthanides from the fission products in the spent nuclear fuel in the TRUEX (Transuranic Extraction) process. Studies are being performed in order to optimize this process since CMPO is a promising extractant as it can simultaneously extract tri, tetra, and hexavalent actinides, but it also extracts lanthanides very efficiently leading to low separation factors (4, 12, 13)

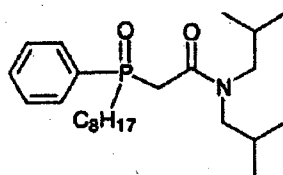
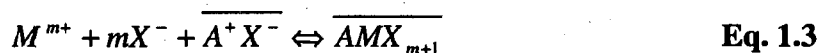


Figure 1.3 CMPO molecule

A third type of extractant for solvent extraction systems is an ion pairing extractant. This class of extractants is made of bulky ionic molecules, most commonly alkylamine salts. These cations can be either quaternary amines or tertiary amines which have been protonated (4). A general reaction for this type of extraction is as follows:



where  $M^{m+}$  is the metal ion of interest,  $X^{-}$  is the complexing anion,  $A^{+}$  is the ion pairing extractant cation, and the bar again denotes organic phase species. The mechanism of this extraction is similar to that of anion exchange resins, in which the associated anion in the organic phase readily exchanges for negatively charged metal coordination complexes

formed in the aqueous phase (9). Due to their polar properties, ion pairing extractants tend to form reverse micelles in most organic solutions (4). One example of this type of extractant, which has been studied for use in actinide separation, is tri-iso-octyl amine (TIOA) (Figure 1.4) (14, 15). This molecule is a tertiary amine, which must be protonated before extraction. Commonly the complexing anion is chloride, forming the extracting organic complex  $R_3NH^+Cl^-$ , where R is the iso-octyl group (15, 16). Separation factors between uranium and fission products are greater than 100 during extraction with TIOA (14).

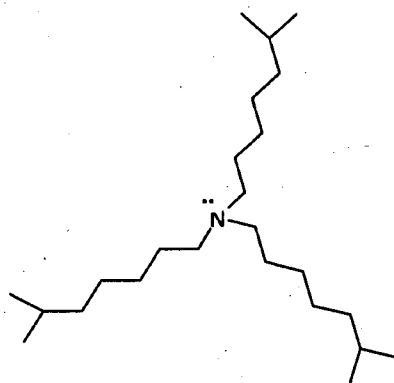


**Figure 1.4** TIOA molecule

Some important concepts when discussing solvent extraction are distribution ratios and separation factors. The distribution ratio is simply the concentration of metal brought into the organic phase divided by the concentration left in the aqueous phase (Eq. 1.4). The distribution ratio provides a quantitative value for the efficiency of an extraction. A separation factor assesses the ability to separate two solutes, and is calculated as the ratio of distribution ratios for two different metals (M and A) in a specific extraction system (Eq. 1.5). This work focuses on another important concept, the stability constant. The

stability constant describes the speciation, and is given by the equilibrium expression (Eq. 1.6) (53). The stability constant in Eq. 1.6 represents the general equation for extraction by the solvating mechanism shown in Eq 1.2. Stability constant expressions can be used to experimentally demonstrate stoichiometry of the reaction (see Section 1.2.2). As discussed in Section 1.2.2.2, the stability constant can also provide thermodynamic information.

$$K_d = \frac{\text{concentration of solute in organic phase}}{\text{concentration of solute in aqueous phase}} = \frac{[MX_mSn]}{[M^{m+}]} \quad \text{Eq. 1.4}$$

$$SF = \frac{K_{d(M)}}{K_{d(A)}} \quad \text{Eq. 1.5}$$

$$\beta = \frac{[MX_mSn]}{[M^{m+}][X^-]^m[S^-]^n} = \frac{K_d}{[X^-]^m[S^-]^n} \quad \text{Eq. 1.6}$$

### 1.2.2 Extraction studies of actinides in TBP

Due to past interest in reprocessing, many studies on TBP extraction systems have been performed (9, 17, 21, 24, 25, 26). Most of the literature reports  $K_d$  as a function of different initial conditions, such as nitric acid concentration, actinide concentration, TBP concentration, and temperature. This section briefly introduces previous work on actinide extraction by TBP, but will focus on U(VI). A discussion of uranium distribution ratios follows, with an explanation of how they vary with initial acid and nitrate ion concentration. Next, there is a review of some nitrate and perchlorate species that may be extract into the organic phase, as it pertains to this work. Finally, there is a discussion of

previous attempts to determine the stability constant of the TBP extraction of uranium as well as other actinides.

In investigations into TBP extraction of other components in spent nuclear fuel such as the lanthanides and technetium, it was found that uranium is far more extractable than the other metal nitrates (Table 1.1) (25). The data shown in Table 1.1 are from extractions performed with 50% TBP in kerosene as the organic phase and an aqueous phase of 1 M HNO<sub>3</sub> containing trace concentrations of all the metal ions. It is important to note that when the acid concentration was increased to 5 M HNO<sub>3</sub>, the distribution ratios of Pu and Np equaled those of U at a value of about 60 (Figure 1.5) (25). This is an example, as mentioned in the previous section, of how varying the acid concentration can dramatically change the efficiency of a separation.

**Table 1.1** Distribution ratios for spent fuel components in 50% TBP from 1 M HNO<sub>3</sub> (25)

Component	K <sub>d</sub>
Uranium	20
Plutonium, Neptunium	1
Remaining Actinides	< 0.1
Lanthanides	< 0.1
Technetium	4
Remaining Fission Products	< 1

Since only the tetra and hexavalent oxidation states of actinides are known to be extracted by TBP, the dependence of distribution ratios on oxidation state has also been studied. Table 1.2 summarizes the findings of two sources for extractions of trace metal concentrations in 5 M HNO<sub>3</sub> into 19% (v.) TBP in kerosene (21, 24). For the tetravalent actinides, extraction into TBP increases with increasing atomic number, following the

same trend as the lanthanides. For the hexavalent actinides the extraction decreases with atomic number, the opposite trend. The extraction of Pu(III) measured under the same conditions as above has a  $K_d$  of  $10^{-2}$ , which is considered inextractable (24).

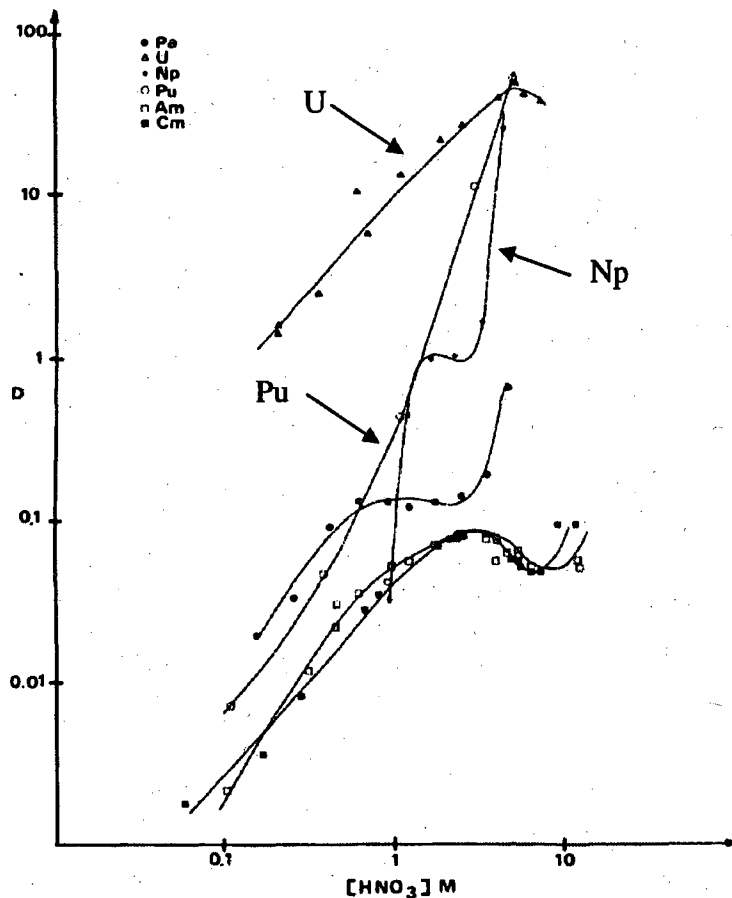


**Figure 1.5** Distribution of actinides in 50% TBP /kerosene (25)

The actinide nitrates are extracted into TBP as neutral disolvate salts, where the coordinating molecules are nitrate and TBP. The metal cation must be neutralized and a complex formed with two solvate molecules before it transfers to the organic phase. In the examined systems the extracted species are  $An(NO_3)_4 \cdot 2TBP$  for tetravalent actinides and  $AnO_2(NO_3)_2 \cdot 2TBP$  for hexavalent actinides (4, 17, 21, 22, 24).

**Table 1.2**  $K_d$  values of actinides in 19% TBP from 5 M  $\text{HNO}_3$  (21, 24)

Actinide	Oxidation State	
	IV	VI
Th	2	
U		30
Np	4	10
Pu	18	3

The speciation in the organic phase has been demonstrated by plotting the measured distribution ratio of the actinide against the varied concentrations of either the nitrate or TBP; the slope then gives the stoichiometry of the extracted species (18, 22, 24, 33). This process for evaluating stoichiometry is based on Eq. 1.8 which is manipulated from Eq 1.6 by taking the logarithm of both sides as shown in Eq. 1.7, and then rearranging. A linear relationship is generated based on  $y = mx + b$ , where  $y$  is  $\log K_d$ ,  $m$  is the stoichiometric coefficient,  $x$  is either  $[\text{NO}_3^-]$  or  $[\text{TBP}]$  as a variable, and  $b$  is a constant since  $\beta$  and either  $[\text{NO}_3^-]$  or  $[\text{TBP}]$  remain unchanged. One example is provided below (Figure 1.6) and displays data from the extraction of trace amounts of Pu(IV) with varied TBP in kerosene and  $\text{HNO}_3$  concentrations. The slope is two, demonstrating the formation of a complex with two TBP molecules. Some acid adducts of the known species, such as  $\text{HPu}(\text{NO}_3)_5 \cdot 2\text{TBP}$ , have been reported to be extracted in TBP (19, 20). No such acid adducts of the  $\text{UO}_2(\text{NO}_3)_2 \cdot 2\text{TBP}$  species have been discussed in the literature under normal extraction conditions and will not be considered in this work (4).

$$\log \beta = \log \left( \frac{K_d}{[\text{NO}_3^-]^m [\text{TBP}]^n} \right) \quad \text{Eq. 1.7}$$

$$\log K_d = \log \beta + m \log [\text{NO}_3^-] + n \log [\text{TBP}]$$

Eq. 1.8

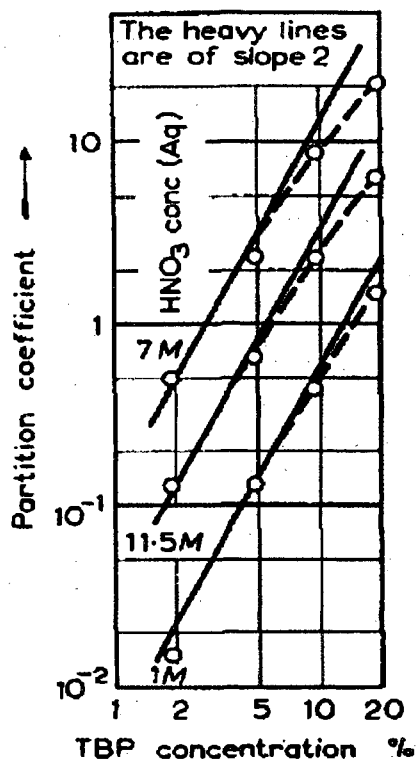


**Figure 1.6** Plot of Pu(IV) distribution ratio against vol. % TBP in kerosene to establish stoichiometry of extraction (24)

#### 1.2.2.1 The U(VI)- HNO<sub>3</sub>-TBP Extraction System

The distribution ratio of uranium depends on several factors, mainly the initial concentrations of nitrate ions and of TBP. It is known that increasing TBP concentration increases the extraction of uranium due to the excess amounts of TBP available for complexing (21, 22). In a reprocessing plant, pure TBP is undesirable due to its physical properties. When diluted, the density and viscosity of the TBP solution become more favorable by shifting towards the properties of the diluent (3). As suggested by the

PUREX and UREX processes (See Section 1.3 and 1.4), the optimum TBP concentration for uranium extraction on a large scale is around 30% (v.) in a hydrocarbon diluent (38).

The distribution ratio of U(VI) depends greatly on nitrate concentration. The nitrate ion concentration is usually varied as nitric acid. Many reports have shown that  $K_d$  for U increases with nitric acid concentration to a maximum around 5-6 M  $\text{HNO}_3$  and then decreases due to the competition of  $\text{HNO}_3$  complexing with TBP (21, 22, 23, 24, 25). Figure 1.7 shows this general trend at two different TBP concentrations. This trend is true for all uranium concentrations up to 1 M, and it is interesting to note that the  $K_d$  values do depend on U concentration at higher values, but it has been shown that for concentrations on the order of millimolar and less there is no change in the distribution ratios (21).

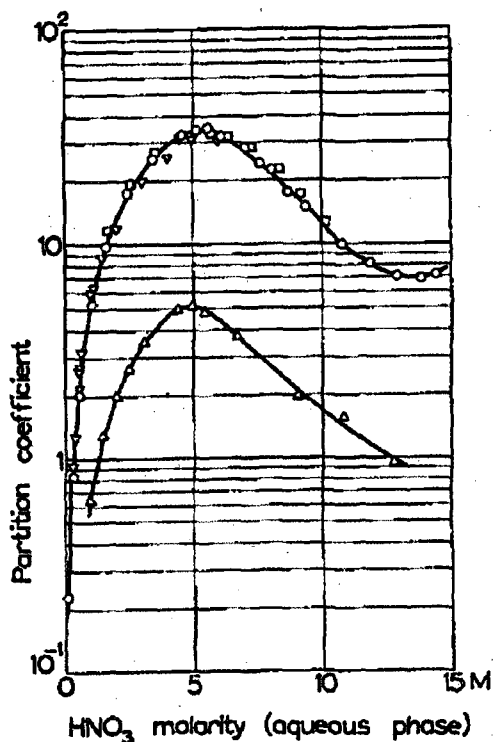


**Figure 1.7** U(VI) distribution ratio as a function of nitric acid concentration, the lower curve is in 4.8% TBP/kerosene and the upper is 19% TBP/kerosene, and the uranium concentration was 4mM. (21)

A commonality in solvent extraction systems is the salting out effect which describes the increase in uranium extraction when additional nitrate ions are present in the initial aqueous phase at a given acid concentration (4, 23, 24). The excess nitrate ions can drive the complexation between uranyl and the nitrates, which in turn promotes extraction. This effect is based on the reaction equilibrium for the system (Eq 1.9). Also at a given nitrate concentration the distribution ratio of U tends to decrease with increasing acid concentration due to competition of acid extraction into TBP (24). Figure 1.8 exhibits both of these trends, and provides data taken at varied nitric acid and total nitrate concentrations. The TBP concentration is 19% in kerosene, and the metal is at a concentration of  $4 \times 10^{-4}$  M.



Eq 1.9

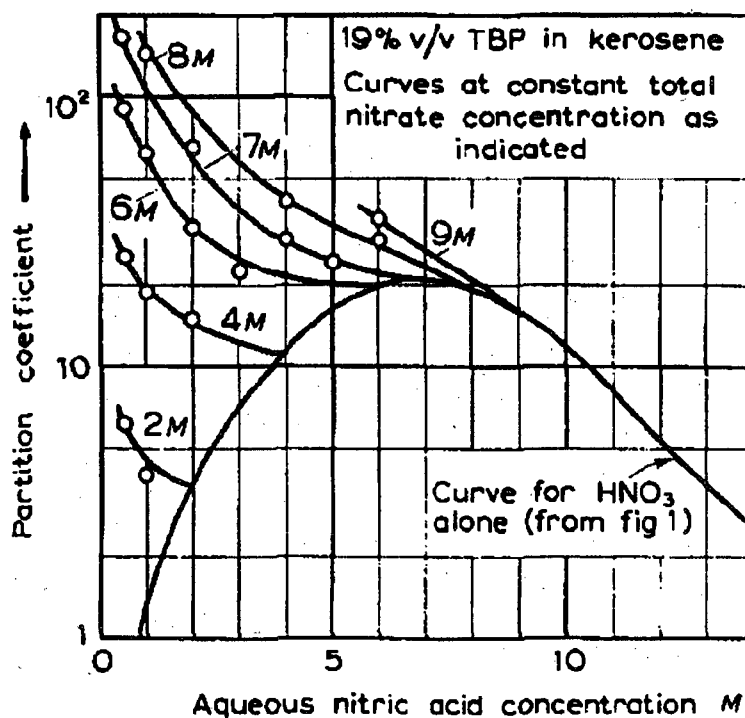


Figure 1.8 Distribution of U(VI) from solutions of varying nitric acid and total nitrate concentration (24)

Though it is known that additional nitrate ions increase distribution, different salts can have varied results when it comes to the amount of enhancement. The cation associated with the nitrate impacts the effectiveness of the salting-out agent. The distribution ratio increases as the ionic radius of the metal cation of the salting agent decreases (4). For example the effectiveness of the salting-out agent decreases as follows:  $\text{Al}(\text{NO}_3)_3 > \text{LiNO}_3 > \text{NaNO}_3 > \text{NH}_4\text{NO}_3$  (4, 23, 24). The smaller cation essentially provides more free nitrate in solution since the dissociation of the ions is greater (9).

In order to fully understand the extraction, it is necessary to know if other species can form in the organic phase. In the U(VI) –  $\text{HNO}_3$  – TBP system, an organic species that must be considered is  $\text{HNO}_3 \cdot \text{TBP}$  since it is known to extract (9, 17, 20, 25, 26, 29). The distribution ratio of nitric acid has a maximum value at an aqueous nitric acid concentration of 2 M; the  $K_d$  is as high as 0.8 in 100% TBP, 0.4 in 50% TBP/kerosene, and 0.25 in 30% TBP/dodecane (25, 26, 69). Typically distribution ratios above 0.1 will lead to competitive extraction into TBP (25). The  $\text{HNO}_3 \cdot \text{TBP}$  species will be considered in the next section when the stability constant is discussed.

The addition of  $\text{LiNO}_3$  is used in this work as a means of probing the speciation during extraction. It should be examined as a species in the organic phase since it is a neutral salt. It has been reported that solid  $\text{LiNO}_3$  is soluble in 100% TBP after 5 days of mixing (17). This would imply that  $\text{LiNO}_3$  could possibly be extracted as well as uranyl nitrate and nitric acid, but this solubility does not directly correlate to extractability. The nitrates mentioned above which are used as salting-out agents, including  $\text{LiNO}_3$ , are considered inextractable based on previous reports in the literature, and they have not

been reported to extract into TBP in the presence of U(VI) (27, 28). There are no reported values for the distribution ratio of lithium or sodium nitrate in TBP, but the  $K_d$  of cesium is reported to be less than 0.001 in 50% TBP/kerosene (25). As mentioned before, species with distribution ratios less than 0.1 are negligibly extracted. These studies indicate that  $\text{LiNO}_3$  will not significantly extract into TBP and can be eliminated as a possible organic species.

The extraction of perchlorate species is discussed since  $\text{NaClO}_4$  is used as an ionic strength adjuster in this work. The extraction of  $\text{UO}_2(\text{ClO}_4)_2$ ,  $\text{HClO}_4$ , and  $\text{NaClO}_4$  into TBP have all been reported (9, 22, 26, 28, 29). The distribution ratio of U(VI) into 100% TBP from a solution of 1 M  $\text{HClO}_4$  is equal to 1, as compared to a value of 20 for the nitrate system at the same conditions (22). The salting-out effect causes the  $K_d$  of U(VI) to increase to over 100 when the aqueous phase contains 3 M  $\text{NaClO}_4$  and the organic is 100% TBP. The  $K_d$  of this system decreases dramatically to a value of about  $10^{-2}$  when the TBP is diluted to 20% (22). This decrease in  $K_d$  with TBP dilution shows the uranium extraction from perchlorate medium has a much stronger dependence on the organic ligand concentration than does the nitrate system. This is explained by the extraction of the reported species,  $\text{UO}_2(\text{ClO}_4)_2 \cdot 4\text{TBP}$ , into the organic phase, since four TBP molecules are needed for uranyl extraction from perchlorate, while only two are needed to form the nitrate complex,  $\text{UO}_2(\text{NO}_3)_2 \cdot 2\text{TBP}$  (22). Since  $K_d$  is less than 0.1 in diluted TBP, the uranyl perchlorate species is considered inextractable in the current system.

The distribution ratio of  $\text{HClO}_4$  extracted into 100% TBP is very close to that of  $\text{HNO}_3$ , but when the TBP is diluted, the extraction of  $\text{HNO}_3$  is much more favored (26, 29). The  $\text{NaClO}_4$  salt has been shown to be soluble in TBP (9). When  $\text{NaClO}_4$  is extracted into 30% TBP in dodecane, the distribution ratio has a maximum value of only  $10^{-2}$  (28). As mentioned before species with  $K_d$  values less than 0.1 are considered inextractable (24, 25). The extraction of  $\text{NaClO}_4$  into TBP thus has a negligible effect on uranyl and nitrate speciation in the organic phase.

#### 1.2.2.2 Review of reported stability constants for actinide-nitrate-TBP

There have been a few investigations of the stability constants of actinide nitrate TBP complexes. Some reported values for the tetravalent actinides are:  $\log \beta = 1.65$  and  $2.13$  for Th(IV) and Np(IV) respectively (19, 30). Based on trends in stability constants for the actinides, it would be assumed that the stability constant for U(VI) would be lower than those values reported for Th(IV) and Np(IV) since the stability constants of actinides with any complexant normally increase in the order:  $\text{AnO}_2^+ < \text{An}^{3+} < \text{AnO}_2^{2+} < \text{An}^{4+}$  (31). There have been studies on the stability constant of  $\text{UO}_2(\text{NO}_3)_2 \cdot 2\text{TBP}$ , but the stability constants reported vary by more than an order of magnitude. The average reported value of  $\log \beta$  is  $2.12 \pm 0.44$ . The value for the uranyl species is high when compared to the tetravalent actinides, but within an expected range when considering the error. Figure 1.9 compares the stability constant values to experimental distribution data from literature (69). The reported stability constants were used to predict distribution ratios for different conditions based on equations 1.6 and 1.8. The  $K_d$ s calculated from those  $\beta$ s are higher than the experimentally determined values, but the lowest reported stability constant,  $\log \beta = 1.65$ , gives a result that approaches the measured values. The following table (Table

1.3) is a summary of the findings on reported stability constants of  $\text{UO}_2(\text{NO}_3)_2 \cdot 2\text{TBP}$  (19, 32, 33, 34).

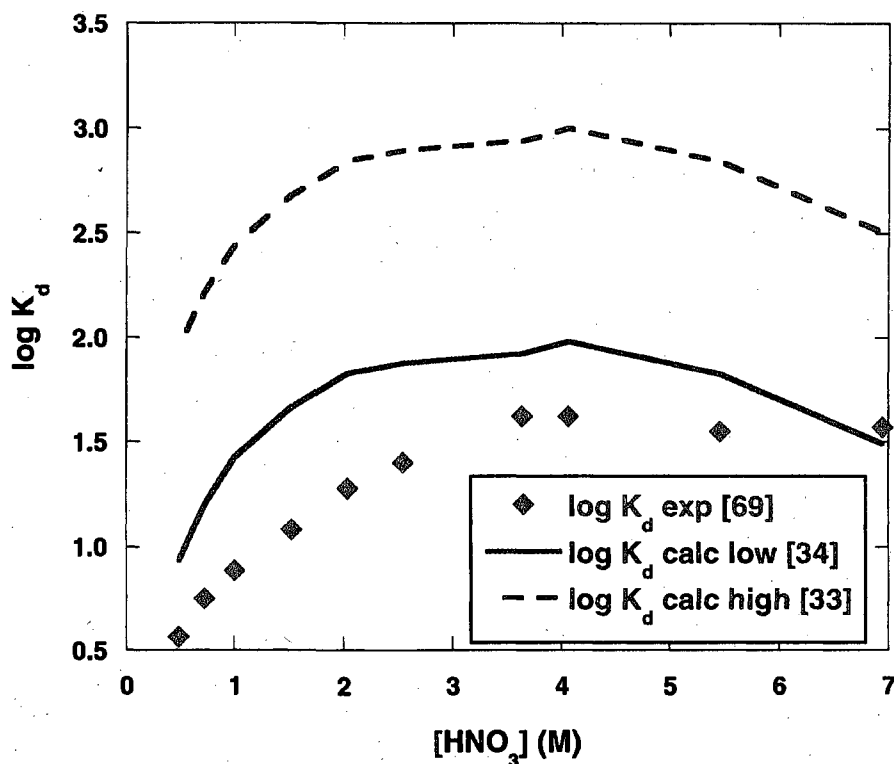


**Figure 1.9** Comparison of distribution ratios determined from the reported stability constant values of 1.65 and 2.67 with experimental data (33, 34, 69)

In order to understand possible reasons for the discrepancy between measured and calculated distribution coefficients, it is necessary to know how the stability constants were obtained. The method of thermodynamic fit consists of measuring  $K_d$  values at different temperatures then using Equation 1.6 to calculate the  $\beta$  values. Then the natural log of  $\beta$  is plotted against  $1/T$  to obtain a line, the slope of which is used to determine thermodynamic values for the Gibbs free energy, enthalpy, and entropy based on the equations:  $\Delta G = -RT \ln \beta$ , and  $\Delta G = \Delta H - T \Delta S$ . As stated in Table 1.3, this method only

uses equilibrium concentrations instead of activities, and does not measure equilibrium concentrations of nitrate or TBP which are necessary for Eq. 1.6.

**Table 1.3** Table of  $\beta$  values found in the literature for  $\text{UO}_2(\text{NO}_3)_2 \cdot 2\text{TBP}$

Reference	19	32	33	33	34
Log $\beta$	1.73*	2.11±0.18	2.46*	2.67*	1.65±0.21
[HNO <sub>3</sub> ] M	0.25	0.1 – 4	0.5	1	2
[U(VI)] M	0.0001 - 0.00015	0.1 – 1.2	0.126	0.126	0.03 – 0.65
[TBP] M	0.25	1.1	0.1 – 0.3	0.1 – 0.3	0.1 – 0.5
Temp.	25°C	**	25°C	25°C	20°C
Diluent	dodecane	AMSCO	kerosene	kerosene	AMSCO
K <sub>d</sub> used	Measured	Literature	Measured	Measured	Measured
Activity Considered	No	Yes	No	No	No
Method	Thermo-dynamic fit	Empirical fit	Graphically	Graphically	Graphically

\*Deviations were not reported.

\*\*Temperature not reported

The next method listed in Table 1.3, empirical fit, uses reported K<sub>d</sub> values and activity coefficients. At first this appears to be a reliable method, but the activity coefficients used above were those reported at standard state (infinite dilution), whereas, as shown in Table 1.3, concentrations up to 4 M were used for the log  $\beta$  calculations. The last method listed in Table 1.3 is graphical, determines log  $\beta$  by plotting measured log K<sub>d</sub> values against log TBP concentration while holding the nitrate concentration constant. This method is based on Eq. 1.8, but the intercept, not the slope, is used to calculate a value for log  $\beta$ , since [NO<sub>3</sub><sup>-</sup>] is known. This method was used to calculate three of the reported stability constants, which led to a variation in values of log  $\beta$  from

1.65 to 2.67. None of the methods used in the previous studies evaluated the equilibrium concentrations of  $\text{NO}_3^-$  or TBP as part of determining the complexation constants.

Another reason for the variation is that the stability constant is known to change with ionic strength. In order to obtain the stability constant at zero ionic strength,  $\beta_0$ , the stability constant as a function of I must be determined. As a first approximation, the Specific Ion Interaction Theory Model (SIT) may be used through the relation:

$$\log \beta_i = \log \beta_0 + \Delta Z^2 \cdot D - \Delta \epsilon I \quad \text{Eq. 1.10}$$

$$D = \frac{0.5091\sqrt{I}}{1+1.5\sqrt{I}} \quad \text{Eq 1.11}$$

where Z is ionic charge,  $\epsilon$  is the specific ion interaction coefficient,  $\beta_i$ , and I is ionic strength in molality (35). This theory accounts for both long range electrostatic ion interactions and for short range non-electrostatic interactions. The long range interactions are accounted for by using the extended Debye-Hückel equation which is incorporated in the second term of the SIT equation above and approximates the activity coefficient. The short range interactions need to be accounted for by the summation of the ion interaction coefficients of all the participating ionic species (36).

One recent study applied the SIT theory to a series of solvent extractions of Th(IV) nitrate with TBP in order to determine the equilibrium constant of  $\text{Th}(\text{NO}_3)_4$  extraction with TBP (28). This work considered the extraction system in  $\text{NaNO}_3$  medium, where  $[\text{NaNO}_3]$  varied from 0.05 to 3 M,  $[\text{HNO}_3]$  was 0.02 M, and  $[\text{Th}^{4+}]$  was 0.002 M. Only low concentrations of thorium and acid were examined in order to ignore the effects of changing free TBP concentration. The stability constants determined are conditional equilibrium constants for a given TBP concentration. The same set of experiments was

repeated for perchlorate and chloride systems. The equilibrium constants obtained were used to calculate the necessary specific ion interaction coefficients and were compared to the literature (37). Two out of the three coefficients calculated were in excellent agreement with values in earlier literature. The value for the coefficient that did not agree, for the  $\text{Th}^{4+}$  -  $\text{NO}_3^-$  interactions, was shown to have a better linear fit with the coefficients of other metal nitrates, as reported in the literature, than the previously determined value. Therefore this new specific ion interaction coefficient should be added to the NEA-TDB (Nuclear Energy Agency – Thermodynamic Database). Overall, this study demonstrates that using a solvent extraction system along with SIT corrections to obtain stability constants is a viable method.

### 1.3 PUREX

Presently the most developed and widely used separation method used for reprocessing in the nuclear industry is the PUREX process. “PUREX” is an acronym for **Plutonium URanium Extraction, Plutonium Uranium Recovery by Extraction, or Plutonium Uranium Reduction Extraction** (4, 5, 8). The PUREX process was developed by the General Electric Company and was operated at a pilot plant at Oak Ridge National Laboratory in 1950. Two U.S. plants used PUREX for plutonium production: the Savannah River plant (put into operation in 1954) and the Hanford plant, which switched from the Redox process in 1956 (2, 38). A plant in West Valley, New York, in operation from 1966-1972 and owned by Nuclear Fuel Services, Inc., was the only plant in the U.S. to use PUREX to reprocess fuel from privately owned nuclear power plants (2).

The PUREX process is a solvation mechanism solvent extraction method (see Section 1.2.1). This process consists of an organic phase with TBP as the extractant molecule. Typically, the concentration of TBP is about 30% by volume in a paraffinic hydrocarbon diluent. The aqueous feed contains the dissolved fuel in about 3 M HNO<sub>3</sub>, with a uranium concentration on the order of 1 M (1). The exact conditions vary by plant, and a comparison of five flowsheets indicates variations in TBP concentration from 20-30%, [HNO<sub>3</sub>] from 1 to 4 M, and uranium feed concentration from 0.5 to 1.76 M (3).

As discussed in Section 1.2.2, the extraction is based on the formation of neutral organic phase complexes, with UO<sub>2</sub>(NO<sub>3</sub>)<sub>2</sub>•2TBP and Pu(NO<sub>3</sub>)<sub>4</sub>•2TBP being the most extractable species. It is important to note that only tetravalent and hexavalent metals are extracted with TBP, so this process depends heavily on maintaining the proper oxidation states of uranium, plutonium, and neptunium. Pu(IV), Pu(VI), and U(IV) are readily extracted into the organic phase with U(VI), while Pu(III) is not. Neptunium is maintained in the pentavalent state, so it does not extract with the hexavalent uranium and extractable plutonium. There are many steps involved in this process that can be placed in five main categories:

- (1) feed preparation
- (2) co-decontamination cycle
- (3) partition cycle
- (4) second uranium and plutonium extraction cycle
- (5) final purification of plutonium (2, 4, 5, 39).

Details of the PUREX process are described below (Figure 1.10) (4, 38, 40).

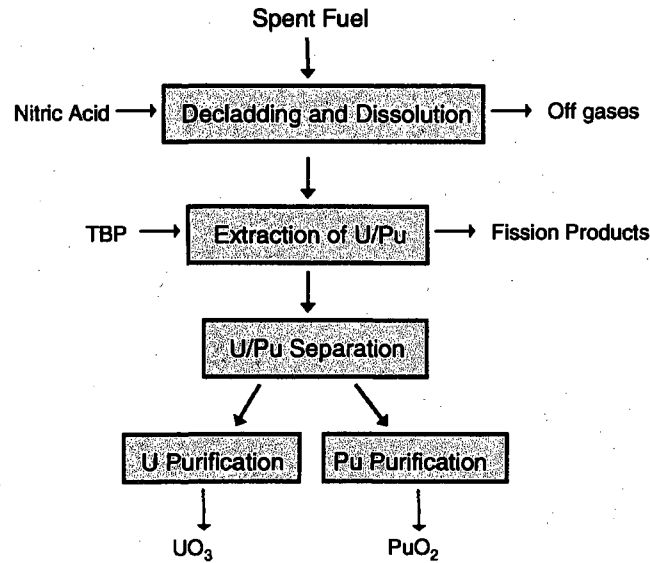


**Figure 1.10** PUREX process

Step (1) consists of the spent fuel being decladded and dissolved in nitric acid. During decladding, radioactive gases are released from the fuel and must be collected and treated. After dissolution, the nitric acid concentration is adjusted to 2-3 M, and the Pu is brought to its most extractable valence of +4, usually by the addition of  $\text{H}_2\text{O}_2$  or  $\text{HNO}_2$ . In step (2), U(VI) and Pu(IV) are co-extracted into the TBP phase, leaving over 99% of the fission products, trivalent actinides, and Np(V) in the aqueous raffinate. During step (3), Pu is then separated from U by reducing Pu to the organic-insoluble trivalent state, Pu(III). The reductant must be strong enough to reduce plutonium but not so strong as to reduce uranium. Commonly used reductants are ferrous sulfamate, U(IV), or hydroxylamine. This reduction results in Pu(III) being stripped into the aqueous phase while uranium remains in the TBP phase. Uranium is subsequently stripped with very dilute nitric acid solution. During step (4), a cleanup is performed by repeating step (3)

for both of the aqueous phases separately. This is done in order to increase the amount of recovered material. The final step consists of purification of the Pu and U streams, and is done using additional TBP solvent extraction steps, as well as ion exchange chromatography. Then plutonium and uranium nitrates are converted into the final products, commonly  $\text{PuO}_2$  and  $\text{UO}_3$ , by either evaporation or precipitation (5, 38, 41).

There are several benefits of PUREX over previously used processes, the most significant being the decreased volume of radioactive waste generated. This decrease is because no additional salting agent is used, and because the solvent is recycled to eliminate secondary by-products such as dibutyl phosphate (DBP) and monobutyl phosphate (MBP) (4, 38). In a well designed reprocessing plant, materials are recycled as much as possible, which further minimizes the volume of wastes and the cost of chemicals. Another advantage is that the TBP solvent is less volatile, less flammable, and more stable against attack by nitric acid than hexone or di-butyl carbitol used in the REDOX process (2, 42, 43). All of these advantages have the overall effect of lower operating costs for a PUREX plant than for a plant using older technologies (4, 44).

#### 1.4 UREX

Several different separation schemes have been investigated for advanced separation technology, but the best studied are in the suite of UREX + solvent extraction processes. These are not to be confused with the UREX process, which is the first step of any UREX + process. The UREX + processes are composed of a series of extraction processes designed to separate the U, Tc, Cs/Sr, and transuranic actinides from the lanthanides and remaining fission products. Currently there are four basic variations: UREX +1, +2, +3,

and +4; which is chosen depends on the desired degree of separation of the remaining actinides (45). Figure 1.12 is a diagram of the proposed UREX +3 reprocessing scheme, representative of UREX +. The first step removes the uranium, most of the liquid waste volume, and the Tc, which contributes to long term radioactivity of the spent fuel.

Since the separation of a pure plutonium stream is a proliferation concern, the PUREX process has evolved into the UREX (URanium EXtraction) process, which uses the same solvent of 30% TBP in a hydrocarbon diluent, typically kerosene or dodecane. In the UREX process, the interaction of acetohydroxamic acid (AHA) (Figure 1.11) with Pu is exploited to achieve separation of U and Tc from other radionuclides in spent fuel by maintaining Pu in the aqueous phase. The interaction of AHA with Pu(IV) decreases its extraction into the organic phase by either hydrophilic complex formation or reduction to inextractable Pu(III) (46). The aqueous phase contains AHA and 1 M HNO<sub>3</sub>. This concentration is lower than the PUREX process, and enhances the complexation of Pu and Np with AHA as well as increases the extraction of Tc as the pertechnetate ion TcO<sub>4</sub><sup>-</sup> (47). After the coextraction of U and Tc, the Tc is stripped with a concentrated nitric acid solution. The UREX process has been demonstrated at a laboratory scale at both Argonne National Laboratory and at the Savannah River Technology Center with uranium recovery of over 99.95% and technetium recovery of over 95%, while over 99.98% of plutonium and the other actinides remain in the aqueous phase (47, 48).

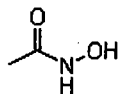


**Figure 1.11** AHA molecule

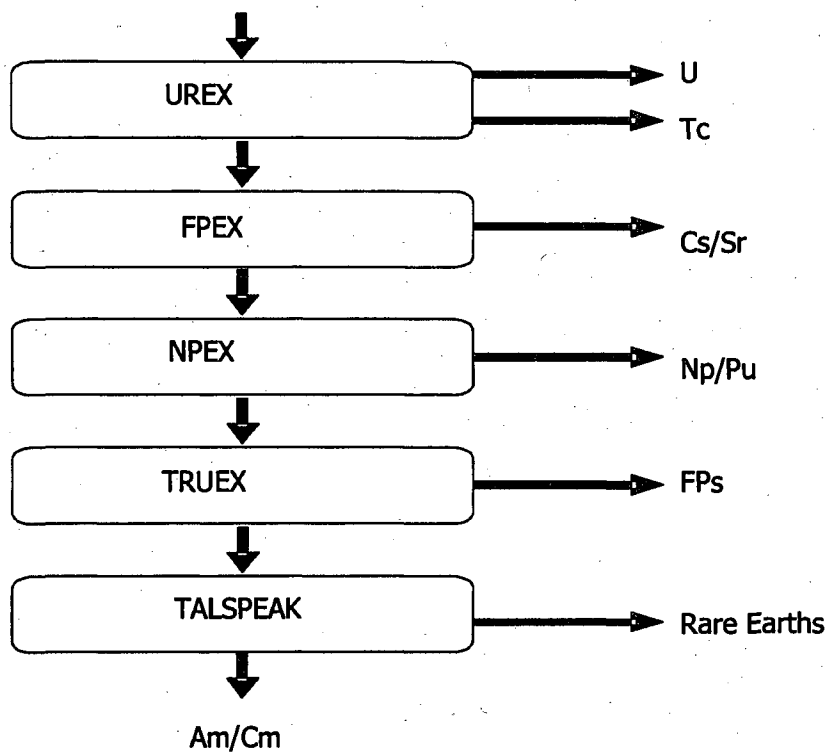


**Figure 1.12** Diagram of UREX +3 reprocessing scheme

During the next step cesium and strontium are removed via the FPEX (Fission Product Extraction) process. These radioactive isotopes generate most of thermal heat of spent fuel, which impacts the spacing of waste casks and therefore capacity in the repository (49). The third step of the process, NPEX (Neptunium Plutonium Extraction), extracts neptunium with plutonium in order to avoid the proliferation issues of a pure plutonium stream while maintaining the Pu for reuse as new fuel. The remaining actinides, americium and curium, are removed during the fourth and fifth steps (Section 1.2.1) in order to further decrease the radioactivity and heat of the waste. This example is just one of many variations of this basic scheme, and researchers are continuously optimizing this process for commercial use (50).

## 1.5 Process Modeling

A solvent extraction flow sheet is being developed for large scale, plant based separations. The Argonne Model for Universal Solvent Extraction (AMUSE) code aims to predict the chemical behavior of all the major components of the dissolved spent nuclear fuel during the UREX + process segments (51, 52). The AMUSE code calculates the component distribution ratios by using kinetic and thermodynamic data found in literature. The calculated distribution ratios, along with user input information such as equipment specifications, fuel composition, and temperature, are used to design multistage countercurrent flowsheets. These flowsheets are the basis of the process parameters, adjusted to ensure that the required recoveries of the products of each segment are achieved. The AMUSE code has been used for several different processes as part of the UREX + suite, including PUREX, UREX, TRUEX, CCD-PEG (extraction of Cs and Sr), and TALSPEAK (51, 52).

The code is made of two separate parts: SASSE (Spreadsheet Algorithm for Stagewise Solvent Extraction) and SASPE (Spreadsheet Algorithm for Speciation and Partitioning Equilibria) (51) (Figure 1.13). The SASPE portion calculates distribution ratios of the major components based on user inputs of initial compositions of each phase. This calculation requires accurate thermodynamic activity data for actinides, fission products and matrix components of spent nuclear fuel. The SASSE portion refines the calculated distribution ratios and uses them to determine stage compositions, which are then put back into SASPE. This iteration process repeats until convergence is

met (51). The output of the code is a flowsheet that gives compositions of both phases at each stage of the process.

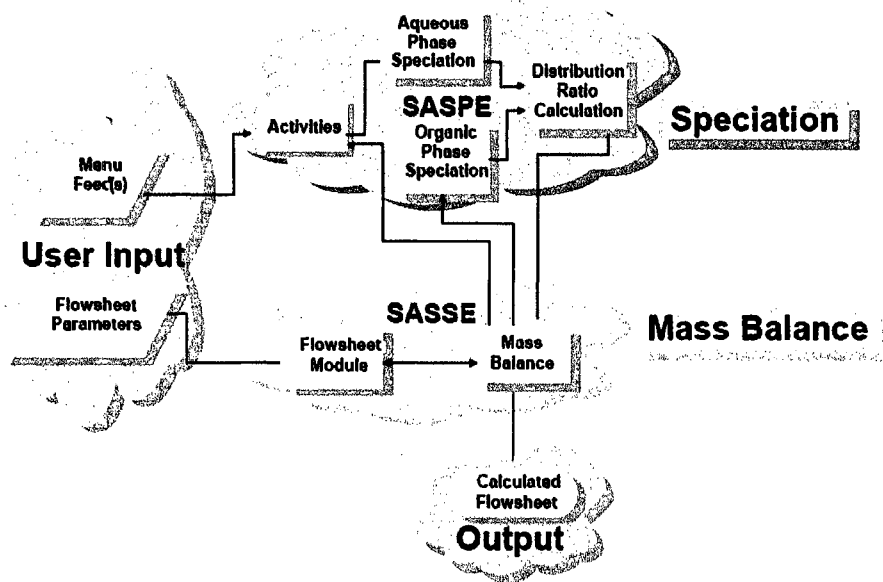


**Figure 1.13** Schematic of AMUSE code (51)

## 1.6 Project Rationale

As mentioned in Section 1.1, this thesis project is part of the larger task of understanding the fundamental chemistry involved in the UREX+ separation schemes. This research will be used to improve the AMUSE code for reprocessing modeling. The AMUSE code has been able to predict actinide extraction behaviors for most, but not all, reprocessing conditions. In particular, it has been stated that some aspects of the plutonium extraction system are not well understood. For example, Pu(IV) is theoretically extracted with four nitrates, but data indicate the extraction actually has a second order dependence (20). This implies that the dinitrate complex of Pu(IV) in the aqueous phase is preferred, and the different species may account for difficulties in

modeling Pu extraction under some nitrate conditions (20). This leads to questions about the speciation of Pu(IV) in both the aqueous and organic phases. Even with these uncertainties, the AMUSE code predicts the Pu(IV) extraction behavior fairly well under a variety of conditions, such as changing temperature,  $[\text{HNO}_3]$  and  $[\text{AHA}]$ , except when additional nitrate is added as a salting-out agent (20). Not only are the predicted  $K_d$  values different from the measured values, but the expected trends are nearly a mirror image of the experimental data (20). This suggests a flaw in the model, implying that other Pu(IV) extracted species besides  $\text{Pu}(\text{NO}_3)_4 \cdot 2\text{TBP}$  and  $\text{HPu}(\text{NO}_3)_5 \cdot 2\text{TBP}$  (19, 20, 21, 24) need to be considered.

This thesis project investigated the U(VI) –  $\text{HNO}_3$  – TBP extraction system with  $\text{LiNO}_3$  as a salting-out agent. Extractions were performed under a variety of aqueous phase conditions, described in detail in Chapter 2. The organic phase was 30% by volume TBP diluted in dodecane. The speciation was investigated by measuring equilibrium concentrations of  $[\text{H}^+]$ ,  $[\text{NO}_3^-]$ , and  $[\text{UO}_2^{2+}]$ , and then calculating the stability constant based on Equation 1.6. The aqueous phase of the extraction was held under constant ionic strength as adjusted by  $\text{NaClO}_4$ . The stability constant obtained was then used for predicting  $K_d$  values of literature data.

## CHAPTER 2

### EXPERIMENTAL METHODS

#### 2.1 Reagents

All reagents used in this work are listed in Table 2.2. Some solid reagents from Table 2.2 were used to make stock solutions by dissolving the appropriate mass of salt in purified water in a volumetric flask. Stock solutions using liquid reagents were prepared by volume percent using graduated cylinders and volumetric flasks. The stock solutions prepared are listed in Table 2.1.

**Table 2.1** List of stock solutions

Chemical	Formula	Concentration	Diluent
Nitric acid	$\text{HNO}_3$	0.1 M (1%)	water
Lithium nitrate	$\text{LiNO}_3$	12 M	water
Uranyl nitrate	$\text{UO}_2(\text{NO}_3)_2$	1 M	water
Sodium perchlorate	$\text{NaClO}_4$	8 M	water
Tributyl phosphate (TBP)	$(\text{C}_4\text{H}_9\text{O})_3\text{PO}$	1.1 M (30 %)	dodecane
Ammonium oxalate	$(\text{NH}_4)_2\text{C}_2\text{O}_4$	0.1 M	water

**Table 2.2** List of reagents

Chemical	Formula	Maker	Description	CAS #
Nitric acid	HNO <sub>3</sub>	J.T. Baker	69-70% ACS grade	7697-37-2
Lithium nitrate, granular	LiNO <sub>3</sub>	Mallinckrodt AR	99.9% pure	7790-69-4
Uranyl nitrate, hexahydrate	UO <sub>2</sub> (NO <sub>3</sub> ) <sub>2</sub> · 6H <sub>2</sub> O	Int Bio Analytical	99% pure	13520-83-7
Sodium perchlorate, anhydrous	NaClO <sub>4</sub>	EMD	ACS grade	7601-89-0
Tributyl phosphate (TBP)	(C <sub>4</sub> H <sub>9</sub> O) <sub>3</sub> PO	J.T. Baker	99%	126-73-8
n-Dodecane	C <sub>10</sub> H <sub>22</sub>	Alfa Aesar	99+%	112-40-3
Ammonium oxalate, monohydrate	(NH <sub>4</sub> ) <sub>2</sub> C <sub>2</sub> O <sub>4</sub> · H <sub>2</sub> O	EMD	99% ACS grade	6009-70-7
Sodium hydroxide, 0.1N volumetric solution	NaOH	J.T. Baker	Baker Analyzed Reagent	1310-73-2
Methanol	CH <sub>3</sub> OH	Fisher Scientific	99.9% ACS certified	67-56-1
Ultima Gold AB, liquid scintillation cocktail		Perkin Elmer	Suited for strong acids	9016-45-9

## 2.2 Extractions

Studies were performed under a range of conditions to investigate the extraction of uranium(VI) and nitric acid into TBP. Variations in concentrations of acid, nitrate, and uranium were examined as a function of ionic strength. The experiments can be categorized into three sets. One set of extractions was performed under a large range of conditions in order to test the validity of the extraction procedure and to understand the salting-out effect discussed in Section 1.2.2.1. The next set of extractions was performed

at constant acid concentration in order to examine the effects of total nitrate concentration. The final experiments were performed at constant ionic strength in order to calculate the stability constant. Details of these experiments are in the following sections, and Table 2.3 provides an overview of the concentration ranges examined.

**Table 2.3** Range of concentrations

<u>Experiment</u>	<u>[H<sup>+</sup>] (M)</u>	<u>[NO<sub>3</sub><sup>-</sup>] (M)</u>	<u>[U] (M)</u>	<u>I</u>
Varied acid	0 – 12	[H <sup>+</sup> ] – 12	0.05 – 0.1	varied
Constant acid	1	1 – 10	0.01 – 0.02	varied
Constant ionic strength	1 – 2	[H <sup>+</sup> ] – 1	0.01 – 0.02	4, 6

### 2.2.1 General Extraction Procedure

The samples were composed of an aqueous phase and an organic phase. The aqueous phase initially consisted of varying amounts of nitric acid, lithium nitrate, uranyl nitrate, and sodium perchlorate. The initial organic phase of each sample consisted of 30% tributyl phosphate in dodecane which were pre-equilibrated by extracting and separating the corresponding uranium-free nitric acid matrix prior to experiments. The aqueous components were mixed in vials to a final volume of 0.75 mL, and an equal volume of the organic phase was added by pipette. The phases were contacted by mixing for 2 minutes with a vortexor, which is sufficient time to reach equilibrium (33). Then the samples were centrifuged for 3 minutes to ensure complete separation of the two phases. The organic phase was removed and stored separately. The analyses of [U], [NO<sub>3</sub><sup>-</sup>], and [H<sup>+</sup>] were performed on both the organic and aqueous phases.

## 2.2.2 Aqueous Phase Variation

The aqueous phase was varied as shown in Table 2.3. The TBP concentration and extraction procedure were held constant during the experiments. The sample sets are organized as described in Section 2.2. The following tables provide the initial conditions of the aqueous phases of the extractions.

**Table 2.4** Initial aqueous phase conditions with 0.1 M  $\text{UO}_2(\text{NO}_3)_2$

Sample #	[ $\text{HNO}_3$ ] M	[ $\text{LiNO}_3$ ] M	[ $\text{NO}_3^-$ ] M
1	0	0	0.2
2	0	3.8	4
3	0	7.8	8
4	0	9.8	10
5	2	0	2.2
6	2	1.8	4
7	2	3.8	6
8	2	5.8	8
9	2	7.8	10
10	4	0	4.2
11	4	1.8	6
12	4	3.8	8
13	4	5.8	10
14	6	0	6.2
15	6	1.8	8
16	6	2.8	9
17	6	3.8	10
18	8	0	8.2
19	8	0.8	9
20	8	1.8	10
21	10	0	10.2
22	10	0.8	11
23	10	1.8	12
24	12	0	12.2

The first set of experiments was done to investigate the extractions under a wide variety of initial conditions described in Table 2.4 and Table 2.5. Each series consisted

of 24 extractions, where the concentration of nitric acid varied from 0 M to 12 M. The total nitrate concentration was changed by addition of  $\text{LiNO}_3$  and ranged from the acid concentration up to 12 M total nitrate. The uranium concentration was held at 0.1 M  $\text{UO}_2(\text{NO}_3)_2$  and 0.05 M  $\text{UO}_2(\text{NO}_3)_2$ .

**Table 2.5** Initial aqueous phase conditions with 0.05 M  $\text{UO}_2(\text{NO}_3)_2$

Sample #	[ $\text{HNO}_3$ ] M	[ $\text{LiNO}_3$ ] M	[ $\text{NO}_3^-$ ] M
1	0	0.1	0.2
2	0	3.9	4
3	0	7.9	8
4	0	9.9	10
5	2	0.1	2.2
6	2	1.9	4
7	2	3.9	6
8	2	5.9	8
9	2	7.9	10
10	4	0.1	4.2
11	4	1.9	6
12	4	3.9	8
13	4	5.9	10
14	6	0.1	6.2
15	6	1.9	8
16	6	2.9	9
17	6	3.9	10
18	8	0.1	8.2
19	8	0.9	9
20	8	1.9	10
21	10	0.1	10.2
22	10	0.9	11
23	10	1.9	12
24	12	0.1	12.2

Experiments were performed at a constant initial acid concentration in order to determine how nitrate concentrations affect extraction chemistry. The experimental conditions are listed in Table 2.6 and Table 2.7. Each set consisted of 10 extractions at 1

M HNO<sub>3</sub> varied LiNO<sub>3</sub> concentration from 0 to 10 M. The uranium concentrations were 0.01 M and 0.02 M UO<sub>2</sub>(NO<sub>3</sub>)<sub>2</sub>.

**Table 2.6** Initial aqueous phase conditions with 0.01 M UO<sub>2</sub>(NO<sub>3</sub>)<sub>2</sub> and 1 M HNO<sub>3</sub>

Sample #	[HNO <sub>3</sub> ] M	[LiNO <sub>3</sub> ] M	[NO <sub>3</sub> <sup>-</sup> ] M
1	1	0.18	1.2
2	1	1.18	2.2
3	1	2.18	3.2
4	1	3.18	4.2
5	1	4.18	5.2
6	1	5.18	6.2
7	1	6.18	7.2
8	1	7.18	8.2
9	1	8.18	9.2
10	1	9.18	10.2

**Table 2.7** Initial aqueous phase conditions with 0.02 M UO<sub>2</sub>(NO<sub>3</sub>)<sub>2</sub> and 1 M HNO<sub>3</sub>

Sample #	[HNO <sub>3</sub> ] M	[LiNO <sub>3</sub> ] M	[NO <sub>3</sub> <sup>-</sup> ] M
1	1	0.16	1.2
2	1	1.16	2.2
3	1	2.16	3.2
4	1	3.16	4.2
5	1	4.16	5.2
6	1	5.16	6.2
7	1	6.16	7.2
8	1	7.16	8.2
9	1	8.16	9.2
10	1	9.16	10.2

The final set of experiments was performed at constant ionic strength. One set of 18 extractions was performed at an ionic strength of 6 M, maintained by the addition of NaClO<sub>4</sub> (Table 2.8). The concentrations of nitric acid were 1 and 2 M, and the total nitrate concentration varied from 1.2 to 5.2 M by addition of LiNO<sub>3</sub>. The uranium

**Table 2.8** Initial aqueous phase conditions with I = 6 M

Sample #	[UO <sub>2</sub> (NO <sub>3</sub> ) <sub>2</sub> ] M	[HNO <sub>3</sub> ] M	[LiNO <sub>3</sub> ] M	[NaClO <sub>4</sub> ] M	[NO <sub>3</sub> <sup>-</sup> ] M
1	0.01	1	0.18	4.8	1.2
2	0.01	1	1.18	3.8	2.2
3	0.01	1	2.18	2.8	3.2
4	0.01	1	3.18	1.8	4.2
5	0.01	1	4.18	0.8	5.2
6	0.02	1	0.16	4.8	1.2
7	0.02	1	1.16	3.8	2.2
8	0.02	1	2.16	2.8	3.2
9	0.02	1	3.16	1.8	4.2
10	0.02	1	4.16	0.8	5.2
11	0.01	2	0.18	3.8	2.2
12	0.01	2	1.18	2.8	3.2
13	0.01	2	2.18	1.8	4.2
14	0.01	2	3.18	0.8	5.2
15	0.02	2	0.16	3.8	2.2
16	0.02	2	1.16	2.8	3.2
17	0.02	2	2.16	1.8	4.2
18	0.02	2	3.16	0.8	5.2

**Table 2.9** Initial aqueous phase conditions with I = 4 M

Sample #	[UO <sub>2</sub> (NO <sub>3</sub> ) <sub>2</sub> ] M	[HNO <sub>3</sub> ] M	[LiNO <sub>3</sub> ] M	[NaClO <sub>4</sub> ] M	[NO <sub>3</sub> <sup>-</sup> ] M
1	0.01	1	0.18	2.8	1.2
2	0.01	1	1.18	1.8	2.2
3	0.01	1	2.18	0.8	3.2
4	0.02	1	0.16	2.8	1.2
5	0.02	1	1.16	1.8	2.2
6	0.02	1	2.16	0.8	3.2
7	0.01	2	0.18	1.8	2.2
8	0.01	2	1.18	0.8	3.2
9	0.02	2	0.16	1.8	2.2
10	0.02	2	1.16	0.8	3.2

concentrations were 0.01 and 0.02 M  $\text{UO}_2(\text{NO}_3)_2$ . The last set (Table 2.9) includes 10 extractions of the same  $\text{HNO}_3$  and U concentrations at an ionic strength of 4 M, maintained by the addition of  $\text{NaClO}_4$ , with a total nitrate concentration of 1.2 to 3.2 M.

### 2.3 Determination of Analysis Methods

In order to measure the concentrations of acid, nitrate and uranium in each phase after extraction, accurate and reproducible methods had to first be developed. Some existing methods were examined to determine which available techniques would be best suited for this work. Titration was the only method used to determine acid concentration. In order to measure nitrate, two common methods were investigated: ion specific electrode potentiometry and ion chromatography. To measure uranium concentration, several different analytical and radiochemical were explored: UV-visible spectroscopy (UV-visible), inductively coupled plasma atomic emission spectroscopy (ICP-AES), and liquid scintillation counting (LSC).

#### 2.3.1 Acid Concentration Determination

Titration with a strong base was used to determine nitric acid concentration. Titration is based on the concept of an equivalence point, where the concentrations of acid and base are equal. The equivalence point occurs where the change in pH is greatest, as plotted against the volume of base added. The true equivalence point is in an ideal, infinitely dilute solution, and titrations actually measure the end point, the closest approximation. When titrating a strong acid with a strong base, the endpoint should occur at a pH of 7 (53). The acid concentration can easily be calculated based on the moles of base needed to reach the end point, when sample and titrant volume as well as titrant concentration are known precisely.

A Brinkmann Instruments Metrohm Titrino 799 using Tiamo software and equipped with an autosampler was employed for the titrations. The system included stirring and inert gas purging capabilities as well as caps for nonactive samples. The electrode was a Metrohm micro LL combination electrode with a fill solution of 3 M KCl. The titration procedure used 0.1 mL of each sample diluted into 20 mL 0.02 M  $(\text{NH}_4)_2\text{C}_2\text{O}_4$ .

Ammonium oxalate binds to and prevents the hydrolysis of the uranium(VI) (54). Each sample was stirred under argon gas before and during titration to eliminate interfering carbonic acid from the dissolution of atmospheric  $\text{CO}_2$ . The titrant used was a 0.1 N NaOH standard solution. The titrations were performed using a 0.01 mL step volume. An electrode was calibrated using three buffers before running and between sets of 20 samples. This method was optimized to achieve both accurate and precise endpoint measurements. The software calculated the endpoint value, which was used to determine the original acid concentration of each sample. The calculation was performed by the software by finding the inflection point, where the change in slope is at a maximum, of the titration curve.

The effect of purging with Ar gas was analyzed by titrating 0.1 mL of 1 M  $\text{HNO}_3$  standards with and without the gas bubbling (Table 2.10). In the presence of argon, a mean endpoint of  $1.02 \pm 0.01$  M was reached, vs.  $1.04 \pm 0.03$  M without Ar, indicating some carbonic acid effect. Therefore all experimental titrations were performed after Ar purging. The influence of ammonium oxalate on the titration was also investigated by titrating six 0.05 mL samples of 2 M nitric acid, three in 20 mL of water and three in 20 mL of 0.02 M ammonium oxalate. Both sets resulted in mean measured values of  $2.01 \pm$

0.03 M  $H^+$  (Table 2.11). Figure 2.1 shows that the presence of ammonium oxalate does not change the titration curve. In order to estimate the error involved in using this titration method to determine acid concentration, six identical samples were prepared and titrated, indicating a relative standard deviation of 2.1% (Table 2.12).

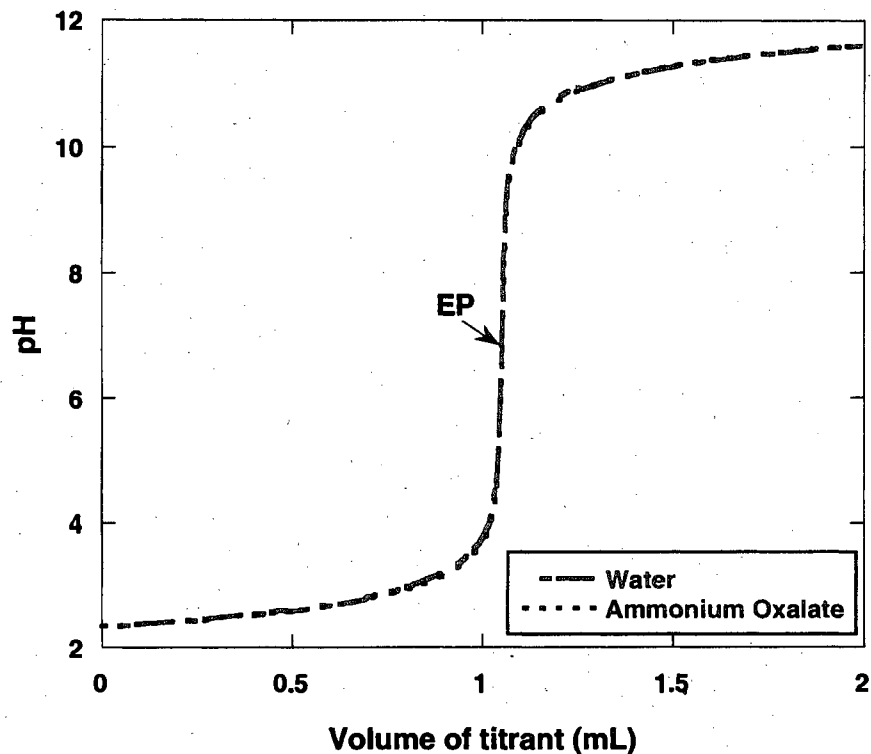


**Figure 2.1** Comparison of titrations performed in  $H_2O$  and in  $(NH_4)_2C_2O_4$

**Table 2.10** Effects of bubbling argon gas on  $[H^+]$  (M) measured during titration

Trial #	Ar bubbling	no Ar bubbling
1	1.02	1.07
2	1.03	1.03
3	1.01	1.01
average	1.02	1.04
standard deviation	0.01	0.03

**Table 2.11** Effects of ammonium oxalate on  $[H^+]$  (M) measured during titration

Trial #	H <sub>2</sub> O	(NH <sub>4</sub> ) <sub>2</sub> C <sub>2</sub> O <sub>4</sub>
1	2.00	2.04
2	2.03	2.00
3	1.98	1.99
average	2.01	2.01
standard deviation	0.03	0.03

**Table 2.12** Relative standard deviation in titration measurements

Trial #	$[H^+]$ (M)
1	1.01
2	1.03
3	1.00
4	1.03
5	1.01
6	1.06
average	1.02
standard deviation	0.02
% RSD	2.11

### 2.3.2 Nitrate Concentration Determination

Two different methods were investigated to measure the nitrate concentration in each phase: a nitrate ion specific electrode (ISE) and ion chromatography (IC). Both of these methods are commonly used to measure nitrate ion concentrations in food and water (55, 56, 57). Both ISEs and IC are fundamentally based on an ion exchange mechanism where the stationary phase consists of a counter ion coordinated with a mobile ion. The mobile ion is replaced by the desired ion, in this case  $NO_3^-$ .

An ISE is composed of a reference electrode surrounded by an aqueous salt solution housed in a small polyvinyl chloride (PVC) tube with an ion exchange membrane at the tip. There are four main classes of ISEs based on membrane materials: polymer

membrane electrodes, solid state electrodes, gas sensing electrodes and glass membrane electrodes (53). The ISEs selective for nitrate are made with polymer membrane electrodes, which consist of ion exchange materials incorporated into a polymer membrane. Most commonly, the ion exchange material is a quaternary ammonium compound and the polymer membrane is PVC (58). When nitrate ions interact with the membrane an electrode potential develops, which is measured against the internal reference electrode potential. These potentials can then be used to determine nitrate ion concentration by creating a calibration curve.

The ISE used in this work was a nitrate specific refillable combination Beckman electrode with a fill solution of 0.1 M  $(\text{NH}_4)_2\text{SO}_4$ . The calibration range was from  $10^{-4}$  M to 0.1 M lithium nitrate, so the samples were diluted to fit in this range. A solution of 0.04 M ammonium sulfate was used as the diluent for the standards and samples. This solution was suggested by the manufacturer to be used as an ionic strength adjuster. The measurements were taken in 100 mL of solution with constant stirring. The measurements were taken in 100 mL of solution with constant stirring. The electrode was allowed to reach equilibrium, indicated by stabilization of the voltammeter for a period of 1 minute. The standards were within the linear range of the electrode's response, and the equation of the calibration curve was used to calculate the concentrations of the unknown samples. The electrode was rinsed and soaked for at least 5 minutes in deionized water between samples.

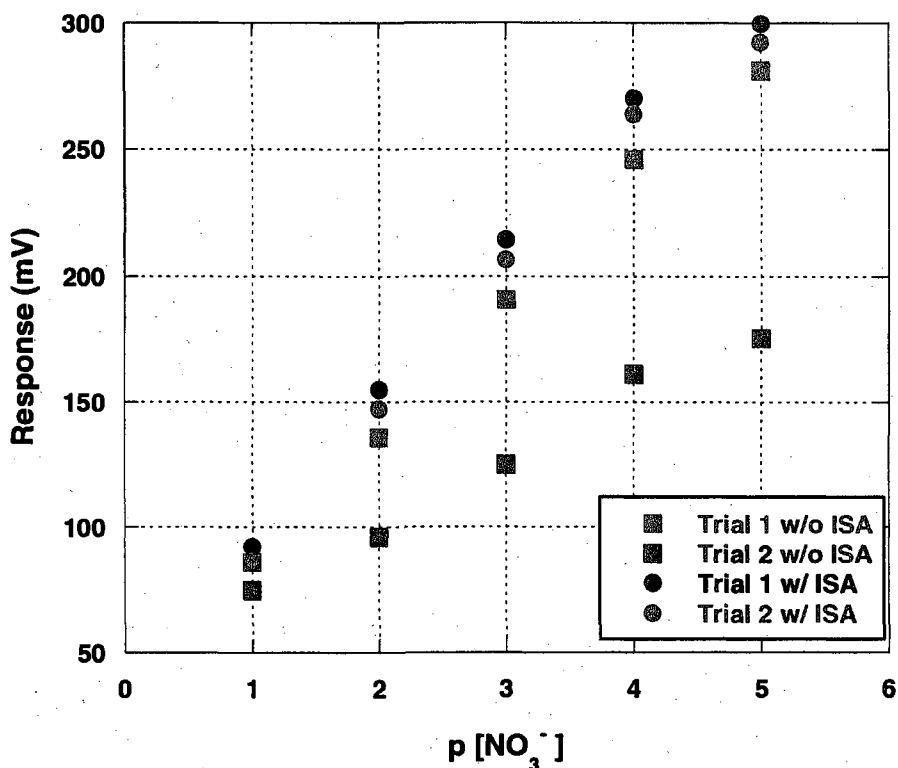


**Figure 2.2** Calibrations of the nitrate specific ion selective electrode with and without the presence of an ionic strength adjuster

As mentioned, the manufacturer suggests the use of an ionic strength adjuster (ISA) when using the ISE as the response of ion-specific electrodes is known to depend on ionic strength. First experiments were performed without ISA added, and the results show that the electrode response was not reproducible. Figure 2.2 shows two different calibrations of the same  $\text{LiNO}_3$  standards prepared in water as well as two calibrations of  $\text{LiNO}_3$  standards prepared in 0.04 M  $(\text{NH}_4)_2\text{SO}_4$ . The ordinate axis represents the digital reading on the meter, while the abscissa represents the nitrate concentration, where  $p[\text{NO}_3^-] = -\log([\text{NO}_3^-])$ . The use of this ISA made the electrode's response much more stable and reproducible (Table 2.13).

**Table 2.13** Effects of ionic strength adjuster on calibration slope  $\left(\frac{\text{mV}}{p[\text{NO}_3^-]}\right)$

Trial #	H <sub>2</sub> O	(NH <sub>4</sub> ) <sub>2</sub> SO <sub>4</sub>
1	50.28	53.05
2	29.76	52.87
3	39.97	53.91
average	40.00	53.27
standard deviation	10.26	0.56
% RSD	25.65	1.04

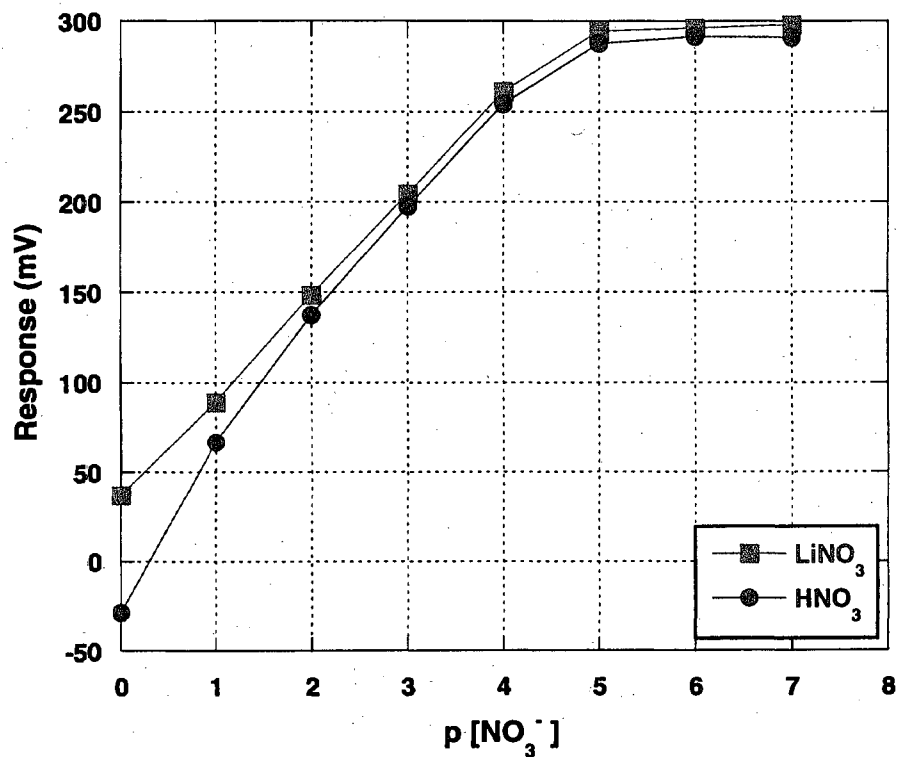


**Figure 2.3** Response of the ion selective electrode as a function of nitrate

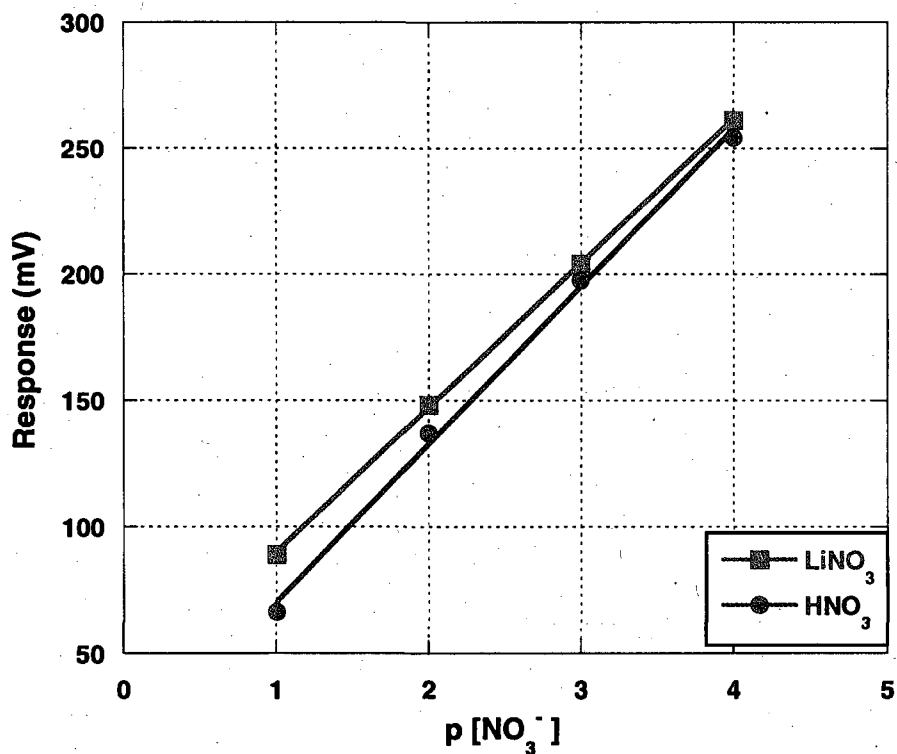


**Figure 2.4** Response of ion selective electrode over linear range

Figure 2.2 also shows the electrode not to respond linearly to nitrate concentrations below  $10^{-4}$  M. In order to determine the dynamic range of the electrode, HNO<sub>3</sub> and LiNO<sub>3</sub> standards with concentrations ranging over several orders of magnitude were measured. By removing the end data points until the remaining numbers can be fit to a line, the dynamic range of the electrode was found to be from  $10^{-1}$  to  $10^{-4}$  M nitrate. Figure 2.3 shows the electrode response for the nitrate standards in the concentration range from 1 to  $10^{-7}$  M, and Figure 2.4 illustrates the calibration curves generated from the data.

Nitric acid causes an obvious decrease in the electrode conductivity measurements when compared to nitrate salt alone. It was previously shown that using ISE to measure

nitrate was accurate in the presence of acid (59). The previous study only investigated acid concentrations less than  $10^{-4}$  M. This change in the response seems to be intensified by increasing concentrations of nitric acid. By calibrating the electrode with nitric acid and measuring lithium nitrate standard solutions of the same concentration, an increase of 21% of the measured nitrate concentration was observed at 0.1 M nitrate, yielding a response slope of  $1.12 \pm 0.03$ . The inverse experiment, where the electrode was calibrated with nitrate salts and used to measure nitric acid concentrations, demonstrated a decrease of 36% of the measured nitrate concentration at 0.1 M nitrate, yielding a response slope of  $0.85 \pm 0.01$  (Figure 2.5).

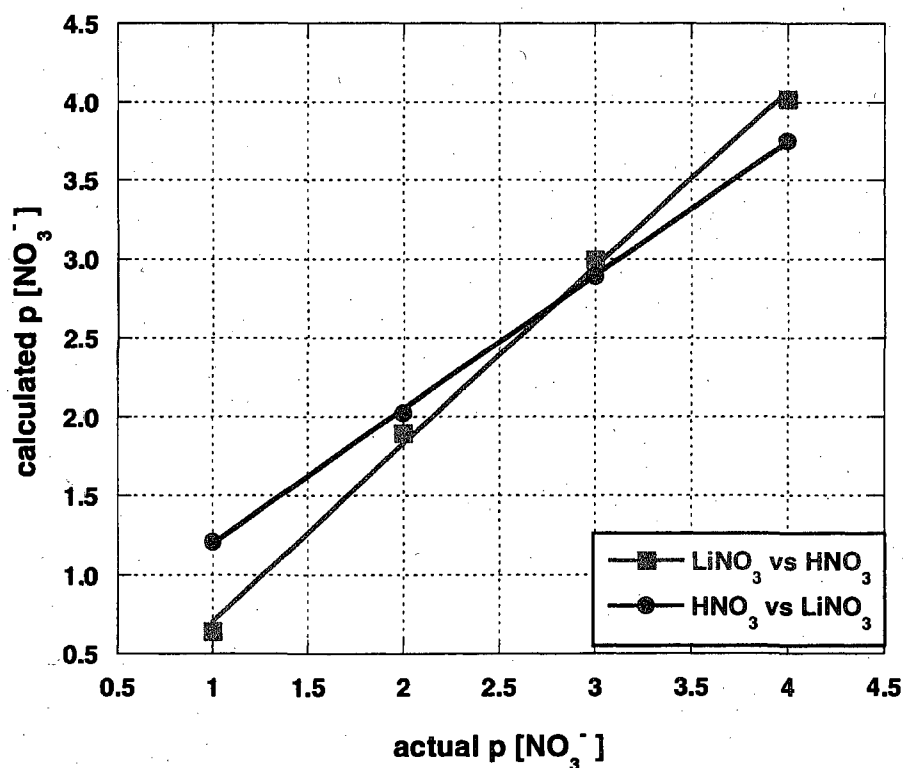


**Figure 2.5** Measurement of  $\text{LiNO}_3$  and  $\text{HNO}_3$  standards as calculated based on opposing calibration curve

An experiment was devised to determine a correction factor based on the amount of nitric acid in the sample. Standards from  $10^{-2}$  to  $10^{-4}$  M total nitrate with varying concentrations of nitric acid were generated. The acid concentration is given in pH units. The slopes of nitrate calibration curves were plotted against the pH at which they were obtained. This is shown in Figure 2.6 and the equation of the line is  $y = -3.5x + 72.1$  and can be used to minimize the error caused by the presence of acid.

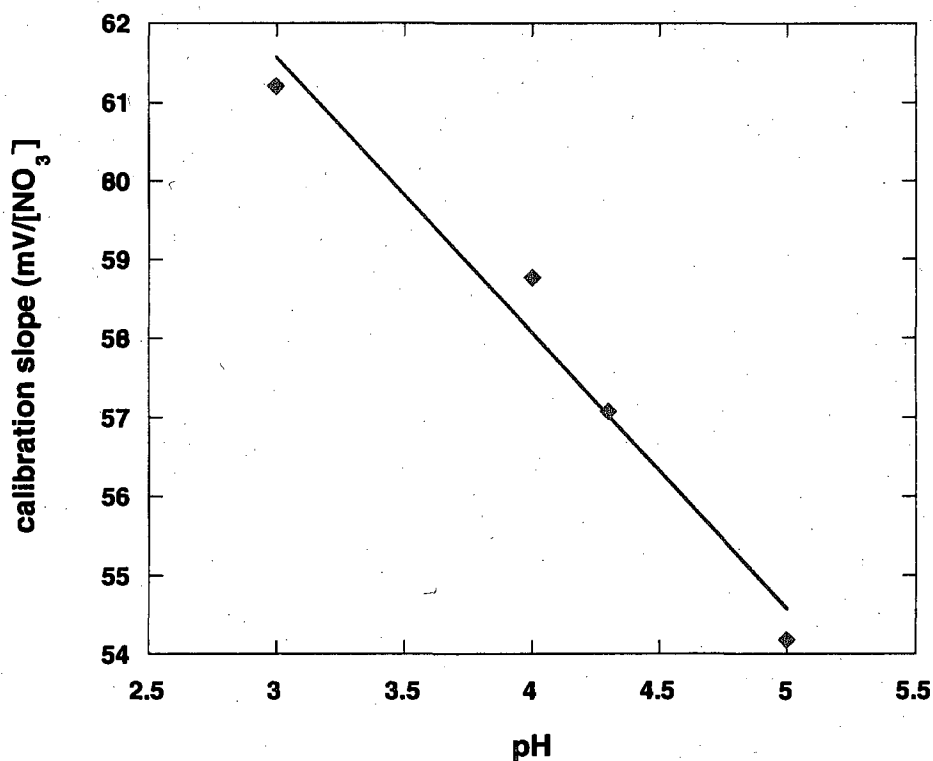


**Figure 2.6** Response slope as a function of pH

Ion chromatography as a means of nitrate determination was also examined. Ion chromatography is based on ion exchange, which involves an exchange equilibrium between ions in solution (mobile phase) and ions on the surface of a solid (stationary phase) found in the column. A typical anion exchange column contains quaternary amine

groups with hydroxide ions as the anionic exchangers (60). An IC system first pumps the eluent through the column, and then injects the sample. Each of the selected ions will remain in the column due to ionic interactions for a certain amount of time, called the retention time, which depends on the column's selectivity for that particular ion. The solution is then pumped through a conductivity suppressor before being sent to the detector. In the absence of a suppressor, the conductivity detector would detect all ions in the solution. This would result in a noisy chromatogram since there are more ions in the eluent than in the sample. The suppressor exchanges the eluent cations for  $H^+$ , which converts the eluent to water so that the detector will only detect the anions from the sample (53, 60). The detector measures the conductivity of the solution and the chromatogram represents the ions present in the sample. The area of the peak is used to determine the concentration of the ion of interest by first establishing a calibration curve of known standards.

The system used in this work was a Dionex ICS 3000, which is specialized for measuring anion concentrations in aqueous solutions and includes autosampling capabilities. This instrument was used with a Dionex AS 18 micro (2x250 mm) column along with a Dionex AG 18 micro (2x50 mm) guard column, and the eluent was a 30 mM KOH solution. The calibration range was 16  $\mu M$  to 1600  $\mu M$  nitrate. The samples were diluted accordingly, with the aqueous samples being diluted by a factor of 10,000 in water and the organic samples diluted by a factor of 1,000 in methanol. The prepared samples were then filtered before being run which, along with the use of the guard column, prevents the column from clogging so it can be reused many times.

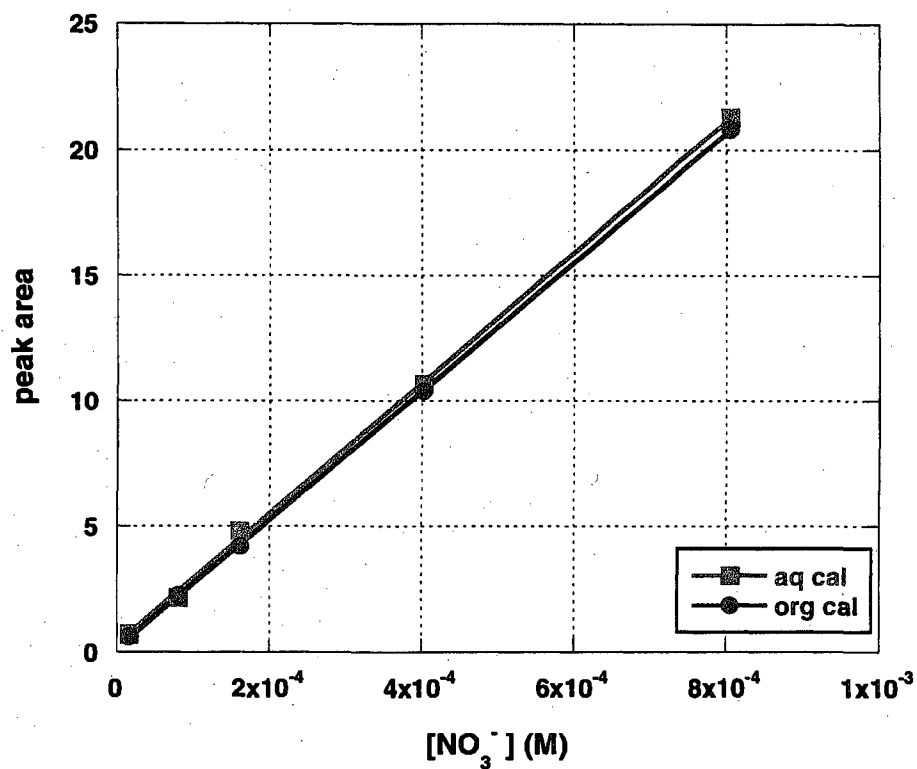
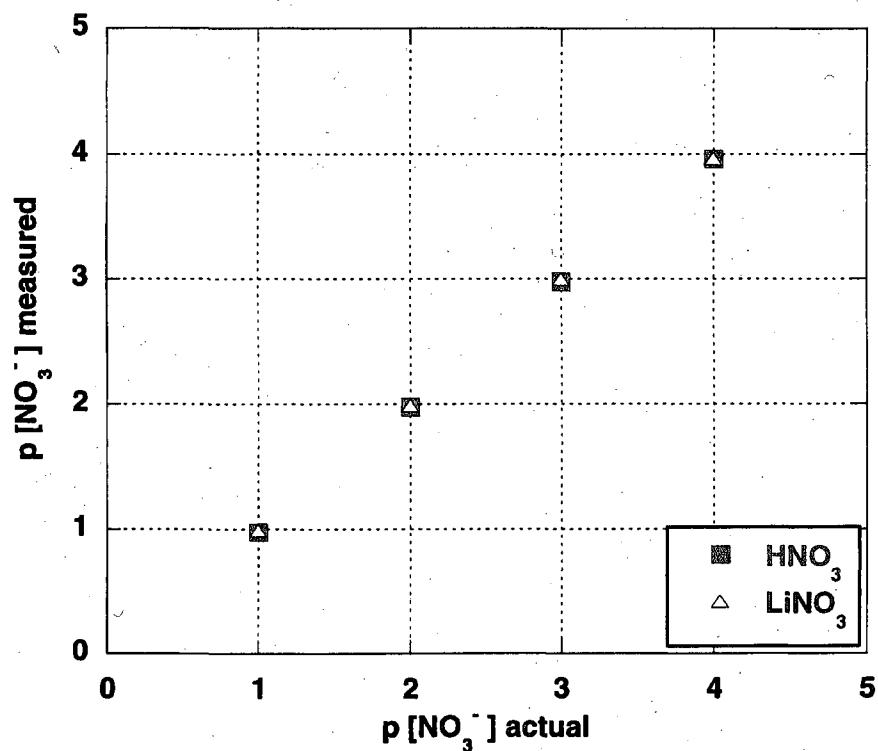


Figure 2.7 Nitrate calibration curves as determined by ion chromatography

Table 2.14 Method detection limit of [NO<sub>3</sub><sup>-</sup>] determination by ion chromatography (M)

Trial #	H <sub>2</sub> O	MeOH
1	1.54x10 <sup>-6</sup>	7.50x10 <sup>-7</sup>
2	1.72x10 <sup>-7</sup>	5.42x10 <sup>-7</sup>
3	5.22x10 <sup>-7</sup>	8.28x10 <sup>-7</sup>
4	2.31x10 <sup>-6</sup>	9.84x10 <sup>-7</sup>
5	7.91x10 <sup>-7</sup>	3.37x10 <sup>-7</sup>
6	6.22x10 <sup>-7</sup>	2.59x10 <sup>-7</sup>
7	2.13x10 <sup>-6</sup>	8.87x10 <sup>-7</sup>
average	1.15x10 <sup>-6</sup>	6.55x10 <sup>-7</sup>
standard deviation	8.37x10 <sup>-7</sup>	2.80x10 <sup>-7</sup>
MDL	3.67x10 <sup>-6</sup>	1.50x10 <sup>-6</sup>

Ion chromatography was demonstrated to have a large linear range for calibration and also to provide reproducible results in the presence of acid. Another advantage to using IC for nitrate determination was that a method was developed to measure the organic phase directly which was not possible with the ISE. Figure 2.7 shows typical calibration curves for nitrate ions in aqueous and organic matrices. Table 2.14 provides the data on the method detection limit, as determined by the  $b+3\sigma$ , where  $b$  is the mean of seven measurements of the blank and  $\sigma$  is the standard deviation (53).



**Figure 2.8** Test for accuracy and acid effects of ion chromatography based measurements

In order to test IC for accuracy and acid effects, the same standards used to calibrate the ISE were used. The  $10^{-1}$ ,  $10^{-2}$ ,  $10^{-3}$ , and  $10^{-4}$  M  $\text{HNO}_3$  and  $\text{LiNO}_3$  standards were

tested as unknown aqueous samples. A comparison of the measured versus known nitrate concentrations is shown in Figure 2.8 as a log plot. The slopes were  $0.994 \pm 0.005$  for  $\text{LiNO}_3$  samples and  $0.997 \pm 0.004$  for  $\text{HNO}_3$  samples. The slopes approach unity, implying accuracy in using IC to measure nitrate concentration. Also, since the two data sets are indistinguishable, the acid effect seems to be eliminated by using IC.

**Table 2.15** Relative standard deviation in nitrate concentration of 1.2 M  $\text{LiNO}_3$  determined by ion chromatography

Trial #	$[\text{NO}_3^-]$ (M)
1	1.19
2	1.34
3	1.27
4	1.20
5	1.36
6	1.21
average	1.26
standard deviation	0.07
% RSD	5.90

Ion chromatography was used to determine total nitrate concentration in both the organic and aqueous phases of the extraction samples. In order to estimate the precision of this method, a set of six identical samples were prepared from the  $\text{LiNO}_3$  stock solution. Each sample was diluted and filtered in the same manner as described above, and then measured using the Dionex ICS 3000. The standard deviation in the obtained results was 5.9% of the mean value and was used as an estimation of the uncertainty in the nitrate measurement (Table 2.15). A new calibration was performed prior to each set of aqueous or organic samples. During the analysis of the extraction samples, a calibration check was performed by measuring a calibration standard as an unknown

sample. If the calibration check was more than 10% different from the actual value, that set of samples was reanalyzed to eliminate errors from instrument drift.

### 2.3.3 Uranium Concentration Determination

As stated in Section 2.3, the three methods investigated for the determination of uranium(VI) concentration were ICP-AES, UV-visible spectroscopy, and LSC. All of these methods have been used in literature reports to obtain quantitative measurements of uranium concentration in nuclear fuel processing, nuclear forensics, and environmental monitoring (61, 62, 63, 64). These methods are discussed and compared to determine the most reliable means of measuring uranium concentration for this project.

The first method explored was ICP-AES. A schematic of the components included in a typical ICP-AES system is shown in Figure 2.9. The sample is made into a plasma with an argon carrier gas, which breaks up the molecules in the sample and ionizes each atom. The excited atoms emit photons at characteristic wavelengths, and spectroscopy is used to detect and quantify the concentration of each element.

The inductively coupled plasma torch is made of three concentric quartz tubes through which argon gas flows. Initiation of the plasma occurs when the argon atoms are ionized with a Tesla coil. A water-cooled radio frequency (RF) generating induction coil, which surrounds the top of the torch, produces magnetic field (60). This magnetic field causes the ions to flow in a circular path, which creates heat due to the ohmic resistance to this flow. A typical plasma torch will maintain temperatures from 6,000 to 10,000 K (60). Liquid samples are introduced into the plasma as an aerosol produced by a nebulizer.

In the plasma, the sample is atomized and then ionized. Each element in the sample gives off photons of characteristic wavelengths. The transfer optics focuses the emitted light into the polychromator, where a diffraction grating separates the spectrum. The intensity of photons at each specified wavelength then amplified with a photomultiplier tube (PMT) before being sent to the detector. In a PMT, photon interactions produce electrons which are amplified by a system of dynodes, and a detector converts these into an electronic signal. The intensity of this signal is used to determine the concentration of the element with a calibration curve from solutions of known concentrations.

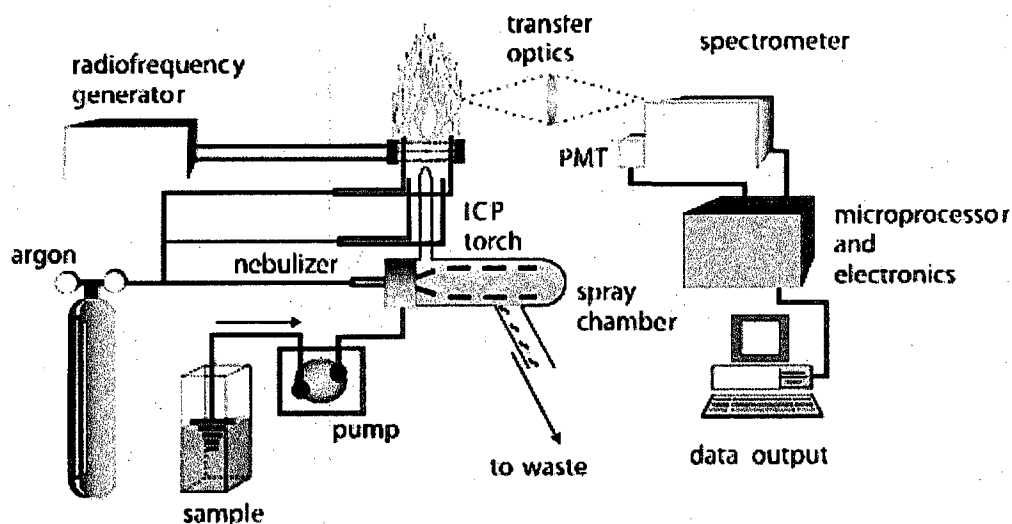


Figure 2.9 ICP-AES diagram (65)

The ICP-AES instrument used in this work was a Thermo Scientific iCAP 6000 Series. The uranium emission wavelength was monitored at 419 nm, which has few interfering emissions from other components of the samples. The lower detection limit for uranium at this wavelength was found to be  $6.9 \times 10^{-6}$  M (Table 2.16). The calibration standards used for this project ranged from  $2 \times 10^{-5}$  to  $1 \times 10^{-3}$  M uranium and

were prepared in a 1% nitric acid matrix. The aqueous samples were diluted by a factor of 20 in 1% HNO<sub>3</sub>, while the organic samples were back extracted and diluted by a factor of 500 in 1% HNO<sub>3</sub>. A comparison of the organic phase measurement and determination based on a mass balance of the aqueous phase measurement gave an average difference of 7.9% (Table 2.17), which suggests the method of back extracting and using ICP-AES to determine uranium concentration is fairly reliable.

**Table 2.16** Method detection limit of [U] determined by ICP-AES (M)

Trial #	[U]
1	3.80x10 <sup>-6</sup>
2	2.42x10 <sup>-6</sup>
3	1.58x10 <sup>-6</sup>
4	4.44x10 <sup>-6</sup>
5	3.25x10 <sup>-7</sup>
6	3.10x10 <sup>-6</sup>
7	3.30x10 <sup>-6</sup>
average	2.71x10 <sup>-6</sup>
standard deviation	1.40x10 <sup>-6</sup>
MDL	6.91x10 <sup>-6</sup>

**Table 2.17** Comparison of [U] (mM) in organic phase as determined by direct ICP-AES measurement vs. by mass balance

[U] initial	[U] aq	[U] org	[U] mass	% difference
11.1	0.130	11.90	10.97	8.16
11.1	0.126	12.11	10.97	9.83
11.1	0.343	11.29	10.76	4.83
11.1	0.422	9.82	10.68	8.35
11.1	0.325	11.55	10.78	6.94
22.2	0.562	23.37	21.64	7.71
22.2	0.303	24.05	21.90	9.35
22.2	2.659	17.94	19.54	8.52
22.2	0.348	23.29	21.85	6.36
22.2	0.615	23.60	21.29	8.94
			average	7.90

The second method investigated for uranium determination was UV-visible spectroscopy. In UV-vis a spectrophotometer measures the amount of light passing through a sample and references it to a blank or a matrix sample, thereby determining the amount of light being absorbed by the species of interest (Figure 2.10). The most common sources of photons for UV-visible systems are the deuterium lamp for wavelengths in the UV region (160-375 nm) and the tungsten filament lamp for the visible-NIR (near infrared) region (350-2500 nm) (60). Light generated by the lamps, called the incident beam, is sent to the monochromator, where a diffraction grating separates the light into its spectrum and each desired wavelength is isolated. In a double beam set up, the incident beam is split and the reference and sample transmittance are measured simultaneously. The photon beam passing through the sample with intensity  $I$ , as well as the incident beam with intensity  $I_0$ , is directed to the photomultiplier and detector.

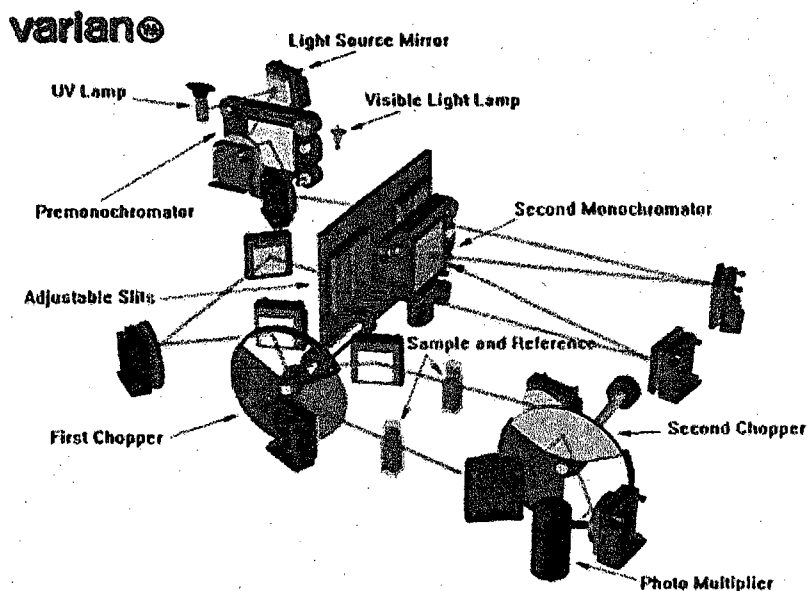


Figure 2.10 Diagram of UV-visible system (66)

The output is usually a spectrum displayed as measured absorbance over a user-defined range of scanned wavelengths. Eq 2.1 shows the relation between absorbance ( $A$ ), transmittance ( $T$ ) and intensity ( $I$ ) ( $I_0$ ):

$$A = -\log T = -\log\left(\frac{I}{I_0}\right) \quad \text{Eq. 2.1}$$

The absorbance measured at a specific wavelength can be used to determine the concentration of a species. The following equation (Beer's Law) correlates absorbance with concentration, which allows for calibration and quantification.

$$A = \epsilon bc \quad \text{Eq. 2.2}$$

In Eq. 2.2,  $A$  is absorbance,  $b$  is pathlength (in cm) of the cuvette,  $c$  is concentration (in M) of the analyte, and  $\epsilon$  is the molar absorptivity. The molar absorptivity of a given species is constant at each particular wavelength.

The absorbance occurs at specified wavelengths due to the bond energetics of the molecule being probed. When photons of a characteristic absorbance wavelength are passed through the sample, the absorbing species acquires an electronically excited state. The wavelength is inversely proportional to the energy of the excitation. There are several types of electronic transitions possible involving transitions of pi, sigma, nonbonding electrons and charge transfer electrons.

Based on electronic configurations, metals can undergo a variety of transitions between orbitals. Typically, the orbitals involved in UV-visible absorbance transitions are located in the outermost shell. The transition metals can undergo transitions in the d orbitals, while lanthanides and actinides can have f orbital transitions as well. The transitions of the 5f orbital electrons are of concern in this work, since the molecule being excited is the uranyl ion ( $\text{UO}_2^{2+}$ ), and the 5f shell contains the highest occupied orbital

(60). A molecular orbital diagram of the uranyl ion demonstrates orbital mixing of the 5f (U) and 2p (O) and shows the lowest unoccupied orbitals, which are important in excitation and bonding, have only f orbital contributions (Figure 2.11) (67).

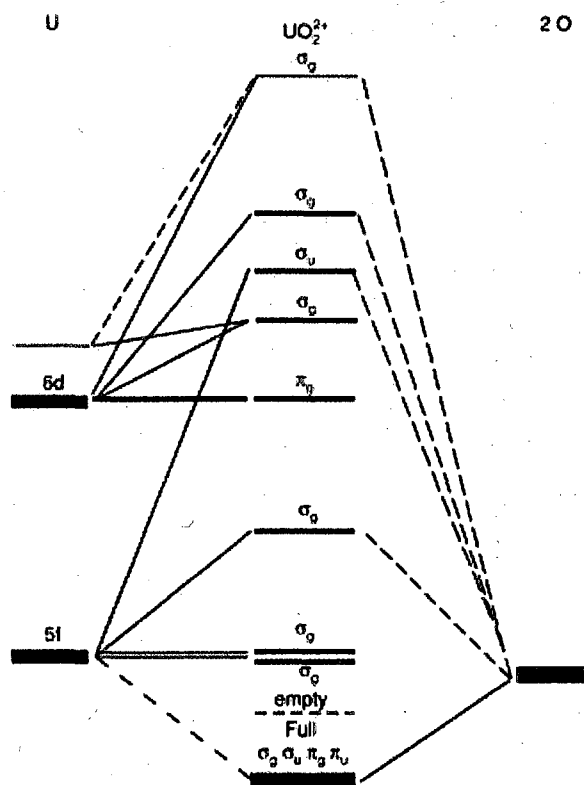


**Figure 2.11** Molecular orbital diagram of uranyl ion (67)

The uranyl ion has characteristic absorption spectra containing three fingerlike peaks between 400 and 430 nm (63) (Figure 2.12). The uranyl absorption spectra change shape and shift absorbance maxima with changes in speciation, since the spectrophotometer detects variations in the uranium electron configuration and transition energies. These variations are caused by the shifts in energies of the molecular orbitals when bonding with the uranyl ion occurs. For example, it was shown in previous work that as nitric

acid concentration increases from 2 to 6 M the characteristic uranyl peaks broaden and merge into one large peak (63). Each specific species still absorbs light according to Beer's Law (Eq. 2.2), and linear calibrations are achievable.

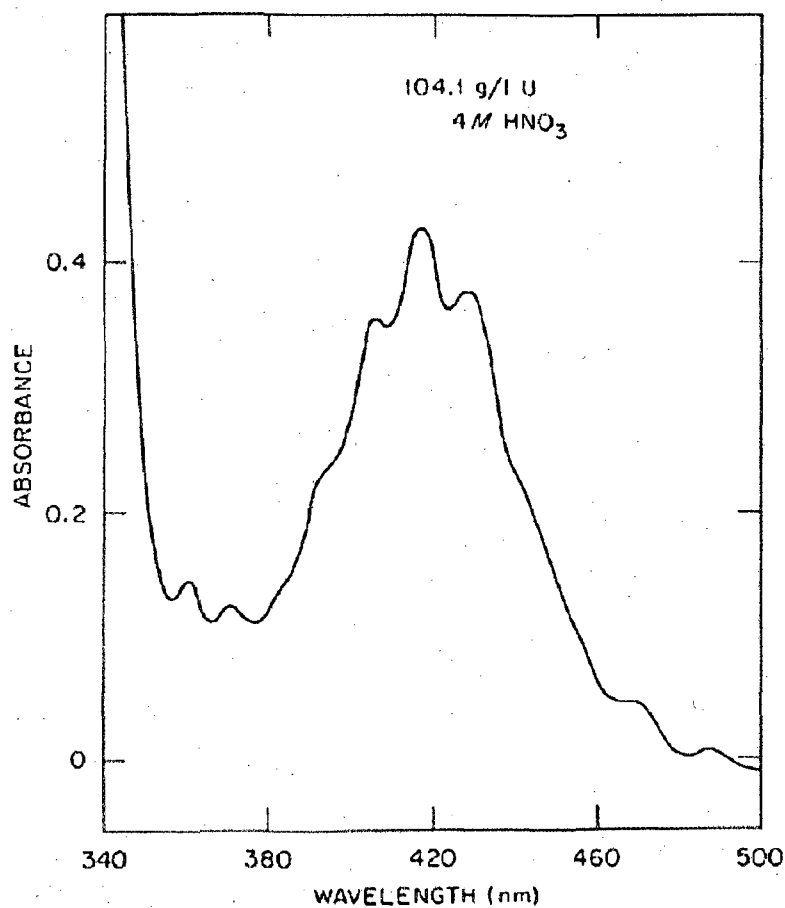


**Figure 2.12** Absorption spectrum of uranyl ion (63)

The instrument used for the determination of uranium was a Varian Cary 6000i UV-Visible-NIR Spectrophotometer. This analysis was performed on the organic phase directly, and 1 mm glass cuvettes were used. The aqueous phase uranyl nitrate concentration after extraction was below the minimum detection limit, which was found

to be  $7.8 \times 10^{-3}$  M. In order to evaluate the UV-visible technique for accuracy and reliability in determining uranium concentration, samples containing uranyl nitrate solutions of known concentrations were analyzed in 1 cm or 1 mm glass or plastic cuvettes with light from 350 to 800 nm. Figure 2.13(a) shows the spectra collected, and Figure 2.13(b) is an expansion of the spectra of the solutions with lower concentrations, which shows that the structure of each spectrum is the same.

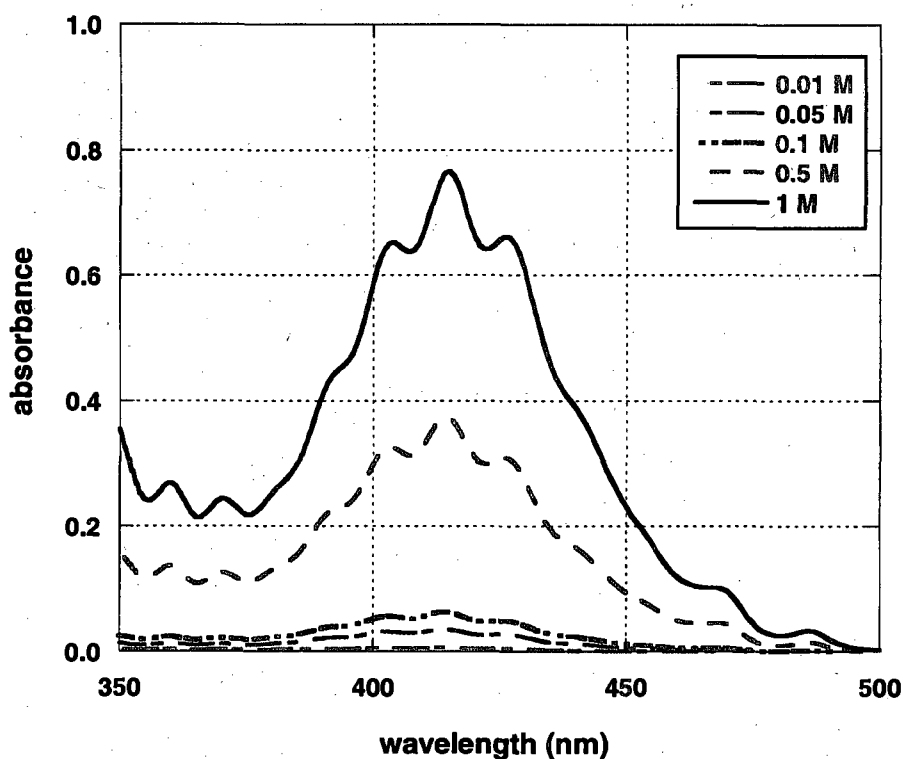


**Figure 2.13(a)** UV Spectra of  $\text{UO}_2(\text{NO}_3)_2$  aqueous solutions in 1 mm cuvettes

These figures demonstrate the characteristic absorption peaks of the uranyl ion (63), and the data were used to create a uranium calibration curve at 415 nm (Figure 2.14). Calibration checks were performed by measuring a standard and using the linear equation generated by the curve to calculate the concentration of uranium, and the results were

within 5% of the actual value. The calibration gave an molar absorptivity of  $8.9 \pm 0.8$   $M^{-1}cm^{-1}$ , which is close to a reported value of  $9.7 M^{-1}cm^{-1}$  (63) (Table 2.18).

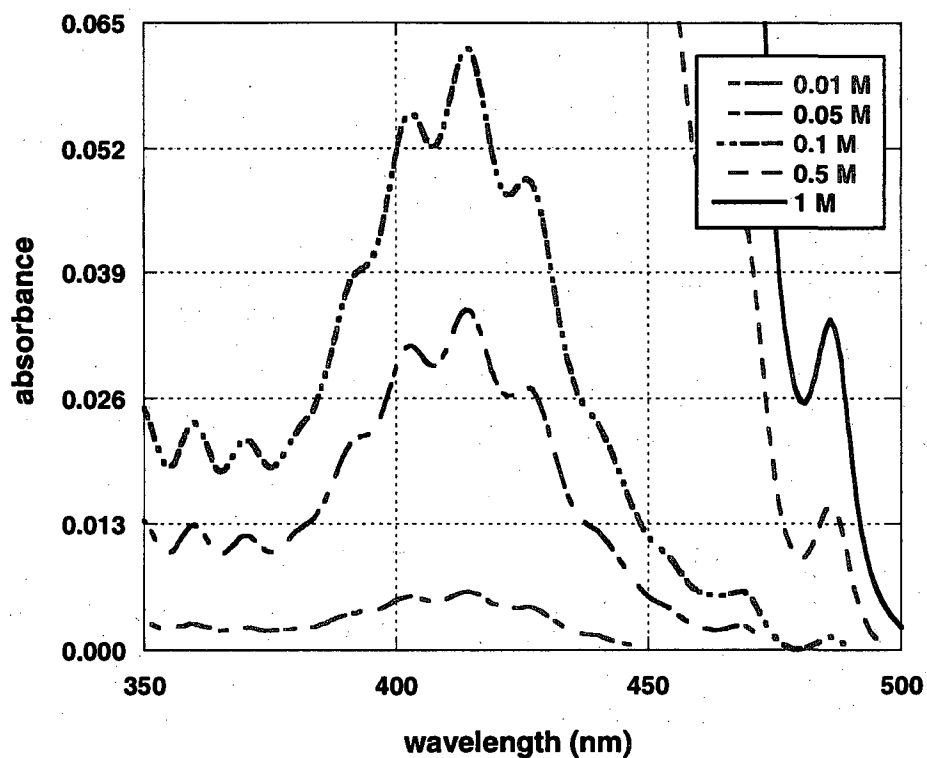


**Figure 2.13(b)** Expansion of spectra of  $UO_2(NO_3)_2$  aqueous solutions in 1 mm cuvettes

**Table 2.18** Molar absorptivity measured at 415 nm

Trial #	$\epsilon (M^{-1}cm^{-1})$
1	8.74
2	7.75
3	9.34
4	9.59
average	8.85
standard deviation	0.82

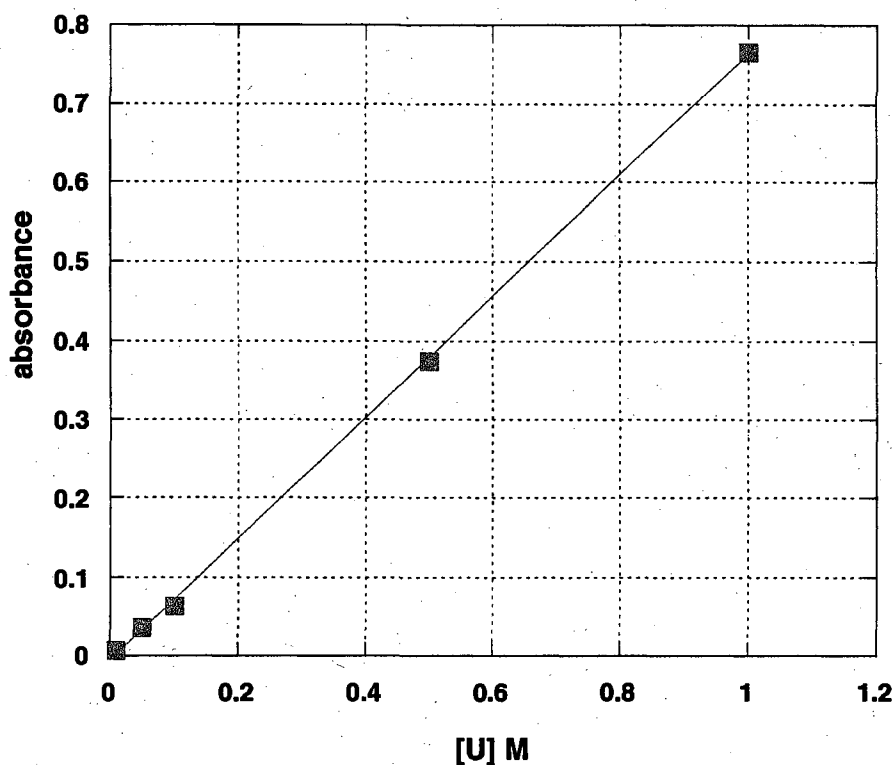


**Figure 2.14** Calibration using maximum UV absorbance at 415nm

**Table 2.19** Difference between [U] (mM) in organic phase of samples extracted from 20 mM  $\text{UO}_2(\text{NO}_3)_2$  as determined by UV-Visible spectroscopy and ICP-AES

UV-Vis	ICP-AES	% difference
17.78	16.48	7.62
19.16	18.47	3.63
18.78	18.97	1.01
19.37	19.14	1.19
18.56	19.26	3.67
20.91	19.29	8.07
18.46	19.25	4.18
17.73	19.34	8.66
17.94	19.21	6.83
17.77	19.34	8.57
	average	5.35

As a comparison, a set of the same 10 organic samples was analyzed by both ICP-AES and UV-visible spectroscopy and the two sets of results were compared. The

percent difference of the two outcomes was calculated based on the difference divided by the average. The two sets of results had an average difference of 5.4%, and ranged from 1.0 to 8.7% (Table 2.19).

The use of UV-visible spectroscopy is a reliable method for uranium determination, in fact the only major drawback found in this study was that the aqueous phase concentration of uranium was below the detection limit and could not be analyzed by this method. One potential problem with uranyl nitrate measurement by UV-visible spectroscopy is that nitrate concentration affects the uranyl absorption spectrum (63). The nitrate effect was not seen in this work, and was deemed to not be a concern, most likely due to the fact that the amount of nitrate extracted into the organic phase is relatively constant.

The final method investigated as a means of measuring uranium concentration was LSC. It is the fastest and simplest of the three methods, due to the minimum sample preparation and ease of use of the instrument. The fundamental principle behind LSC is energy transfer through radioactive decay. When a radionuclide decays, the emitting particle interacts with surrounding molecules and imparts some of its energy. In LSC this interaction is exploited to produce a measurable electronic signal. The radionuclide sample is dissolved in the liquid scintillation cocktail, which contains a scintillating molecule. The radionuclide transfers energy to the organic cocktail solvent, which transfers energy to the scintillator, which can then produce a photon upon relaxation. The light produced is then detected by a photomultiplier. Due to the low  $Z$  (atomic number) of the atoms in the organic scintillators, they are primarily used in the detection of alpha and/or beta particles (68).

The instrument used to determine uranium concentration by LSC was a Perkin Elmer Tri-Carb 3100 TR scintillation counter. Both the aqueous and organic phases were analyzed by this method. Samples were prepared by placing 0.1 mL of uranium solution in 10 mL of Ultima Gold scintillation cocktail and mixing. Samples were then counted for one hour or until the error percent of the count reached 1%. This LSC method was developed based on results from initial uranium counting experiments.

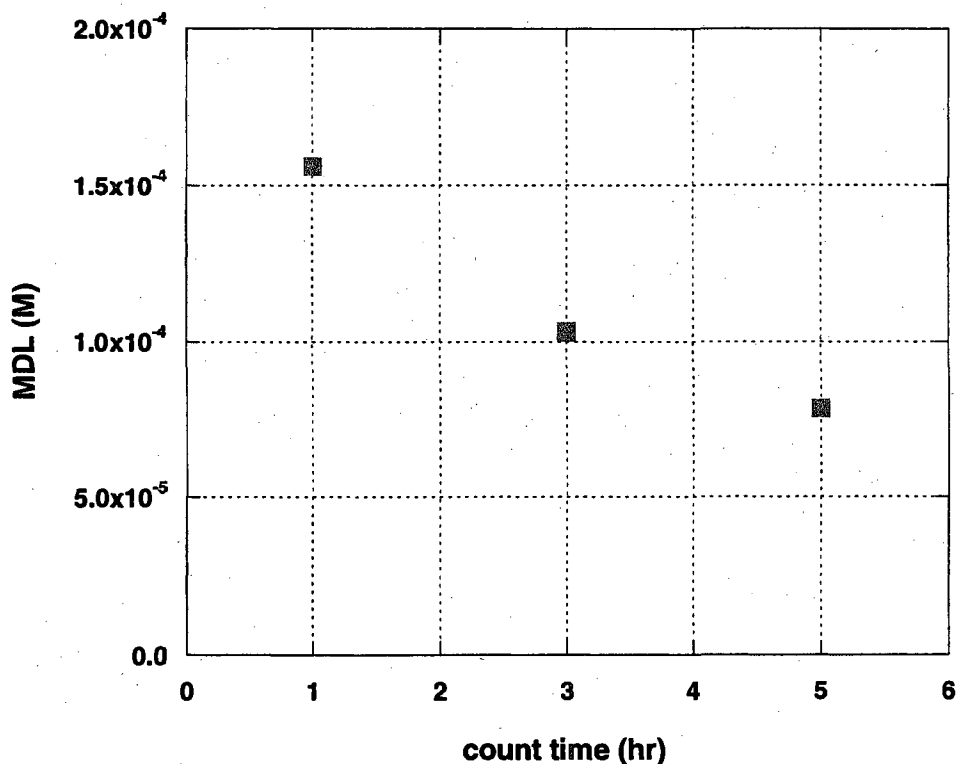


**Figure 2.15** Effect of counting time on the minimum detection limit of liquid scintillation counting

During these initial experiments, three parameters were considered: counting time, sample volume, and scintillation fluid volume. The samples used consisted of uranyl nitrate solutions ranging in concentration from  $10^{-6}$  M to 1 M. Calibration curves were

generated and the detection limits computed and compared. The first test varied counting time while using 0.1 mL of each  $\text{UO}_2(\text{NO}_3)_2$  solution in 10 mL of scintillation cocktail. Figure 2.15 shows that the detection limit decreases with increasing count time. Based on these results, the volume test samples were counted for 5 hours. The volume tests consisted of varying the sample volume of each  $\text{UO}_2(\text{NO}_3)_2$  solution from 0.1 to 0.5 mL in both 10 and 20 mL of scintillation fluid. These data (Figure 2.16) illustrate that sample volume affects the detection limit much more than does scintillation fluid volume, and so 10 mL of cocktail was used in order to minimize waste. A summary of the observed detection limits is in Table 2.20. Based on these results and the extraction conditions, it was determined that a sample volume of 0.1 mL with a count time of 1 hr was sufficient, since the uranium concentration is greater than  $1.56 \times 10^{-4}$  M.

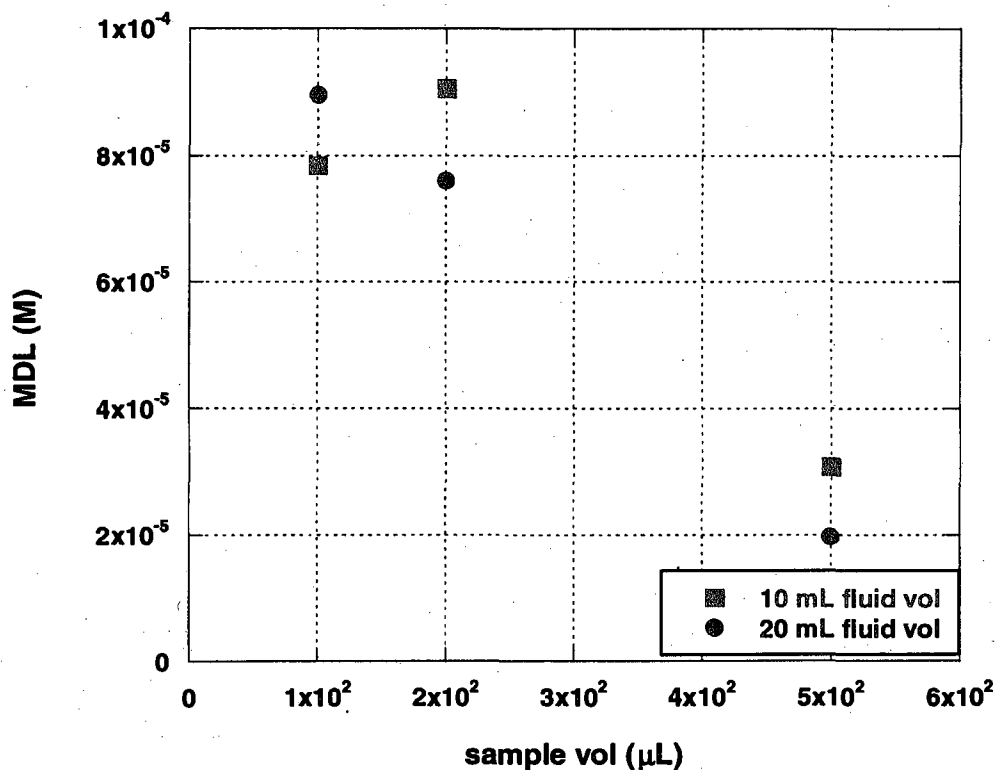


**Figure 2.16** Effects of sample and scintillation fluid volume on the minimum detection limit of liquid scintillation counting

**Table 2.20** Method detection limits of liquid scintillation counting

Time (hr)	Sample vol (mL)	Cocktail vol (mL)	MDL (M)
1	0.1	10	$1.56 \times 10^{-4}$
3	0.1	10	$1.03 \times 10^{-4}$
5	0.1	10	$7.85 \times 10^{-5}$
5	0.2	10	$9.06 \times 10^{-5}$
5	0.5	10	$3.09 \times 10^{-5}$
5	0.1	20	$8.96 \times 10^{-5}$
5	0.2	20	$7.61 \times 10^{-5}$
5	0.5	20	$1.98 \times 10^{-5}$

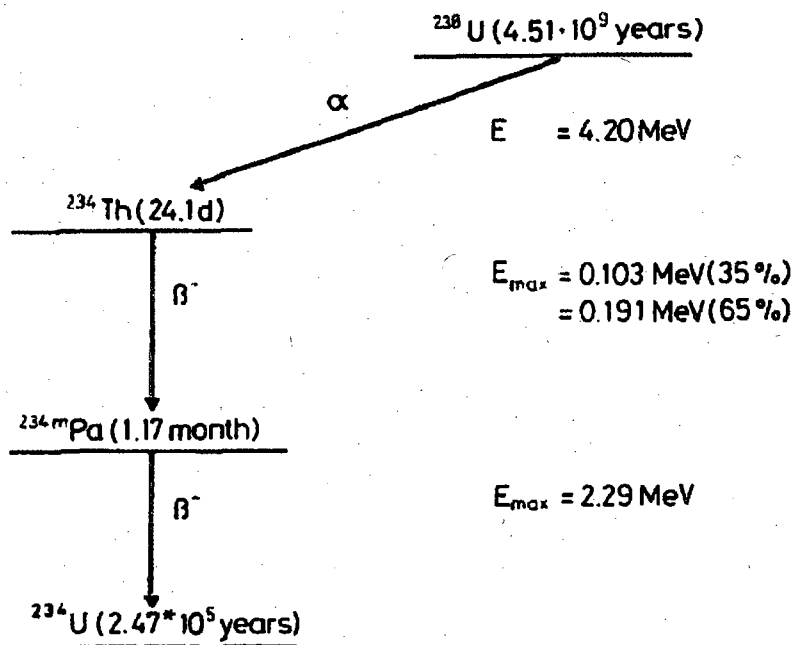


**Figure 2.17** Partial decay chain of  $^{238}\text{U}$  (62)

Determining uranium concentration by LSC requires consideration of the radiation emission of the daughter products. The most important daughters are shown in Figure 2.17. The  $^{238}\text{U}$  will be in secular equilibrium with  $^{234}\text{Th}$ ,  $^{234\text{m}}\text{Pa}$  and  $^{234}\text{U}$  within a year of its purification, and it will take thousands of years for the other daughters to grow in

again. The beta emission peaks generated by these daughter products will overlap with the uranium beta peak, but not its alpha peaks (62). Also, it is known that the amount of nitric acid in the sample matrix can affect the overall count rate through quenching of the scintillation fluid, leading to lower counting efficiency (62). The effects are diminished for organic samples, since Th and the bulk of the nitric acid remain in the aqueous phase; however, to minimize these complications, calibration standards were generated in the same manner as the extraction samples.

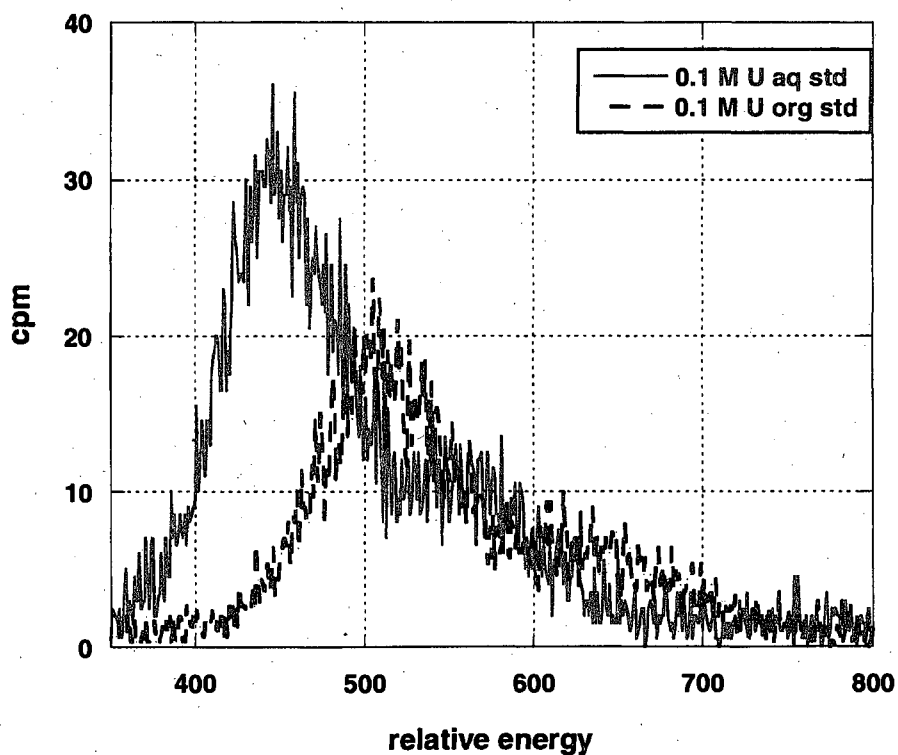


**Figure 2.18** LSC spectra of aqueous and organic standards

Uranium standards varied from  $1 \times 10^{-1}$  to  $5 \times 10^{-4}$  M U, and were prepared in both aqueous and organic matrices containing 1 M nitric acid. The instrument channel gates were set between 350 and 800 in relative energy units since this is where the uranium

peak was observed. Only the counts measured within these gates were used to generate the calibration curves. The spectra of standards containing 0.1 M  $\text{UO}_2(\text{NO}_3)_2$  in both aqueous and organic phases are shown in Figure 2.18. There is a decrease in the count rate and a shift in the peak position for the organic standard since the uranium was separated from the daughter products during the preparation.

**Table 2.21** Deviation in LSC calibration slopes (cpm / [U](M))

Trial #	aqueous	organic
1	19288	11877
2	38002	12240
3	30125	23543
average	29138	15887
standard deviation	9396	6633
% RSD	32.25	41.75

**Table 2.22** Concentration of uranium measured in aqueous and organic phases as determined by LSC and compared to initial [U] (mM)

[U] initial	[U] aq	[U] org	[U] total
11.1	4.57	9.40	13.97
11.1	2.19	12.45	14.64
11.1	1.33	14.09	15.42
11.1	0.68	13.44	14.42
11.1	0.47	13.67	14.14
22.2	4.89	28.08	32.97
22.2	1.63	33.52	35.15
22.2	0.55	32.40	32.95
22.2	0.21	32.65	32.86
22.2	0.13	33.19	33.32

The aqueous and organic calibration curves generated showed excellent linearity (Figure 2.19), but not reproducibility. The slopes of these curves varied up to 40% when standards were counted on different days (Table 2.21). New calibrations using fresh

standards were made each time samples were counted. Based on the linearity between cpm (counts per minute) and uranium concentration in both types of matrices, both the aqueous and organic phases of the extraction samples were measured by LSC. The results gave uranium concentrations that were greater than the initial amounts in each sample (Table 2.22).

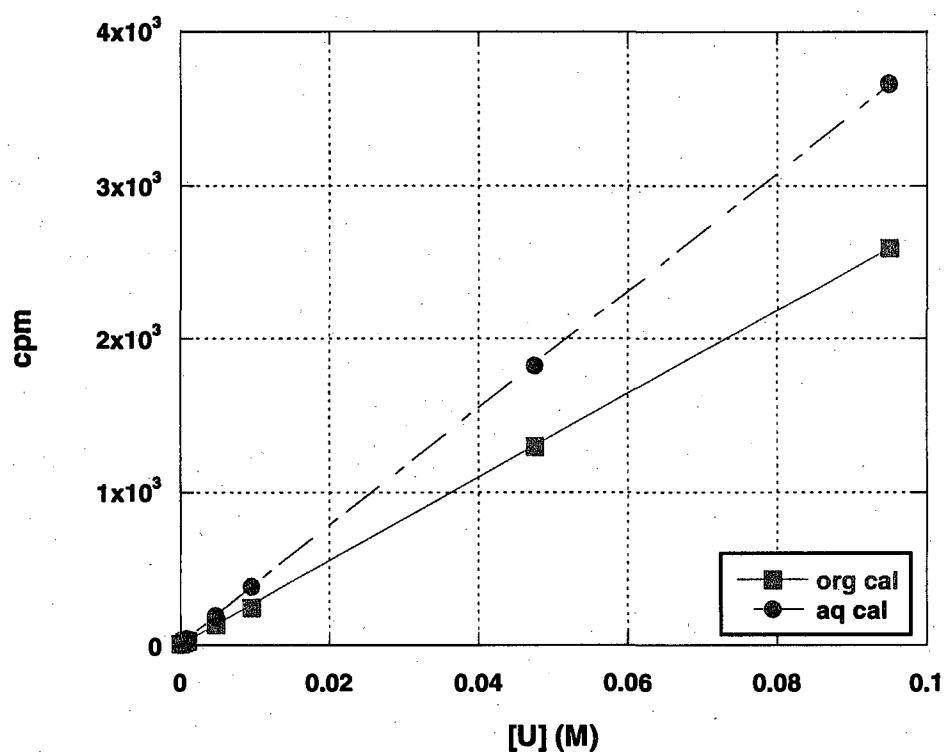


**Figure 2.19** Calibration curves generated by liquid scintillation counting

A comparison of the uranium concentration measurements for the same extraction samples as determined by both LSC and ICP-AES was made. These two methods gave very different results. Figure 2.20 and Figure 2.21 show these comparisons for the aqueous and organic phases respectively. When [U], as determined by LSC, was

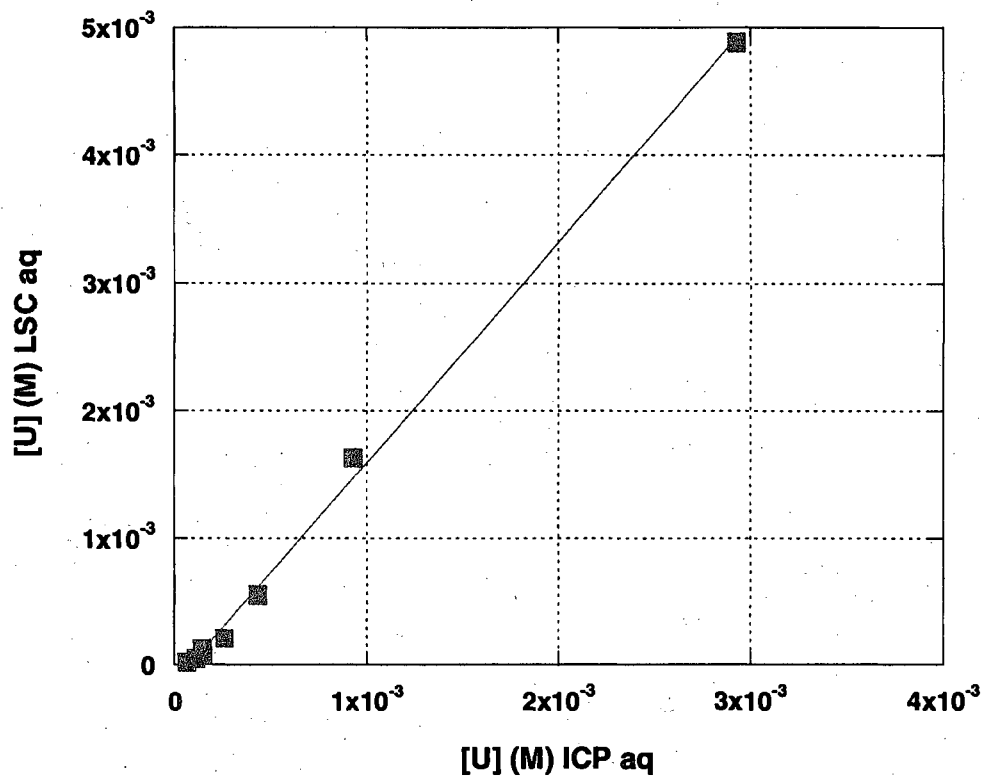
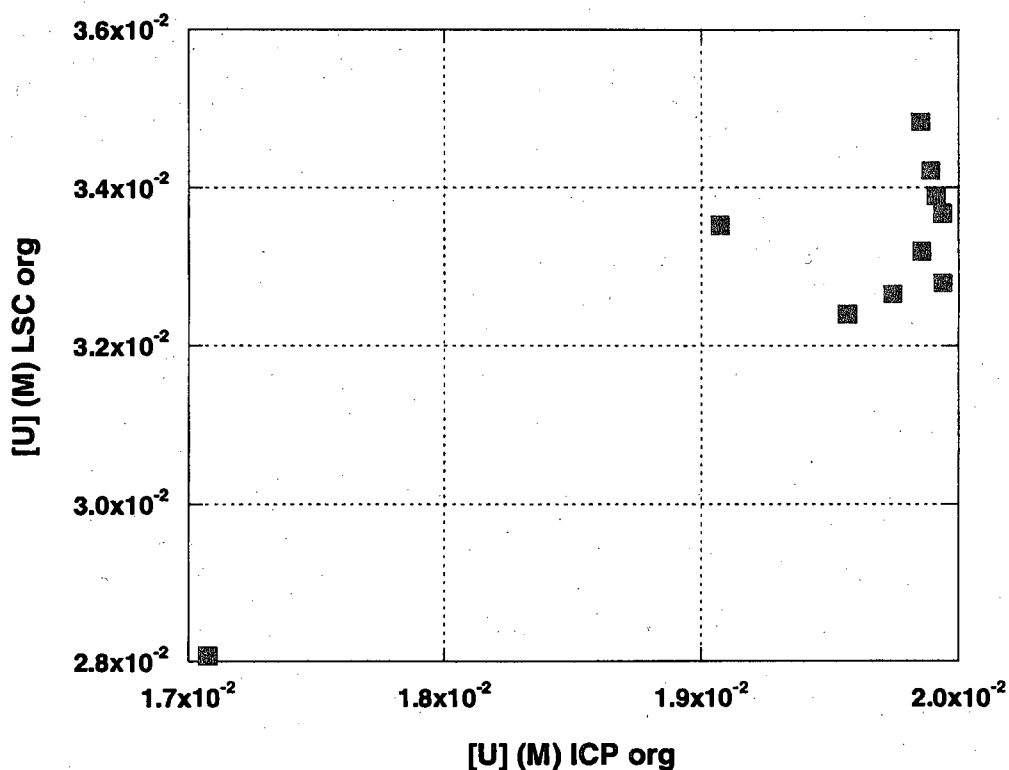


Figure 2.20 Comparison of [U] of aqueous samples determined by liquid scintillation counting and ICP-AES

Table 2.23 Ratio of [U] values as obtained by LSC and ICP-AES

LSC	ICP-AES	ratio
28.08	16.48	1.70
33.52	18.47	1.81
32.40	18.97	1.71
32.65	19.14	1.71
33.19	19.26	1.72
34.21	19.29	1.77
34.83	19.25	1.81
32.80	19.34	1.69
33.89	19.21	1.75
33.67	19.34	1.74
	average	1.74
	$\sigma$	0.04

examined as a function of concentration measured by ICP-AES, there was an apparent linear relationship for the aqueous samples, but not the organic. Also, as shown by the slopes in the figures, the values determined by LSC were nearly twice of those measured by ICP-AES. Data in Table 2.23 provides results of the organic phases of extraction as determined by LSC and ICP-AES and demonstrates the relationship of the two to be a ratio of 1.7. Based on the initial conditions, ICP-AES seemed more reliable.



**Figure 2.21** Comparison of [U] of organic samples determined by liquid scintillation counting and ICP-AES

In order to compensate for the inflated concentration measurements given by LSC, samples of known uranium concentrations in both aqueous and organic phases were analyzed by LSC and ICP-AES. Figure 2.22 exhibits how the difference in the results of

these two methods decreases as uranium concentration increases. The percent difference was calculated as before based on the difference between the two values divided by their average. This convergence of ICP-AES and LSC measured values at higher uranium concentrations was seen for both the aqueous and organic samples. An exponential curve can describe the difference as a function of [U] ( $y=5.3 \times 10^{-0.49}$ ) and could be used to correct for the LSC measurement.

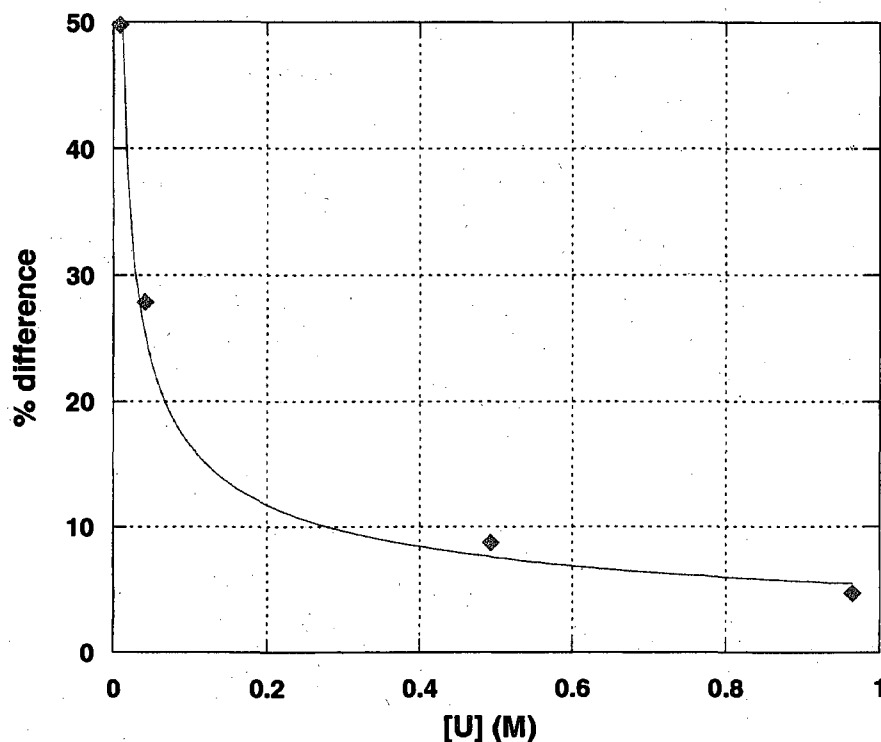


**Figure 2.22** Difference between results based on LSC and ICP-AES

**Table 2.24** Comparison of % difference in [U] results from LSC and ICP-AES with and without the addition of  $^{233}\text{U}$

[U] (M)	without $^{233}\text{U}$ (%)	with $^{233}\text{U}$ (%)
1	4.58	2.71
0.5	8.63	7.84
0.05	27.82	28.39

Based on the previous results, experiments were conducted to determine if increasing the count rate decreased the difference in results of the two methods, since the observed discrepancy could be due to the low activity of  $^{238}\text{U}$ . These experiments were performed by adding  $1\mu\text{Ci}$  of  $^{233}\text{U}$  to 20 mL of the uranyl nitrate stock solution used to make the samples and calibration standards. A congruent set of samples and standards without the  $^{233}\text{U}$  added were analyzed simultaneously. The count rate increased by nearly 1000 cpm due to the  $^{233}\text{U}$  peak (shown in Figure 2.23), but the measured concentrations of uranium was still much higher than the values obtained with ICP-AES (62). The uranium concentration as determined by these two methods still differed by greater than 28% at a  $[\text{U}]$  of 50 mM, and decreased with increasing uranium concentration at the same rate as before (Table 2.24).

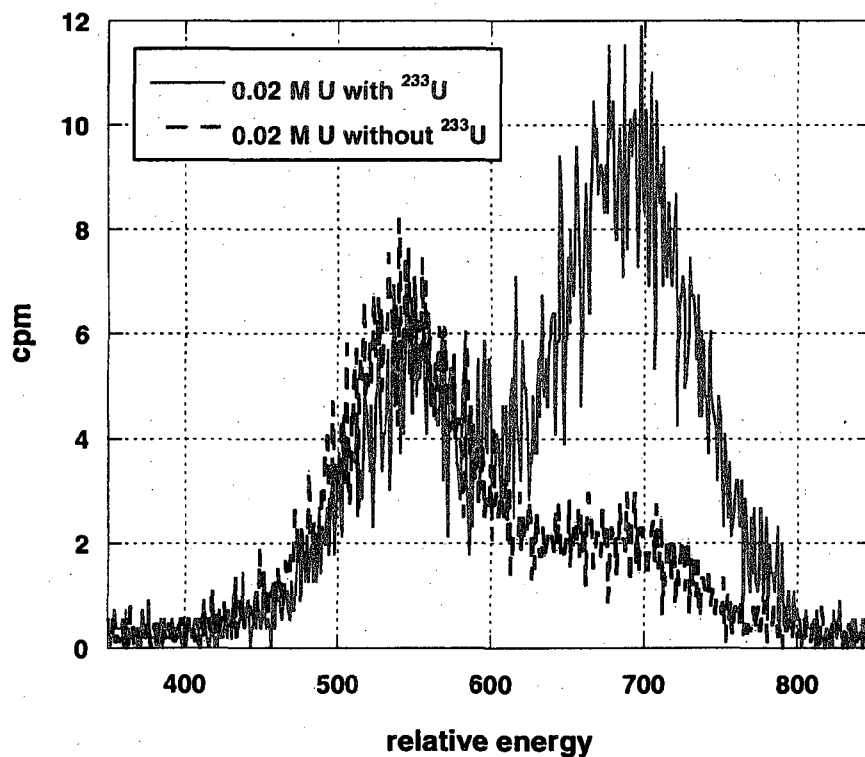


**Figure 2.23** LSC spectra of 0.02 M U standard with and without addition of  $^{233}\text{U}$

In order to compare the three methods for uranium determination, an extraction experiment was performed without the addition of  $^{233}\text{U}$  and the  $[\text{U}]$  in the organic phase was measured by UV-Visible spectroscopy, ICP-AES, and liquid scintillation counting (Figure 2.24). The extractions were performed at initial concentrations of 20mM  $\text{UO}_2(\text{NO}_3)_2$ , 1 M  $\text{HNO}_3$ , and varied total nitrate concentrations. The figure shows while the results based on ICP-AES and UV-visible determinations are comparable, the LSC results are not.

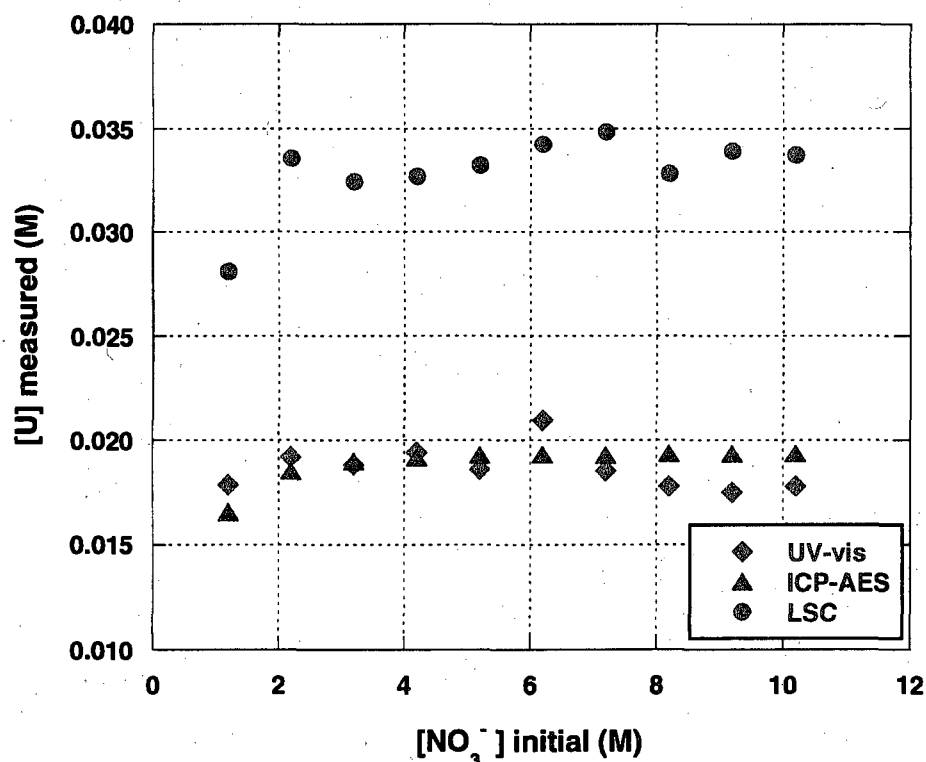


**Figure 2.24** Comparison of three methods used to determine uranium concentration ( $[\text{U}]$  initial of 20mM)

In conclusion, the use of LSC and UV-Visible spectroscopy were both rejected as the method for uranium determination, and based on these experiments ICP-AES was chosen. In order to estimate the precision of this method, an experiment similar to the one described in Section 2.3.2 for IC was performed. The results of this experiment had a relative standard deviation of uranium concentration of 3.7% as an estimation of uncertainty for uranium concentration determined by ICP-AES (Table 2.25). As with IC, a new calibration was performed prior to each analysis. Regular calibration checks were performed, and all samples in that set were reanalyzed if the check standard was not measured to within 10% of the actual value.

**Table 2.25** Relative standard deviation in uranium concentration determined by ICP-AES of 1.1 M uranyl nitrate stock solution

Trial #	[U]
1	1.18
2	1.20
3	1.11
4	1.12
5	1.10
6	1.11
average	1.14
standard deviation	0.04
% RSD	3.66

## CHAPTER 3

### RESULTS AND DISCUSSION

#### 3.1 Uranium Extraction

The amount of uranium extracted into the TBP phase was examined under a variety of initial conditions. All extractions and analysis described in this section were performed as discussed in Section 2.2. The distribution ratio,  $K_d$ , reported in this section was found by the following variation of Eq. 1.7.

$$K_d = \frac{[U]_{org}}{[U]_{aq}} \quad \text{Eq. 3.1}$$

Initial experiments were performed in order to better understand uranium extraction behavior under varied initial  $[HNO_3]$  and  $[NO_3^-]$  and to confirm with literature results (22, 24, 25). These extractions were performed for a large range of nitric acid and total nitrate concentration in the initial aqueous phase of 0-12 M (Table 2.4 and Table 2.5). Figure 3.1 and Figure 3.2 consist of data obtained from extractions of 0.05 M  $UO_2(NO_3)_2$  and demonstrate uranium distribution changes with respect to initial concentration of nitric acid and total nitrate.

Figure 3.1 and Figure 3.2 illustrate that  $K_d$  decreases with increasing acid for each  $[NO_3^-]$  and that  $K_d$  increases with increasing  $[NO_3^-]$  for each acid concentration. These effects are diminished beyond a concentration of 8 M  $NO_3^-$ , where distribution follows the trend found in extraction from nitric acid (25). These data are in good agreement

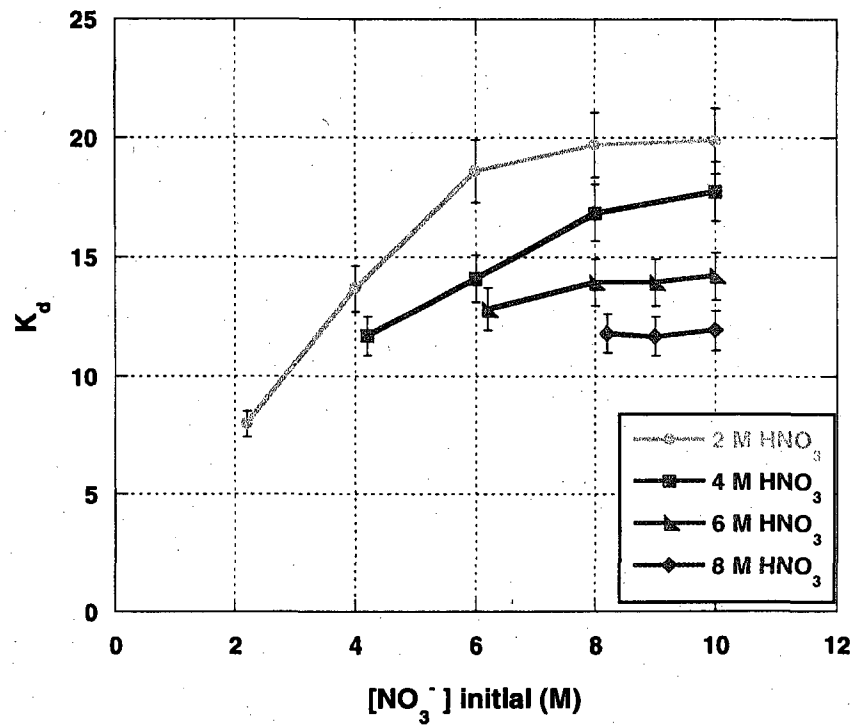


**Figure 3.1**  $K_d$  of U as initial  $[\text{NO}_3^-]$  increases from an aqueous phase of varied nitric acid and of 0.05 M  $\text{UO}_2(\text{NO}_3)_2$

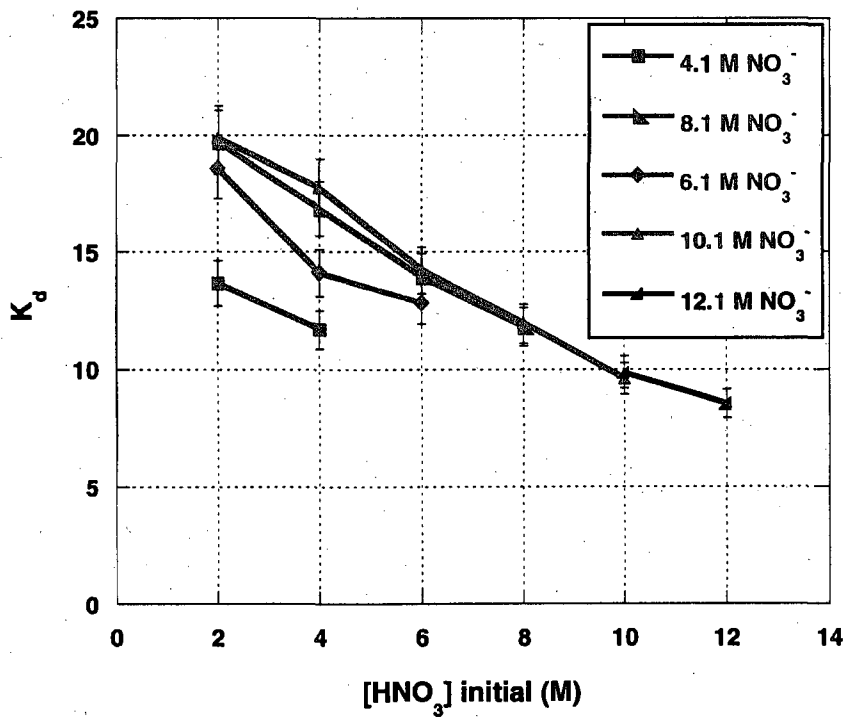


**Figure 3.2**  $K_d$  of U as initial  $[\text{HNO}_3]$  increases from an aqueous phase of varied lithium nitrate and of 0.05 M  $\text{UO}_2(\text{NO}_3)_2$

with the literature (21, 22, 24) and demonstrate the salting-out effect (Section 1.2.2.1).

The obtained  $K_d$  values compare favorably to the literature (Figure 3.3) (69). The

experimental data consisted of samples with an initial aqueous phase of 0.1 M

$\text{UO}_2(\text{NO}_3)_2$  and nitric acid as shown. This plot does not include extraction data at

elevated nitrate levels, and the  $K_d$  values from literature shown here were determined by

extraction from solutions of 0.1 M  $\text{UO}_2(\text{NO}_3)_2$  as well.

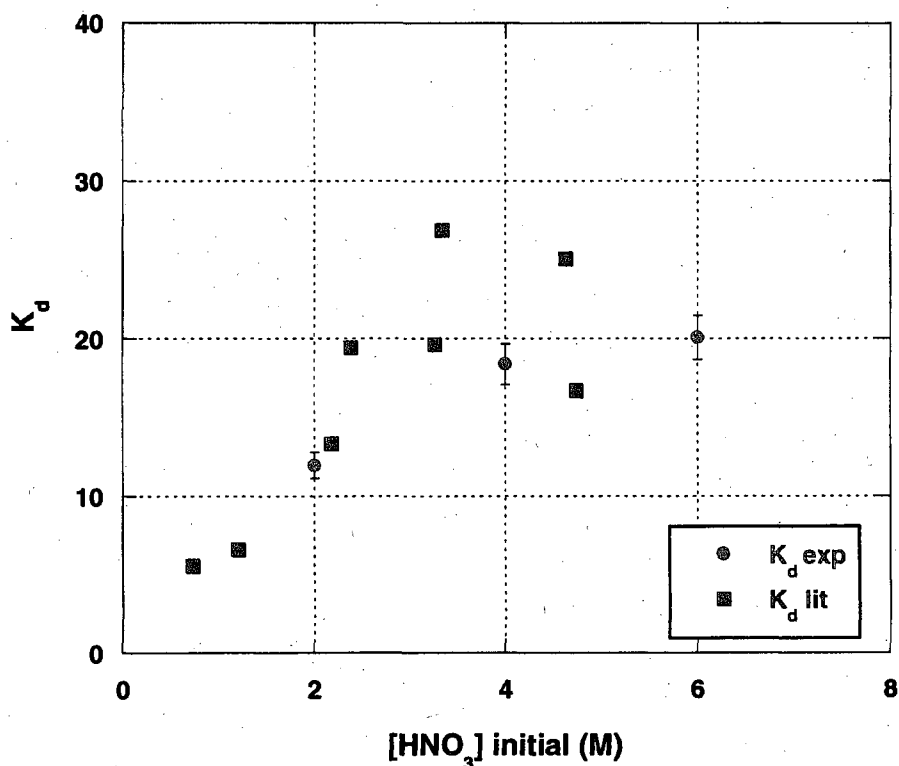
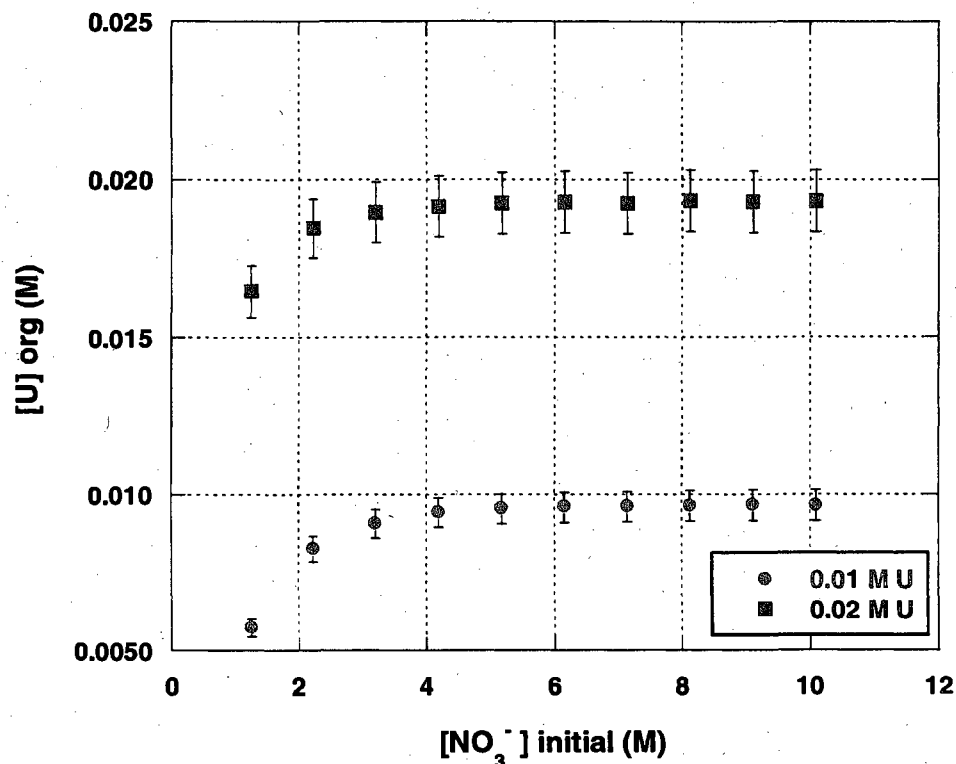


**Figure 3.3**  $K_d$  comparison to literature values at initial [U] of 0.1 M (69)

Extractions were performed under a constant  $\text{HNO}_3$  concentration of 1 M to evaluate effects of  $[\text{NO}_3^-]$ . The initial aqueous phase conditions of these extractions (Table 2.6 and Table 2.7) consist of samples where acid concentration was held at 1 M, and nitrate varied up to 10 M. The results of these experiments will also be used in Section 3.5 as a

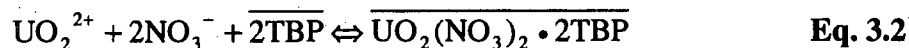
basis to compare the results of the extractions performed under constant ionic strength.

Figure 3.4 shows the [U] extracted into the TBP phase from two different aqueous phase concentrations. It is shown that at 1 M HNO<sub>3</sub> extraction tends toward completion (> 99% of [U] extracted) when the nitrate salt concentration is at 4 M and above.



**Figure 3.4** Extraction of U from 1 M HNO<sub>3</sub> into 30% TBP/dodecane

Further analysis of the data obtained from the experiments at 1 M HNO<sub>3</sub> was performed to verify the expected speciation of uranyl extraction. The assumed uranyl species is UO<sub>2</sub>(NO<sub>3</sub>)<sub>2</sub>·2TBP (see Section 1.2.2) and speciation described by the following equations:



$$\beta = \frac{[UO_2(NO_3)_2 \cdot 2TBP]}{[UO_2^{2+}][NO_3^-]^2[TBP]^2} = \frac{K_d}{[NO_3^-]^2[TBP]^2} \quad \text{Eq. 3.3}$$

$$\log K_d = \log \beta + 2 \log [NO_3^-] + 2 \log [TBP] \quad \text{Eq. 3.4}$$

Based on Equation 3.4, a plot of  $K_d$  against  $[NO_3^-]$  (Figure 3.5) or  $[TBP]$  (Figure 3.6) at equilibrium can give the stoichiometry of the extracted species (Section 1.2.2). These data imply by their slopes of  $2.03 \pm 0.05$  and  $1.9 \pm 0.2$  that 2 nitrates and 2 TBP molecules are extracted with the uranium. This confirms the predicted uranyl extraction species.

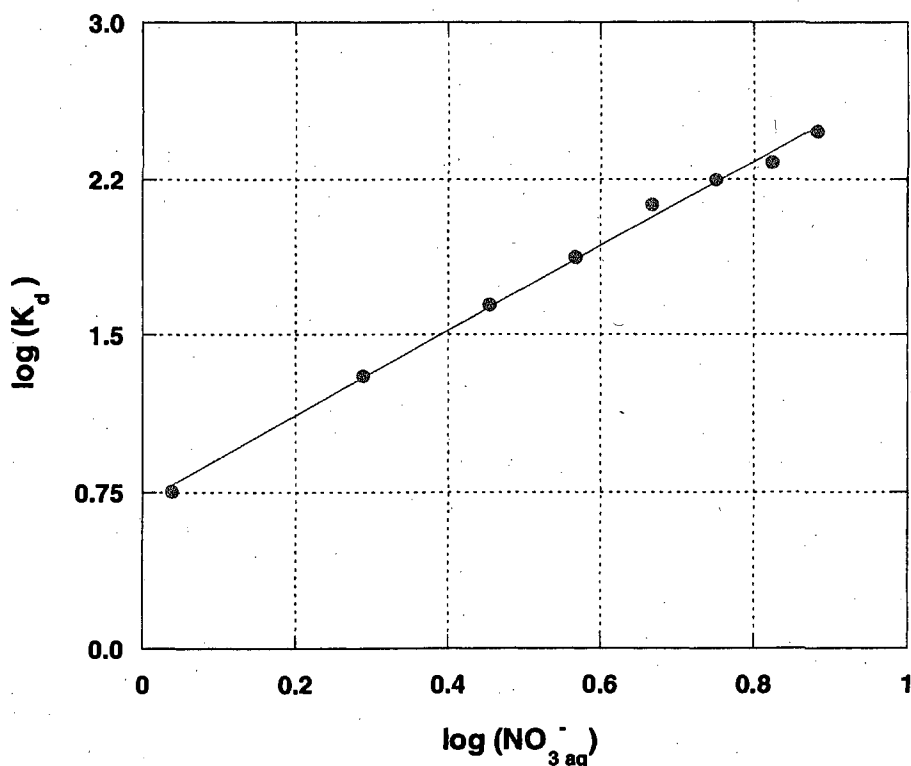


**Figure 3.5**  $NO_3^-$  stoichiometry determined via extraction data from 1 M  $HNO_3$  and 0.01 M U solutions

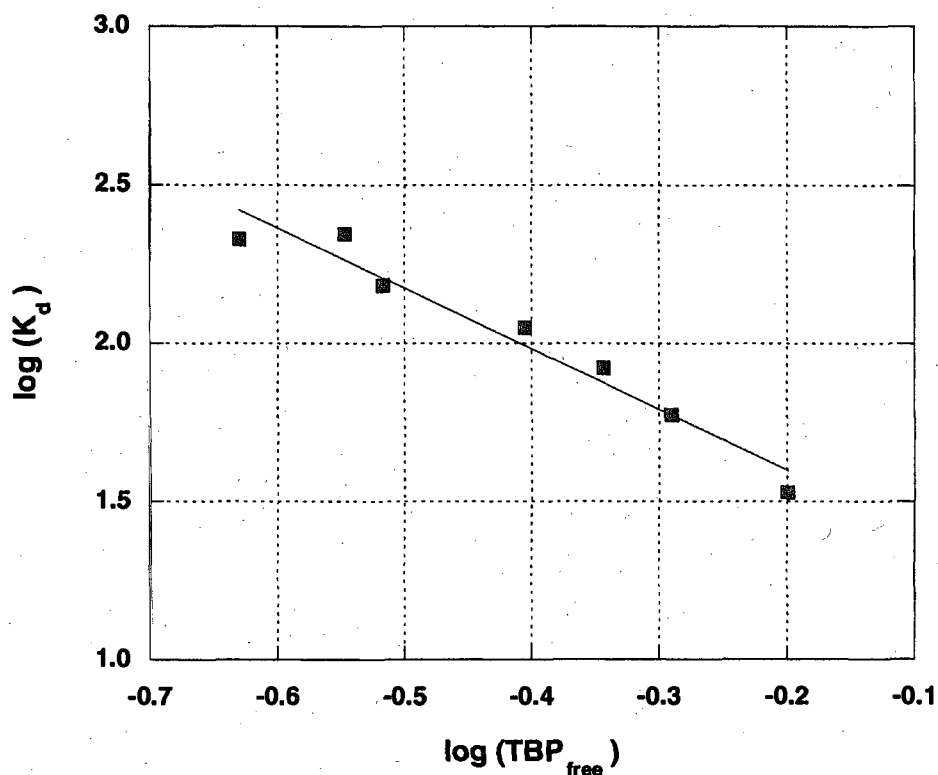


**Figure 3.6** TBP stoichiometry determined via extraction data from 1 M HNO<sub>3</sub> and 0.01 M U solutions

### 3.2 Nitric Acid Extraction

As discussed in Section 1.2.2.1, the extraction of nitric acid by TBP is an important consideration for this system; therefore extraction of the species HNO<sub>3</sub>•TBP was investigated. The amount of acid extracted into the organic phase was examined by titration as discussed in Section 0. The most obvious effect was how the total aqueous nitrate concentration significantly impacts the extraction of acid from a 1 M HNO<sub>3</sub> solution. The extracted acid increased from 15% at 1 M NO<sub>3</sub><sup>-</sup> to 75% at 10 M NO<sub>3</sub><sup>-</sup> (Figure 3.7). This increase of nitric acid in the organic phase when the aqueous nitrate concentration increases from a constant [HNO<sub>3</sub>] shows that the salting-out effect is valid for the extraction of nitric acid as well as for metal nitrates.

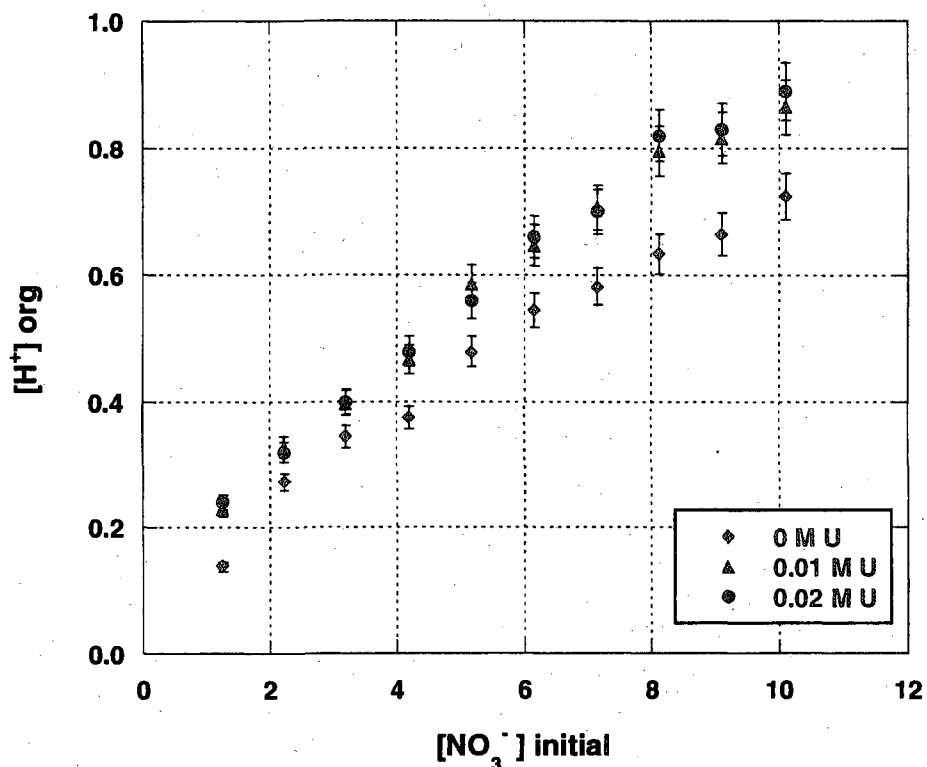
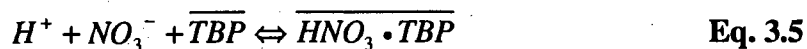


**Figure 3.7** Acid extraction from 1 M HNO<sub>3</sub> and varied [NO<sub>3</sub><sup>-</sup>] with and without the presence of uranium

The extraction of nitric acid was further examined by analysis of data obtained from samples with and without uranium present. In order to verify the speciation of the acid extraction, a similar process was used as for the uranium data in Section 3.1 by plotting the distribution ratio against the nitrate and TBP concentrations. The extraction is based on Eq. 3.5 - Eq. 3.7. Figure 3.8 is a plot based on Equation 3.7 and demonstrates the linear relationship, with a slope of  $1.09 \pm 0.05$ , between acid extraction and the nitrate ion. The details of the extraction conditions are found in Table 2.7.



$$\beta_H = \frac{[\overline{HNO_3 \cdot TBP}]}{[H^+][NO_3^-][\overline{TBP}]} \quad \text{Eq. 3.6}$$

$$\log \left( \frac{[\overline{\text{HNO}_3 \cdot \text{TBP}}]}{[\text{H}^+]} \right) = \log \beta_H + \log [\text{NO}_3^-] + \log [\text{TBP}] \quad \text{Eq. 3.7}$$

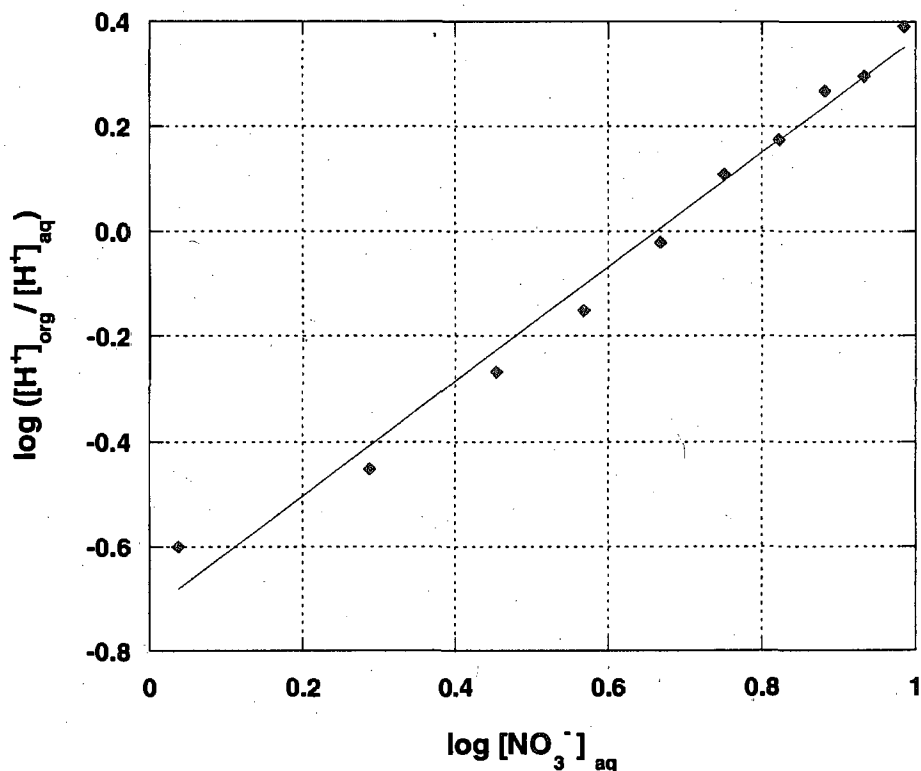
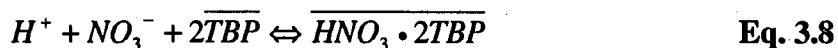


**Figure 3.8**  $\text{NO}_3^-$  stoichiometry determined via acid extraction data from 1 M  $\text{HNO}_3$  and 0.02 M U solutions

Figure 3.9 shows the same acid extraction data used in Figure 3.8 plotted against the amount of free TBP in the organic phase (See equation 3.15). Figure 3.9 illustrates that acid extraction has a clear dependence on  $[\text{TBP}]_{\text{free}}$ . The data can be split into two lines with slopes of  $1.03 \pm 0.04$  and  $1.94 \pm 0.09$ . This suggests that an extracted species of  $\text{HNO}_3 \cdot 2\text{TBP}$  is formed when a majority of the TBP molecules are unbound, which has

been reported in the literature (70, 71). This indicates that in addition to Equations 3.5-3.7, the following Equations 3.8-3.10 are also necessary to model this extraction system.



$$\beta_{H2} = \frac{[\overline{HNO_3 \cdot 2TBP}]}{[H^+][NO_3^-][\overline{TBP}]^2} \quad \text{Eq. 3.9}$$

$$[\overline{H^+}] = \beta_H [H^+][NO_3^-][\overline{TBP}] + \beta_{H2} [H^+][NO_3^-][\overline{TBP}]^2 \quad \text{Eq. 3.10}$$

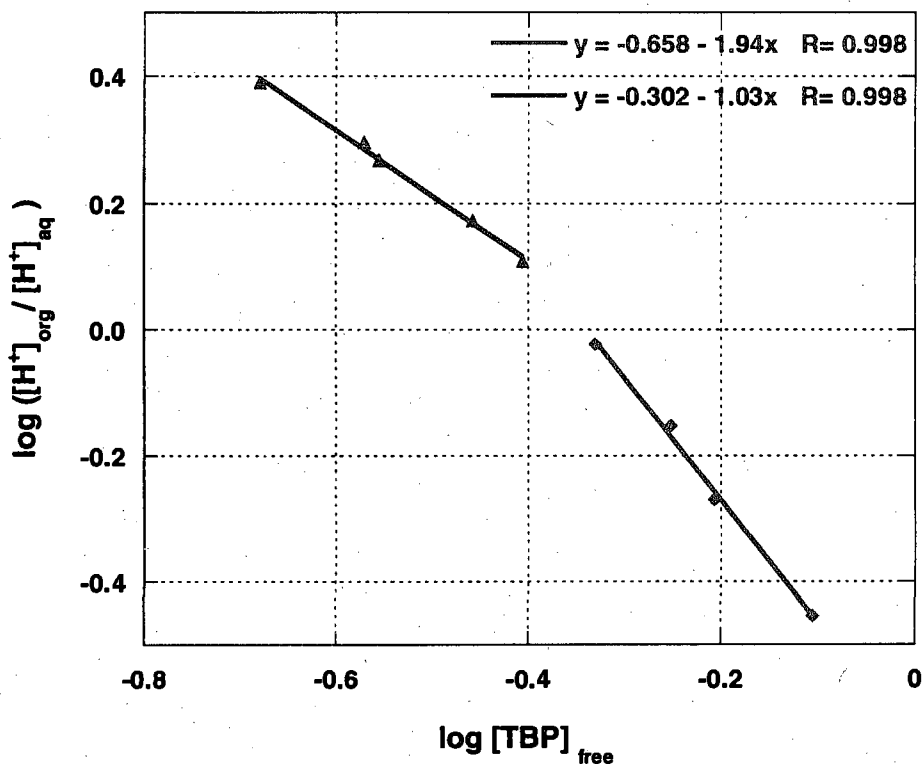


**Figure 3.9** TBP stoichiometry determined via acid extraction data from 1 M HNO<sub>3</sub> and 0.02 M U solutions

Nitric acid – TBP stability constants were calculated from the collected data based on Eq. 3.6 and Eq. 3.9. It was found that HNO<sub>3</sub>•TBP had a log β<sub>H</sub> value of -0.56 ± 0.06 (Table 3.1) and HNO<sub>3</sub>•2TBP had a log β<sub>H2</sub> value of -1.0 ± 0.1 (Table 3.2). These

stability constants close to previously reported values (70, 71), which were obtained by empirically fitting a model to other sources of experimental data. These values (Table 3.3) are compared with those determined in this work. There is good agreement among all the values except for the  $\log \beta_{H2}$  value of 0.76.

**Table 3.1** Calculation of  $\log \beta_H$  for samples with  $[TBP]_{free}$  less than 0.6 M

$[H^+]_{initial}$ (M)	$[NO_3^-]_{initial}$ (M)	I	$[TBP]_{free}$	$\log \beta_H$
2	3	4	0.59	-0.65
2	3	6	0.55	-0.57
2	4	6	0.46	-0.52
2	5	6	0.40	-0.50
			average	-0.56
			$\sigma$	0.06

**Table 3.2** Calculation of  $\log \beta_{H2}$  for samples with  $[TBP]_{free}$  greater than 0.7 M

$[H^+]_{initial}$ (M)	$[NO_3^-]_{initial}$ (M)	I	$[TBP]_{free}$	$\log \beta_H$
1	1	6	0.93	-0.93
1	2	4	0.90	-1.18
1	3	4	0.72	-0.92
2	2	6	0.87	-1.12
2	2	4	0.78	-0.91
			average	-1.01
			$\sigma$	0.13

For further analysis, speciation calculations using two organic phase nitric acid species were performed based on Equation 3.10. The calculation used an initial nitric acid concentration of 2 M and a  $K_d$  for  $[HNO_3]$  of 0.2, which is based on literature data (69) (Table 3.4). The  $[HNO_3]$  of the organic phase was calculated and compared to a

value of 0.33 M. From this it is obvious that the outlying data point for  $\beta_{H2}$  from (70) is inaccurate, with an error of 47% in the calculated organic nitric acid concentration. Moreover, this calculation demonstrates that the two nitric acid-TBP stability constants reported in this work provide the smallest error overall at 4.8%.

**Table 3.3** Reported  $\log \beta_H$  and  $\log \beta_{H2}$  values for nitric acid-TBP

	This work	(70)	(71)
$\text{HNO}_3 \cdot \text{TBP}$	$-0.56 \pm 0.06$	$-0.65 \pm 0.03$	$-0.62 \pm 0.04$
$\text{HNO}_3 \cdot 2\text{TBP}$	$-1.0 \pm 0.1$	$0.76 \pm 0.03$	$-1.00 \pm 0.04$

**Table 3.4** Comparison of error in speciation calculation based on reported stability constants from Table 3.3

Source	$\beta_H$	$\beta_{H2}$	$[\text{HNO}_3]_{\text{org}} \text{ (M)}$	% error
This work	0.28	0.10	0.31	4.8
(70)	0.22	5.75	0.18	46.7
(71)	0.24	0.10	0.30	8.1

### 3.3 Lithium Nitrate Extraction

The possible extraction of  $\text{LiNO}_3$  into TBP was discussed in Section 1.2.2.1, and is not considered to be feasible in this system (25, 27, 28). An analysis was performed to confirm that there is no extraction of  $\text{LiNO}_3$  into TBP. Figure 3.10 shows that in the absence of uranium, the amount of acid extracted into the organic phase correlates to the amount of nitrate extracted by a linear relationship with a slope of  $1.03 \pm 0.03$ . The data presented were obtained from extractions with initial conditions which varied from 1-6 M in  $[\text{NO}_3^-]$  and 1-2 M  $\text{HNO}_3$ .

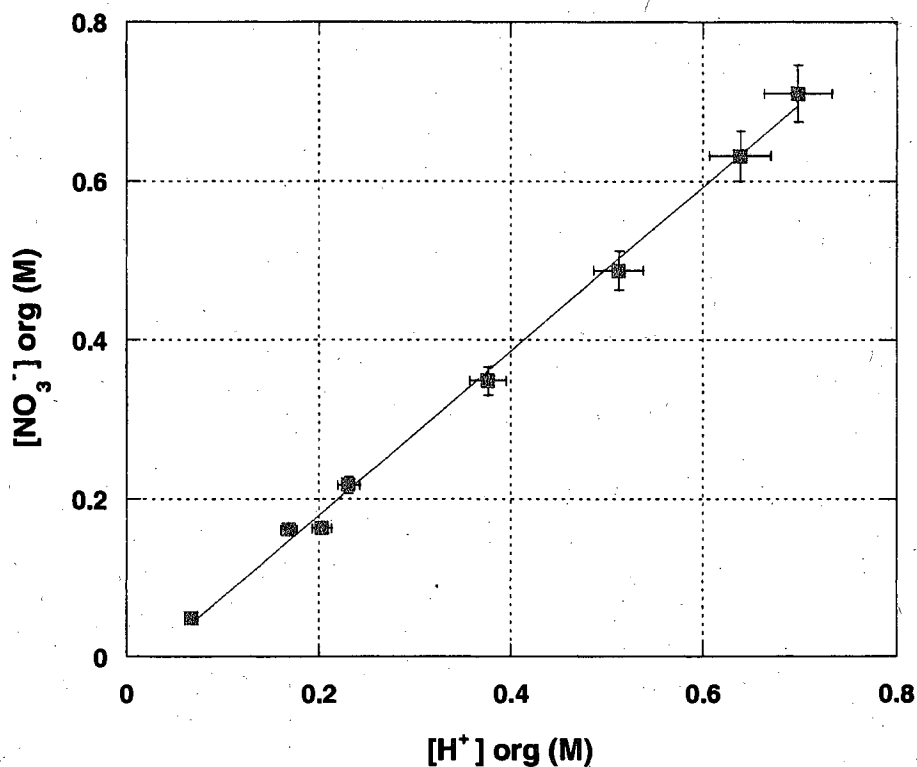


**Figure 3.10** Extraction of  $[\text{NO}_3^-]$  into TBP phase (initial conditions varied from 1-6 M in  $[\text{NO}_3^-]$  and 1-2 M  $\text{HNO}_3$ )

In order to determine if  $\text{LiNO}_3 \cdot \text{TBP}$  is extracted in the presence of uranium, mass balance was used. If  $\text{LiNO}_3$  is not extracted, the total organic nitrate concentration is described by 3.11. If it is extracted, the amount of  $\text{LiNO}_3$  in the organic phase is described by Eq. 3.12.

$$[\text{NO}_3^-]_{\text{org}} = [\text{HNO}_3 \cdot \text{TBP}]_{\text{org}} + [\text{HNO}_3 \cdot 2\text{TBP}]_{\text{org}} + 2[\text{UO}_2(\text{NO}_3)_2 \cdot 2\text{TBP}]_{\text{org}} \quad \text{Eq. 3.11}$$

$$[\text{NO}_3^-]_{\text{org}} - [\text{H}^+]_{\text{org}} - 2[\text{UO}_2(\text{NO}_3)_2 \cdot 2\text{TBP}]_{\text{org}} = [\text{LiNO}_3 \cdot \text{TBP}]_{\text{org}} \quad \text{Eq. 3.12}$$

Figure 3.11 reveals the theoretical amount of  $\text{LiNO}_3$  in the organic phase based on the measured concentrations substituted as values on the left side of Eq. 3.12. Each point represents an average of data from 2 to 6 extractions at each initial nitrate concentration.

All of the difference values shown were obtained from extractions under a variety of

initial conditions (Table 2.6-Table 2.9), a total of 38 samples. Since each set of data averages to a value of 0 within error, this confirms that ignoring  $\text{LiNO}_3$  extraction is reasonable and will not impact data analysis.

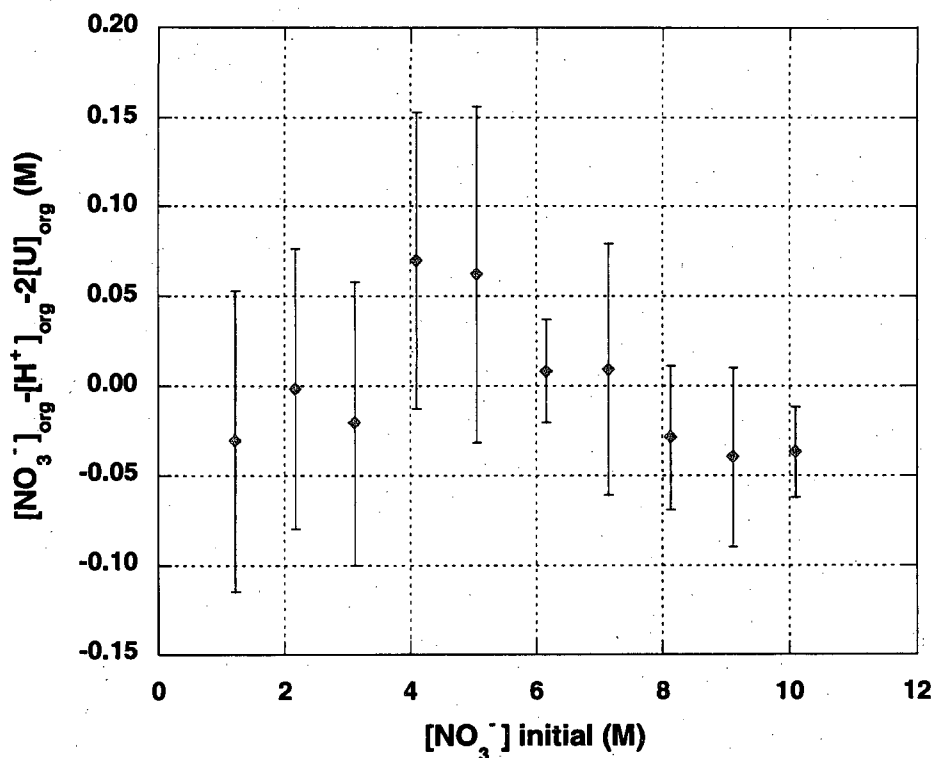


Figure 3.11 Mass balance of nitrate ions based on Eq. 3.12

### 3.4 Perchlorate Species Extraction

Since sodium perchlorate was used to adjust ionic strength, the extraction chemistry of different perchlorate species must be considered. As discussed in Section 1.2.2.1, the previous studies performed on this perchlorate-TBP system suggest that extraction into 30% TBP should be negligible when compared to the extraction of nitric acid (22, 29). Studies were conducted to confirm these results. A similar mass balance calculation was performed on the acid extraction data as with the nitrate data in Section 3.3. Assuming

that  $\text{HClO}_4$  was extracted into the organic phase, the amount would have to be equal to that shown in Equation 3.13.

$$[\text{H}^+]_{\text{org}} - ([\text{NO}_3^-]_{\text{org}} - 2[\text{UO}_2(\text{NO}_3)_2 \cdot 2\text{TBP}]_{\text{org}}) = [\text{HClO}_4 \cdot \text{TBP}]_{\text{org}} \quad \text{Eq. 3.13}$$

Figure 3.12 illustrates how the value on the left side of Equation 3.13 changes with  $[\text{ClO}_4^-]$ . These data points represent averages obtained from extraction samples at each perchlorate concentration, while the initial conditions are as listed in Table 2.8 and Table 2.9. Since the differences are near zero within experimental error, this figure demonstrates that the extraction of acid can be ignored in the chemistry of this system.

As discussed in Section 1.2.2.1, the extraction of  $\text{NaClO}_4$  into 30% TBP/dodecane has been shown in previously, but has a small  $K_d$  ( $<0.1$ ) (28). In order to be certain that species with such a small distribution ratio does not affect the calculation uranyl nitrate-TBP the amount of free TBP was calculated with Eq. 3.15 using the reported  $K_d$  of  $\text{NaClO}_4$  into TBP (28). The calculation of the uranyl nitrate TBP stability constant is discussed in detail in Section 3.5. As predicted, the amount of TBP bound to  $\text{NaClO}_4$  was too small to affect the final calculation (Table 3.5). This comparison demonstrates that the extraction of sodium perchlorate is negligible. More importantly, it shows that the organic phase species of all salts with small distribution ratios ( $<0.1$ ) can be ignored in the speciation calculation of uranyl nitrate-TBP, as suggested in the literature (24).

**Table 3.5** Comparison of the  $\text{UO}_2(\text{NO}_3)_2 \cdot 2\text{TBP}$  stability constant evaluated with and without  $[\text{NaClO}_4]$  extraction

$[\text{NaClO}_4]$ extraction	I = 6 M	I = 4 M
considered	$1.9 \pm 0.3$	$1.5 \pm 0.2$
not considered	$1.9 \pm 0.2$	$1.4 \pm 0.2$

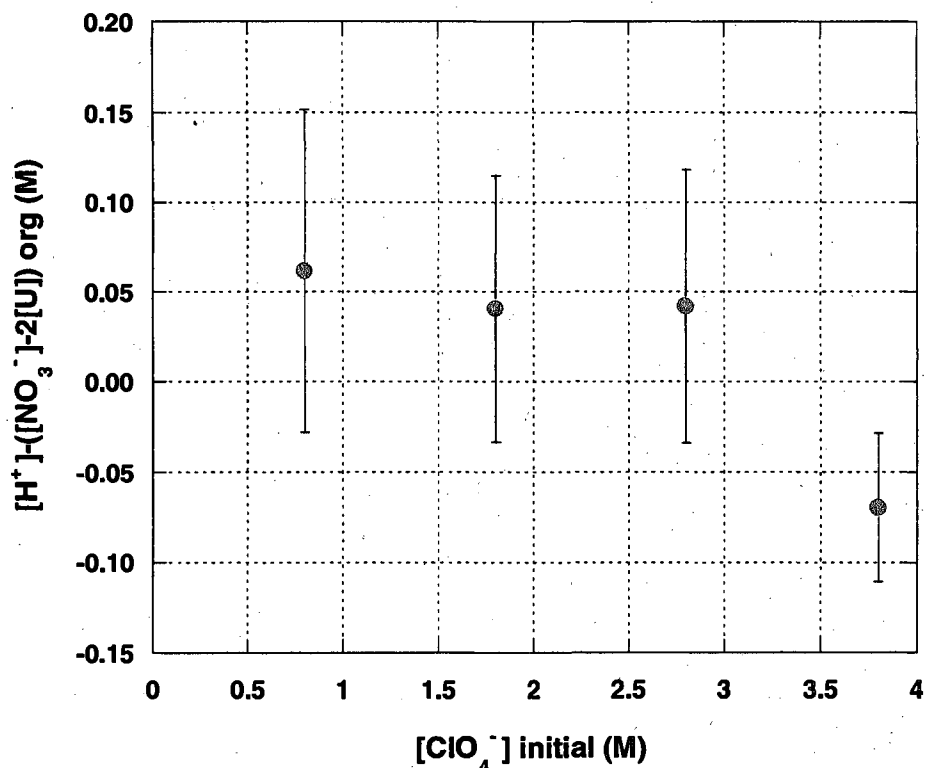


Figure 3.12 Mass balance of acid in the organic phase based on Eq. 3.13

### 3.5 Stability Constant Calculation

The calculation of the desired stability constant discussed in Section 1.2.2.2 was performed after verifying the speciation of the extracted components. It was determined that the dominant extracted species were  $\text{UO}_2(\text{NO}_3)_2 \cdot 2\text{TBP}$ ,  $\text{HNO}_3 \cdot \text{TBP}$ , and  $\text{HNO}_3 \cdot 2\text{TBP}$ ; all others were neglected. The following equations were used, along with the concentrations of  $[\text{U}]$ ,  $[\text{NO}_3^-]$ , and  $[\text{H}^+]$  measured at equilibrium, to calculate the stability constant.

$$\beta = \frac{[\text{UO}_2(\text{NO}_3)_2 \cdot 2\text{TBP}]}{[\text{UO}_2^{2+}][\text{NO}_3^-]^2[\text{TBP}]^2} = \frac{K_d}{[\text{NO}_3^-]^2[\text{TBP}]^2} \quad \text{Eq. 3.14}$$

$$[\text{TBP}]_{\text{free}} = [\text{TBP}]_{\text{init}} - [\text{HNO}_3 \cdot \text{TBP}]_{\text{org}} - 2[\text{HNO}_3 \cdot 2\text{TBP}]_{\text{org}} - 2[\text{UO}_2(\text{NO}_3)_2 \cdot 2\text{TBP}]_{\text{org}}$$

Eq. 3.15

The values for  $\beta_H$  and  $\beta_{H2}$  reported in Section 3.2 were used to determine  $[\text{HNO}_3 \cdot \text{TBP}]_{\text{org}}$  and  $[\text{HNO}_3 \cdot 2\text{TBP}]_{\text{org}}$ . Table 3.6 and Table 3.7 list the values of the stability constant (reported as  $\log \beta$ ) as calculated for the samples at constant ionic strengths of 6 and 4 M, respectively. While there is variation within the  $\beta$  values at each ionic strength, there is a clear difference between the two sets.

**Table 3.6** Calculated  $\log \beta$  values at I = 6 as initial conditions vary

[NO <sub>3</sub> ]	[U]	[H <sup>+</sup> ]	log $\beta$
2.2	0.01	1	2.16
3.1	0.01	1	2.10
4.0	0.01	1	1.93
2.2	0.02	1	1.97
3.1	0.02	1	1.65
4.9	0.02	1	2.27
2.2	0.01	2	1.93
3.1	0.01	2	2.02
4.0	0.01	2	1.78
2.2	0.02	2	1.98
3.1	0.02	2	1.75
4.9	0.02	2	1.42
		average	1.91
		$\sigma$	0.23

A value for the stability constant of  $\log \beta = 1.9 \pm 0.4$  was obtained by averaging results from samples at ionic strength of 6 M and varying nitrate from 1 - 5 M and acid from 1 - 2 M with initial uranyl nitrate of 0.01 and 0.02 M. Another value for the stability constant of  $\log \beta = 1.4 \pm 0.2$  was obtained by averaging results of samples at ionic strength of 4 M and varying nitrate from 1 - 3 M and acid from 1 - 2 M with initial uranyl nitrate of 0.01 and 0.02 M. The same calculation was performed on data obtained from the extractions where [NO<sub>3</sub><sup>-</sup>] varied from 1 to 10 M with out controlling ionic

strength, with an average result of  $\log \beta = 1.5 \pm 0.7$ , which is similar to those at constant ionic strength. The stability constant calculated from varied ionic strength increased with increasing nitrate, which is expected, as discussed in Section 1.2.2.2. The stability constants determined under constant ionic strength do not correlate with increasing nitrate concentration (Table 3.6 and Table 3.7).

**Table 3.7** Calculated  $\log \beta$  values at  $I = 4$  as initial conditions vary

[NO <sub>3</sub> ]	[U]	[H <sup>+</sup> ]	$\log \beta$
1.2	0.01	1	1.54
2.1	0.01	1	1.56
2.1	0.02	1	1.28
3.0	0.02	1	1.56
2.2	0.01	2	1.47
3.1	0.01	2	1.12
2.2	0.02	2	1.67
3.1	0.02	2	1.24
		average	1.43
		$\sigma$	0.19

The values obtained for  $\log \beta$  ( $1.9 \pm 0.2$  at  $I = 6$ , and  $1.4 \pm 0.2$  at  $I = 4$ ) agree with the previously reported values listed in Table 1.3, which range from 1.65 to 2.67. The current experiments differ from the literature studies as the equilibrium values of nitrate and acid were measured in addition to that of uranium, and ionic strength was held constant. The resulting values found in this work were obtained by actively controlling these parameters.

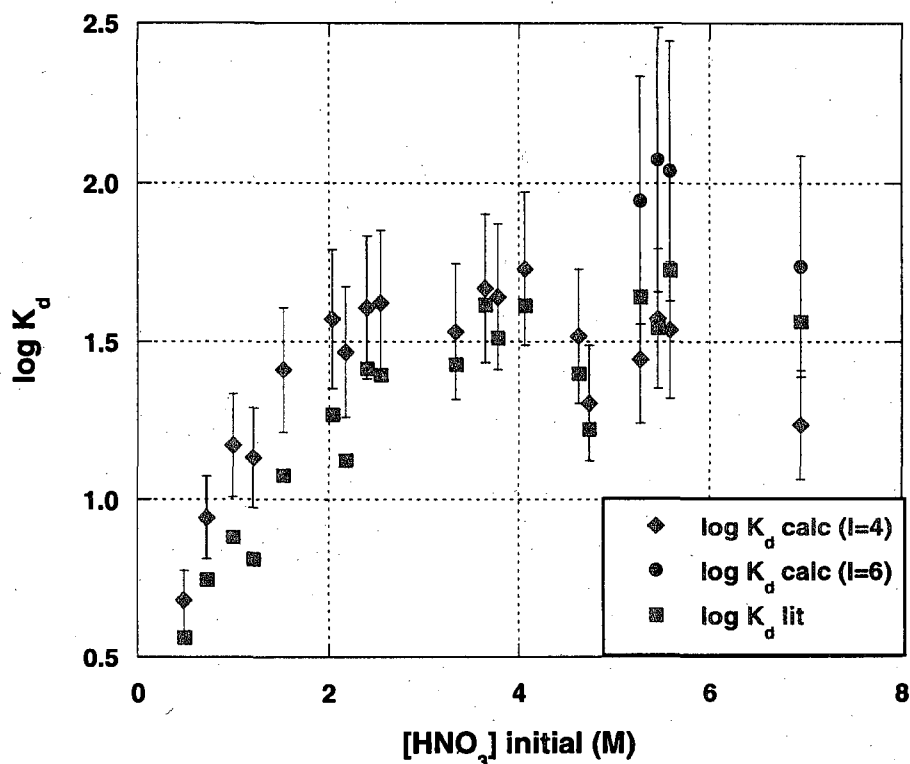


**Figure 3.13** Comparison of calculated  $K_d$  values with those previously reported (69)

The experimentally determined stability constants were used to predict  $K_d$  values, which were compared to literature results (69) using Eq. 3.4. As shown in Figure 3.13, the experimentally determined stability constant value of  $\log \beta = 1.4$  at 4 M ionic strength suitably predicted the distribution ratios that had an initial acid concentration from 3-5 M, concentrations near the experimental conditions of 4 M ionic strength. Similarly, the value determined at 6 M of  $\log \beta = 1.9$  corresponds well with the published  $K_d$  of higher acid concentrations, although the comparison is less thorough, since there were fewer reports in the literature with acid concentrations above 6 M  $\text{HNO}_3$ . The agreement between literature and calculated distribution constants demonstrates that the  $\beta$  values obtained in this work can be used to describe uranyl speciation and evaluate distribution. In summary it was determined that the important species to consider in the uranyl nitrate-

nitric acid-TBP extraction system are  $\text{UO}_2(\text{NO}_3)_2 \cdot \text{TBP}$ ,  $\text{HNO}_3 \cdot \text{TBP}$ , and  $\text{HNO}_3 \cdot 2\text{TBP}$ .

Only these species are extracted into 30% TBP/dodecane to any measurable extent, even when initial  $\text{LiNO}_3$  and  $\text{NaClO}_4$  concentrations are much greater than those of nitric acid or uranyl nitrate. By measuring equilibrium concentrations of  $[\text{U}]$ ,  $[\text{H}^+]$ , and  $[\text{NO}_3^-]$  after extraction, stability constants for each of those three species were obtained. The values for the constants obtained in this work were shown to be accurate.

## CHAPTER 4

### CONCLUSIONS

#### 4.1 Analytical Methods

Experiments were performed to optimize the methods for determination of acid, nitrate, and uranium concentrations. Acid concentration determination was made by titration of samples prepared by diluting 0.1 mL of each phase in 20 mL of 0.02 M ammonium oxalate. The titrant was 0.1 N NaOH and the step volume was 0.01 mL. Each titration was executed under argon gas, and the electrode was calibrated daily. This method provided results with accuracy and precision each within 2%.

Ion specific electrode potentiometry and ion chromatography were both investigated for nitrate determination. The ion specific electrode was only a reliable means of measuring nitrate concentration if the amount of acid in the sample was less than  $10^{-3}$  M, which is much lower than concentrations used in this work. Acid concentration had no effect on the values obtained by ion chromatography, therefore this method was chosen for the analysis of nitrate concentration determination. The aqueous samples were diluted by a factor of 10,000 in water and the organic were diluted by a factor of 1,000 in methanol. Separate calibrations were performed for the aqueous and organic phases before each set of samples were analyzed, and a calibration check was performed every time data were obtained. This method gave measured nitrate concentrations accurate to within 10% and precise to within 6%.

Three methods to measure uranium concentration were examined: inductively coupled plasma atomic emission spectroscopy, UV-visible spectroscopy, and liquid scintillation counting. Uranium determination by UV-visible spectroscopy was a reliable method for the organic phase of the extraction samples, but the aqueous phase concentrations were below the detection limit. Liquid scintillation counting was deemed unreliable for uranium determination in this system. The counts obtained were generally about twice the number there should have been, even in the organic phase, which was free of daughter products after extraction. The uranium concentrations presented in this work were obtained using ICP-AES. The aqueous phases of the extraction samples were prepared for uranium analysis by diluting by a factor of 20 in 1% nitric acid, and the organic phases were diluted by a factor of 500 in 1% nitric acid. Each measurement was made in triplicate and each set of samples was preceded by a calibration curve. The accuracy of each calibration was tested by a calibration check and gave accuracy within 10%. Data obtained was only accepted if the precision of each measurement was within 5%.

#### 4.2 Extractions

The results of uranium extraction distribution ratios (Section 3.1) correlate well with previously reported values. The experimentally determined  $K_d$  values from this work were measured against previously reported values before being used to calculate the desired stability constant and found to be close to literature data, indicating that the extraction and analysis methods used in this work were dependable. At a given acid concentration, the Uranium  $K_d$  value increased with increasing nitrate concentration, as

expected with the salting-out effect. At a given nitrate concentration, the  $K_d$  value decreased with increasing acid concentration due to  $\text{HNO}_3$  competition for TBP molecules. The stoichiometry of the extracted uranyl species was also confirmed to be  $\text{UO}_2(\text{NO}_3)_2 \cdot 2\text{TBP}$ , as is generally accepted.

It is well known that nitric acid is extracted with TBP, but this work demonstrated that the salting-out effect occurs in the extraction of nitric acid as well as of the metal nitrates. At a constant nitric acid concentration of 1 M, the measured concentration of extracted acid increased from 0.15 to 0.75 M as the nitrate ion concentration increased from 1 M to 10 M. One unexpected result of this work was the observation of  $\text{HNO}_3 \cdot 2\text{TBP}$  as well as  $\text{HNO}_3 \cdot \text{TBP}$ , a species of increasing importance as free TBP concentration increases. Nitric acid – TBP stability constants were calculated for both of these species:  $\log \beta$  is  $-0.56 \pm 0.06$  for  $\text{HNO}_3 \cdot \text{TBP}$  and  $-1.0 \pm 0.1$  for  $\text{HNO}_3 \cdot 2\text{TBP}$ . Most of the previous reports on acid extraction in TBP did not consider this second species, which must be incorporated into the calculations of the free TBP concentration when calculating the uranyl nitrate TBP stability constant.

Based on the low reported distribution of the other matrix ions used in this work ( $\text{Li}^+$ ,  $\text{Na}^+$ , and  $\text{ClO}_4^-$ ), they should not affect the extraction of uranium or nitric acid (22, 27, 28, 29). The data obtained here were examined for evidence to the contrary, and no noticeable extraction of  $\text{LiNO}_3$ ,  $\text{NaClO}_4$ , or  $\text{HClO}_4$  occurred.

After these analyses were complete and the methods and equations used were found to be accurate, the uranyl nitrate-TBP stability constant was calculated under different conditions, as discussed in Section 3.5. Nitrate and acid concentrations were varied at two different constant ionic strengths, yielding values for  $\log \beta = 1.9 \pm 0.2$  and  $1.4 \pm 0.2$  at

ionic strengths of 6 M and 4 M, respectively. These values are more accurate than those previously reported, since ionic strength was held constant and the measured equilibrium concentrations of nitrate and acid were included in the calculation. As discussed in Section 1.2.2.2, there were few reported values for this constant in the literature, and the methods used in those reports were not as thorough as the experiments performed for this work. Moreover, the stability constants calculated here were used to successfully predict experimentally determined distribution ratios in the literature.

### 4.3 Future Work

New series of extractions, following this method, should be performed at lower overall concentrations and lower constant ionic strengths. The system must be very dilute in uranium and acid concentration to minimize the change in free TBP concentration so that TBP activity can be ignored. The specific ion interaction theory could be used to calculate the ideal stability constant (28) via extrapolation to an infinitely dilute system. The activities of the organic phase species are still unknown, but can be determined via SIT calculations to more accurately calculate the ideal stability constant, which could then be used to estimate a constant at any ionic strength.

As mentioned in the introduction, the extraction experiments at constant ionic strength should be repeated for the plutonium(VI) and (IV) systems. The methods developed here could be modified to determine the stability constant for plutonium-nitrate-TBP extraction in order to improve the AMUSE code and enable more accurate calculations. Working with plutonium is more complex than working with uranium because plutonium has more available oxidation states, and they can coexist in solution.

In order to produce data reliable enough to be used to calculate the stability constant, care must be taken to ascertain the plutonium is maintained in the desired oxidation state.

Plutonium aqueous oxidation chemistry is well-studied. Combining a good working knowledge of aqueous plutonium nitrate speciation and oxidation state distribution with the methods developed in this work will lead to successful determination of the stability constant for plutonium nitrate TBP complex formation.

## REFERENCES

- 1 Clark, D. L.; Hecker, S. S.; Jarvinen, G. D.; Neu, M. P. Plutonium. In *The Chemistry of the Actinide and Transactinide Elements*, Third ed; Morss, L.R., Edelstein, N.M., Fuger, J., Eds.; Springer: The Netherlands, 2006; Vol. 2, pp 825-844.
- 2 Campbell, D.O.; Burch, W. D. *J. Radioanal. Nucl. Chem.*, Articles **1990**, 142 (1), 303-320.
- 3 Swanson, J. L. Purex Process Flowsheets. In *Science and Technology of Tributyl Phosphate*; Shulz, W. W., Gurger, L. L., Navratil, J. D., Eds.; CRC press: Florida, 1987; Vol. 3, pp 56-77.
- 4 Nash, K.L.; Madic, C.; Mathur, J.N.; Lacquemont, J. Actinide separation science and technology. In *Chemistry of the Actinide and Transactinide Elements*, Third ed.; Morss, L.R., Edelstein, N.M., Fuger, J., Eds.; Springer: The Netherlands, 2006; Vol. 4, pp 2644-2666.
- 5 Choppin G.; Liljenzin J.O.; Rydberg J. *Radiochemistry and Nuclear Chemistry*, 2<sup>nd</sup> edition; Reed: Great Britain, 1996; pp 602-612.
- 6 Choppin G. Overview of chemical separation methods and technologies. In *Chemical Separation technologies and related methods of nuclear wastemanagement*, Choppin G., Khankhasayev M.K, Eds.; NATO science series, Vol 53 pp16
- 7 Lieser K.H. *Nuclear and Radiochemistry*, 2<sup>nd</sup> Edition; Wiley: Germany, 2001; pp 224-229.
- 8 Czerwinski K. Separation Chemistry. In *Advances in plutonium chemistry 1967-2000*, Hoffman, D., Ed., American Nuclear Society: Illinois, 2002; pp 77-88.
- 9 Marcus, Y.; Kertes, A. S. *Ion Exchange and Solvent Extraction of Metal Complexes*, Wiley Interscience, 1969; pp 707-906.
- 10 Nillson, M.; Nash, K. L. *Solvent Extr. Ion Exch.* **2007**, 25(6), 665-701.
- 11 Nash, K.L.; Madic, C.; Mathur, J.N.; Lacquemont, J. Actinide separation science and technology. In *The Chemistry of the Actinide and Transactinide Elements*; Morss, L.R., Edelstein, N.M., Fuger, J., Eds.; Springer: The Netherlands, 2006; Vol. 4, pp 2669-2675.

- 12 Vandergrift G.F.; Leonard R.A.; Steindler M.A.; Horwitz E.P.; Basile L.J.; Diamond H.; Kalina D.G.; Kaplan L. *Transuranic decontamination of nitric acid solutions by the TRUEX solvent extraction process – Preliminary Development studies*; Report ANL-84/85; ANL: Argonne, IL, 1984.
- 13 Horwitz E.P.; Kalina D.G.; Diamond H.; Vandergrift G.F.; Schulz W.W. *Solvent Extr. Ion Exch.* **1985**, 3, 75-109.
- 14 Akatsu, J. *J. Nucl. Sci. Technol.* **1969**, 6(5), 285-289.
- 15 Ding, H. J.; Niu, Y. N.; Xu, Y. B.; Yang, W. F.; Yuan, S. G.; Wu, X. L. *J. Radioanal. Nucl. Chem.* **2007**, 272 (2), 263-266.
- 16 Mandal, D. K.; Bhattacharya, B.; Das, R. D. *Sep. Sci. Technol.* **2004**, 39(9), 2207-2221.
- 17 Healy, T. V.; McKay, H. A. C. *Trans. Faraday Soc.* **1956**, 52, 633-642.
- 18 Wu, S.; Cheng, W.; Chen, L. *He zi ke xue*, **1973**, 10(3-4), 26-37.
- 19 Kalina, D.; Mason, G.; Horwitz, E. P. *J. Inorg. Nucl. Chem.*, **1981**, 43, 159-163.
- 20 Vandegrift, G.F.; et. al. *Letter Report on UREX/PUREX Extraction Models*. ANL, 2001.
- 21 Alcock, K.; Best, G. F.; Hesford, E.; McKay, A. C. *J. Inorg. Nucl. Chem.* **1958**, 6, 328-333.
- 22 Naito, K.; Suzuki, T. *J. Phys. Chem.* **1962**, 66, 989-995.
- 23 Cheng, W. L.; Tsai, Y. M.; Wu, S. C. *Nuclear Science Journal*, **1973**, 10, 12-25.
- 24 Best, G. F.; McKay, A. C.; Woodgate, P. R. *J. Inorg. Nucl. Chem.* **1957**, 4, 315-320.
- 25 Svantesson, I.; Hagstrom, I.; Persson, G.; Liljenzin, J. *J. Inorg. Nucl. Chem.* **1979**, 41, 383-389.
- 26 Hesford, E.; McKay, H. A. C. *J. Inorg. Nucl. Chem.*, **1960**, 13, 156-164.
- 27 Lang, G. P.; Krieg, J. T. U.S. Atomic Energy Comm. MCW-1440, 1960.
- 28 Neck, V.; Altmaier, M.; Fanhanel, T. *Radiochim. Acta.* **2006**, 94, 501-507.
- 29 Oshima, K. *Nihon Genshiryoku Gakkaishi*, **1962**, 4(3), 166-174.
- 30 Moskvina, A. I. *Zhurnal Neorganicheskoi Khimii*, **1971**, 16(3), 759-764.

- 31 Choppin, G.; Jensen, M. Actinides in Solution. In *Chemistry of the Actinide and Transactinide Elements*, Third ed.; Morss, L.R., Edelstein, N.M., Fuger, J., Eds.; Springer: The Netherlands, 2006; Vol. 4, pp 2556-2578.
- 32 Comor, J. J.; Kopečni, M. M.; Petkovic, D. M. *Solvent Extr. Ion Exch.* **1997**, 15(6), 991-1006.
- 33 Stas, J.; Dahdouh, A.; Shlewitt, H. *Periodica Polytechnica Ser. Chem. Eng.* **2005**, 49(1), 3-18.
- 34 Petkovic, D.M. *Bulletin de la Societe Chimique Boegrad*, **1980**, 45, 281-287.
- 35 Grenthe, I., Puyigdomenech. *Modeling in Aquatic Chemistry*, Nuclear energy Agency, OECD: Paris, 1997; p 325.
- 36 Grenthe, I., et. al. (OECD, NEA-TDB): *Chemical Thermodynamics. Vol. 1. Chemical Thermodynamics of Uranium*; Elsevier: Amsterdam, 1992.
- 37 Grenthe, I., et. al. (OECD, NEA-TDB): *Chemical Thermodynamics. Vol. 4. Chemical Thermodynamics of Neptunium and Plutonium*; Elsevier: Amsterdam, 2001.
- 38 Benedict, M.; Pigford, T.H.; Levi H.W., eds. *Nuclear Chemical Engineering*, Second ed.; McGraw-Hill: New York, 1981.
- 39 Long J.T. *Engineering for Nuclear Fuel reprocessing*; American Nuclear Society: Illinois, 1978; pp 236-242.
- 40 Loveland, W.; Morrissey, D.; Seaborg, G. *Modern Nuclear Chemistry*; Wiley Interscience: New York, 2001.
- 41 Madic, C. *Radiation Protection Dosimetry* **1989**, 26, 15-22.
- 42 Cleveland, J.M. *The Chemistry of Plutonium*; American Nuclear Society: Illinois, 1979.
- 43 Wick, O.J., Ed, *Plutonium Handbook, A Guide to the technology*, Vol I and II, 1980.
- 44 Peters, R.; Seshadri, P.; Aubert, G.; Barracco, T.; Billès-Garabédian, L. The Boston Consulting Group, *Economic Assessment of Used Nuclear Fuel Management in the United States*, July 2006.
- 45 Bresee, J. C. *Description of Advanced Fuel Cycle Initiative Separations Technology Program*. Presented in Washington, D. C. in July, 2005.
- 46 Vandegrift, G.F.; et al. *Designing and Demonstration of the UREX+ Process Using Spent Nuclear Fuel*, in ATATLANTE 2004, Advances for Future Nuclear Fuel Cycles. 2004: Nimes, France.

- 47 Vandegrift, G. F. ; et. al. *Lab-Scale Demonstration of the UREX+ Process*, Waste Management 2004 International Symposium, Tucson, AZ, February 29-March 4, 2004
- 48 Rudisill, T. S. ; et. al. *Demonstration of the UREX Solvent Extraction Process with Dresden Reactor Fuel*, WSRC-MS-2003-00089, Rev. 1. Westinghouse Savannah River Company.
- 49 Mincher, B. J.; Mezyk, S. P.; Bauer, W. F.; Elias, G.; Riddle, C.; Peterman, D. R. *Solvent Extr. Ion Exch.* **2007**, 25(5), 593-601.
- 50 Laidler, J.J.; *Advanced Separations Technology Development*. in *AFCI Semi-Annual Review*. 2006. Santa Fe, New Mexico.
- 51 Regalbuto, M. C.; et.al. *Solvent Extraction Process Development for Partitioning and Transmutation of Spent Fuel*. ANL: Illinois, 2005.
- 52 Regalbuto, M. C.; *Chemical Reprocessing Plant Simulation*. Presented at Advanced Simulations: A Critical Tool for Future Nuclear Fuel Cycles, Lawrence Livermore National Laboratory, December, 2006.
- 53 Harris, D. C. *Quantitative Chemical Analysis*, Sixth Edition; W. H. Freeman and Company: New York, 2003.
- 54 Sundar, U.; et al. *Analyst* **1998**, 123, 1875-1877.
- 55 Siu, D. C.; Henshall, A. *J. Chromatogr., A* **1998**, 804(1-2), 157-160.
- 56 Bianchi, E.; Bruschi, R.; Draisci R.; Lucentini, L. *Z Lebensm Unters Forsch* **1995**, 200, 256-260.
- 57 Wilhelm, W. W.; Arnold, S. L.; Schepers, J. S. *Agron. J.* **2000**, 92, 186-189.
- 58 Perez, M. A.; Marin, L. P.; Quintana, J. C.; Pedram, M. Y. *Sensors and Actuators B.* **2003**, 89, 262-268.
- 59 Stana, J. *Agrochimica.* **1982**, 22(4), 119-121.
- 60 Skoog, D. A.; Holler, F. J.; Nieman, T. A. *Principles of Instrumental Analysis*, 5th Edition; Saunders College Publishing: Philadelphia, 1998.
- 61 Halverson, J. E.; Beals, D. M. *Trace Analytical Techniques for Nuclear Forensics*, WSRC-MS-99-00357. Savannah River Technology center, 1999.
- 62 Bower, K.; et. al. *J. Radioanal.Nucl. Chem.*, Articles **1994**, 181, 97-107.

- 63 Bostick, D. T. *The Simultaneous Analysis of Uranium and Nitrate*, ORNL/TM-6292. Oak Ridge National Laboratory, 1978.
- 64 Parrish, R. R.; et al. Depleted uranium contamination by inhalation exposure and its detection after 20 years: Implications for human health assessment, *Sci Total Environ* 2007, doi:10.1016/j.scitotenv.2007.09.044
- 65 Baltic University Environmental science book. *Chapter 12: Metal flows and Environmental Impact*.  
[http://www.balticuniv.uu.se/environmentalscience/ch12/chapter12\\_g.htm](http://www.balticuniv.uu.se/environmentalscience/ch12/chapter12_g.htm)
- 66 The Science of Spectroscopy. *UV-Visible Spectroscopy*.  
[www.scienceofspectroscopy.info/edit/index.php?title=UV-Visible\\_Spectroscopy](http://www.scienceofspectroscopy.info/edit/index.php?title=UV-Visible_Spectroscopy)
- 67 Grenthe, I., Drozdzyński, J.; Fujino, T.; Buck, E. C.; Albrecht-Schmitt, T. E.; Wolf, S. F. Uranium. In *The Chemistry of the Actinide and Transactinide Elements*, Third ed; Morss, L.R., Edelstein, N.M., Fuger, J., Eds.; Springer: The Netherlands, 2006; Vol. 1, pp 577.
- 68 Loveland, W.; Morrissey, D.; Seaborg, G. *Modern Nuclear Chemistry*; Wiley Interscience: New York, 2001.
- 69 Petrich, G., Kolarik, Z. The 1981 Purex Distribution Data Index. Kernforschungszentrum Karlsruhe, 1981.
- 70 Comor, J. J., Kopecni, M. M., and Petkovic, D. M. *Solvent Extr. Ion Exch.* **1997**, 15(6), 991-1006.
- 71 Mokili, B., and Poitrenaud, C., *Solvent Extr. Ion Exch.* **1995**, 13(4), 731-754.

## VITA

Graduate College  
University of Nevada, Las Vegas

Amber Dawn Wright

**Home Address:**

1515 E. Reno Ave. #D-106  
Las Vegas, NV 89119

**Degrees:**

Bachelor of Science, Mathematics, 2005  
University of Nevada, Las Vegas

Bachelor of Science, Chemistry, 2005  
University of Nevada, Las Vegas

**Thesis Title:** Nitrate Ion Effects on Uranium Chemistry in the Tributylphosphate-dodecane System

**Thesis Examination Committee:**

Chairperson, Dr. Kenneth Czerwinski, Ph. D.  
Committee Member, Dr. Al Sattelberger, Ph. D.  
Committee Member, Dr. Cynthia-May Gong, Ph. D.  
Graduate Faculty Representative, Dr. Ralf Sudowe, Ph. D.